

**MATHEMATICAL MODELING AND DETECTION OF  
STATOR ABNORMALITIES IN LINE START  
PERMANENT MAGNET SYNCHRONOUS MOTORS**

BY

**LUQMAN SULYMAN FAEZ MARAABA**

A Dissertation Presented to the  
DEANSHIP OF GRADUATE STUDIES

**KING FAHD UNIVERSITY OF PETROLEUM & MINERALS**

DHAHRAN, SAUDI ARABIA

In Partial Fulfillment of the  
Requirements for the Degree of

**DOCTOR OF PHILOSOPHY**

In

**ELECTRICAL ENGINEERING**

April 2018

KING FAHD UNIVERSITY OF PETROLEUM & MINERALS,  
DHAHRAN- 31261, SAUDI ARABIA  
DEANSHIP OF GRADUATE STUDIES

This thesis, written by **LUQMAN SULYMAN FAEZ MARAABA** under the direction of his thesis advisor and approved by his thesis committee, has been presented and accepted by the Dean of Graduate Studies, in partial fulfillment of the requirements for the degree of **DOCTOR OF PHILOSOPHY IN ELECTRICAL ENGINEERING**.



Dr. ALI AL-SHAIKHI  
Department Chairman



Dr. SALAM A. ZUMMO  
Dean of Graduate Studies

23/7/2018

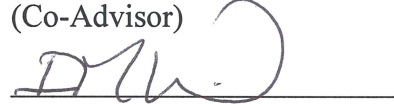
Date



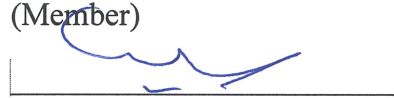
Dr. ZAKARIYA AL-HAMOUZ  
(Advisor)



Dr. MOHAMMAD ABIDO  
(Co-Advisor)



Dr. IBRAHIM ELAMIN  
(Member)



Dr. SAMIR AL-BAIYAT  
(Member)



Dr. IBRAHIM HABIBALLAH  
(Member)

© Luqman Sulyman Faez Maraaba

2018

بِسْمِ اللَّهِ الرَّحْمَنِ الرَّحِيمِ  
{قُلْ إِنَّ صَلَاتِي وَنُسُكِي وَمَحْيَايَ وَمَمَاتِي لِلَّهِ رَبِّ الْعَالَمِينَ}

*This Dissertation is dedicated to*

*The souls of my Mother (Fatima) and Sister (Isra)*

*Dear Father (Sulyman)*

*Beloved Wife (Saraa)*

*Beloved Son (Anas)*

*My Ummah |*



## ACKNOWLEDGMENTS

In the name of Allah, the most gracious, the most merciful all praise is to almighty Allah for having guided me all over my life. Acknowledgement is due to King Fahd University of Petroleum and Minerals for the great support to this work. My deep appreciation is reserved for thesis advisor **Prof. Zakariya Al-Hamouz** for his guidance, valuable time and attention he devoted throughout the course of this work. My numerous intrusions into his office were always met with a considerable response and care. Thanks, are also due to my co-advisor **Prof. Mohammad A. Abido** and committee members **Prof. Ibrahim El-Amin, Prof. Samir Al-Baiyat** and **Dr. Ibrahim O. Habiballah** for their interest, attention and suggestion. I wish also to thank all parties who have contributed to support me in this work, namely Department chairman **Dr. Ali Alshaikhi** and other faculty members for their supports. My great appreciations are also due to all members of my family and to friends who give me the self-confidence to face the challenge

# TABLE OF CONTENTS

ACKNOWLEDGMENTS .....	V
TABLE OF CONTENTS.....	VI
LIST OF TABLES .....	X
LIST OF FIGURES .....	XI
LIST OF ABBREVIATIONS.....	XVII
ABSTRACT .....	XIX
ملخص الرسالة .....	XXI
CHAPTER 1 INTRODUCTION.....	1
1.1 Overview .....	1
1.2 Thesis Motivation.....	3
1.3 Dissertation Objectives.....	3
1.4 Dissertation Methodology .....	4
1.5 Findings and Contributions .....	6
1.6 Dissertation Organization .....	7
CHAPTER 2 LITERATURE REVIEW.....	9

2.1	Overview .....	9
2.2	Line Start Permanent Magnet Synchronous Motors (LSPMSMs).....	10
2.2.1	Dynamic Model for Healthy LSPMSM .....	14
2.2.2	Steady State Model for Healthy LSPMSM .....	16
2.2.3	Basic LSPMSMs Construction Configurations .....	18
2.3	Electric Motors Faults .....	22
2.3.1	Stator Faults .....	23
2.3.2	Eccentricity .....	25
2.3.3	Rotor Faults .....	26
2.3.4	Permanent Magnets Faults.....	28
2.4	Electric Motors Modeling Under Faults .....	29
2.4.1	Modeling of Stator Inter-Turn Fault.....	31
2.5	Faults Indicators .....	33
2.6	Analytical Tools for Electric Motor Faults Diagnosis and Prognosis.....	34
<b>CHAPTER 3 INTERIOR-MOUNT LSPMSM MODELING UNDER STATOR</b>		
<b>WINDING ABNORMALITIES .....</b>		
3.1	Overview .....	40
3.2	Mathematical Modeling of Interior-Mount LSPMSM .....	41
3.2.1	Mathematical Modeling of Interior-Mount LSPMSM Under Asymmetric Stator Windings	42

3.2.2	Mathematical Modeling of Interior-Mount LSPMSM Under Stator Inter-Turn Fault .....	56
3.3	JMAG™ Finite Element Modeling .....	67
3.3.1	JMAG Modeling under Asymmetrical Stator Winding Condition .....	67
3.3.2	JMAG Modeling under Stator Inter-Turns Fault.....	72
 <b>CHAPTER 4 LSPMSM PARAMETERS MEASUREMENTS .....</b>		<b>75</b>
4.1	Overview .....	75
4.2	DC Test .....	76
4.3	Single Phase AC Test (Rotor not Included).....	79
4.4	Blocked Rotor Test .....	81
4.5	DC Step Test.....	86
4.6	Open Circuit Test .....	89
4.7	Parameters Measurement Summary .....	92
 <b>CHAPTER 5 TESTING &amp; VALIDATION FOR THE DEVELOPED MODELS ...</b>		<b>93</b>
5.1	Overview.....	93
5.2	Testing of the Healthy LSPMSM.....	94
5.3	Testing of LSPMSM under Asymmetrical Stator Winding .....	100
5.4	Testing of LSPMSM under Stator Inter-Turn Fault .....	105

<b>CHAPTER 6 DIAGNOSTIC TOOL DESIGN FOR DETECTING STATOR</b>	
<b>WINDING ABNORMALITIES .....</b>	<b>117</b>
<b>6.1 Overview .....</b>	<b>117</b>
<b>6.2 Features Extraction .....</b>	<b>117</b>
<b>6.2.1 Features Extraction for Inter-turn Fault.....</b>	<b>118</b>
<b>6.2.2 Features Extraction for the Asymmetry Condition .....</b>	<b>130</b>
<b>6.3 Neural Network Design .....</b>	<b>134</b>
<b>6.4 Robustness of the developed Diagnostic Tool.....</b>	<b>136</b>
<b>6.5 Diagnostic Tool Deployment .....</b>	<b>142</b>
<b>CHAPTER 7 CONCLUSION AND FUTURE WORK .....</b>	<b>143</b>
<b>7.1 Conclusion .....</b>	<b>143</b>
<b>7.2 Future Work.....</b>	<b>146</b>
<b>REFERENCES.....</b>	<b>147</b>
<b>PUBLICATIONS .....</b>	<b>169</b>
<b>VITAE .....</b>	<b>170</b>

## LIST OF TABLES

Table 2.1 Stator Current as a fault indicator [118] .....	34
Table 3.1 LSPMSM Parameters.....	69
Table 3.2 The Materials assigned to each motor part. ....	70
Table 4.1 DC test results.....	78
Table 4.2 Single phase AC without rotor test Results .....	81
Table 4.3 locked rotor test result (rotor d-axis aligned with phase a).....	84
Table 4.4 locked rotor test result (rotor q-axis aligned with phase a).....	85
Table 4.5 Step DC test result- rotor d-axis aligned with phase-a .....	88
Table 4.6 Step DC test result- rotor q-axis aligned with phase-a .....	89
Table 4.7 Open circuit test results.....	91
Table 4.8 Tested motor measured parameters .....	92
Table 5.1 Tested motor parameters.....	93
Table 5.2 The simulated asymmetrical cases.....	101
Table 5.3 The shorted-turn cases for the faulty LSPMSM .....	106
Table 6.1 Sample of the testing results .....	136
Table 6.2 Sample of the testing results under variation in the supply voltages.....	137
Table 6.3 Sample of the testing results under variation in the motor inertia .....	138
Table 6.4 Sample of the testing results under variation in stator resistance .....	139
Table 6.5 Sample of the testing results under variation in PM flux linkage.....	140
Table 6.6 Sample of the testing results under variation in both supply voltages and motor inertia.....	141



## LIST OF FIGURES

Figure 2.1 1 hp interior-mount LSPMSM.....	11
Figure 2.2 LSPMSM Equivalent circuit: (a) d-axis equivalent circuit; (b) q-axis equivalent circuit.....	16
Figure 2.3 Steady state d-q circuit diagram of LSPMSM (a) d-axis equivalent circuit (b) q-axis equivalent circuit .....	17
Figure 2.4 LSPMSM cross section (a) interior- mount LSPMSM (b) surface-mount LSPMSM [29].....	19
Figure 2.5 Performance comparison between two LSPMSM designs [42].....	20
Figure 2.6 LSPMSM rotor magnets configurations (a) Spoke (b) Series (radial flux rotor) (c) U-type (d) V-type(e) W-type (f) Swastik [29] .....	21
Figure 2.7 Comparison between LSPMSMs with different rotor configurations [29].....	21
Figure 2.8 Fault types in electric motors .....	23
Figure 2.9 Stator inter-turns fault [62].....	24
Figure 2.10 Rotor eccentricity [73].....	26
Figure 2.11 Rotor of induction motor (a) healthy (b) one broken bar (c) three broken bars [45].....	27
Figure 2.12 Permanent magnets damage [65].....	28
Figure 3.1 Mathematical and finite element models deriving steps .....	41
Figure 3.2 LSPMSM ABC-circuit diagram .....	43
Figure 3.3 LSPMSM machine winding displacement .....	48
Figure 3.4 The stator of the LSPMSM under inter-turn fault in phase-a.....	56

Figure 3.5 The steps for JMAG motor modeling.....	68
Figure 3.6 1 HP LSPMSM: (a) stator (b) rotor.....	68
Figure 3.7 The 2-D geometry model parts of LSPMSM in JMAG™.....	70
Figure 3.8 Stator winding circuit.....	71
Figure 3.9 Finite element mesh.....	72
Figure 3.10 2D JMAG™ geometry under stator inter-turn fault.....	73
Figure 3.11 Stator winding circuit.....	74
Figure 4.1 Laboratory tests.....	76
Figure 4.2 DC test setup.....	77
Figure 4.3 DC test circuit diagram.....	77
Figure 4.4 circuit diagram of single phase AC without rotor test.....	79
Figure 4.5 Experimental set-up for single phase AC test without rotor.....	80
Figure 4.6 Voltage and current waveforms using CASSY unit.....	80
Figure 4.7 schematic diagram of locked rotor test.....	82
Figure 4.8 LSPMSM circuit under blocked rotor conditions (a) q-circuit (b) d-circuit.....	82
Figure 4.9 Blocked rotor test experimental set-up.....	83
Figure 4.10 Locked rotor test current and voltage wave form (a) d-axis (b) q-axis.....	85
Figure 4.11 Schematic diagram of step DC test.....	86
Figure 4.12 Equivalent circuit of tested machine under step DC test.....	87
Figure 4.13 Step response of the tested motor.....	88
Figure 4.14 Open circuit test diagram.....	90
Figure 4.15 Experimental set-up of the open circuit test.....	90

Figure 4.16 (a) Induced line voltage at 1060rpm rotor speed (b) relation between rotor speed and induced line voltage .....	92
Figure 5.1 Experimental set-up.....	94
Figure 5.2 Healthy motor at no load (a) Stator phase-a current (b) speed.....	95
Figure 5.3 Healthy motor at 2 N.m load (a) Stator phase-a current (b) speed.....	96
Figure 5.4 Healthy motor at full load (a) Stator phase-a current (b) speed .....	97
Figure 5.5 Rotor three phase current at full load .....	98
Figure 5.6 Motor torque components at full load (a) reluctance torque (b) induction torque (c) excitation torque (d) electromechanical torque .....	99
Figure 5.7 Stator phase-a current at full load.....	101
Figure 5.8 Stator phase-a current at full load (a) Case I (b) Case II (c) Case III.....	102
Figure 5.9 Rotor speed at full load (a) Case I (b) Case II (c) Case III.....	103
Figure 5.10 Motor torque at full load (a) Case I (b) Case II (c) Case III.....	104
Figure 5.11 Configuration of the stator windings of the LSPMSM with center taps added in phase-a. ....	105
Figure 5.12 Experimental setup .....	106
Figure 5.13 Stator phase-a current under no load: (a) healthy conditions, (b) 26 shorted turns, (c) 40 shorted turns .....	108
Figure 5.14 Rotor speed under no load: (a) healthy conditions, (b) 26 shorted turns, (c) 40 shorted turns .....	109
Figure 5.15 Motor testing results under full load with 26 shorted turns: (a) stator phase-a, (b) rotor speed, (c) fault current .....	110

Figure 5.16 Experimental and MATLAB simulation results under no load: (a) fault current as a function of fault resistance, (b) fault current as a function of fault severity .....	111
Figure 5.17 Experimental results under 26 shorted turns occurring at 0.44 sec (a) stator phase-a current and fault (b) three phase current (c) speed.....	112
Figure 5.18 MATLAB simulation results under no load with 9 shorted turns (a) Three-phase stator current (b) speed .....	113
Figure 5.19 Phase-a current under no load for MATLAB simulation.....	114
Figure 5.20 Phase-a current under no load for experimental testing .....	115
Figure 5.21 Speed under no load for MATLAB simulation.....	115
Figure 5.22 Speed under no load for experimental testing .....	116
Figure 6.1 Phase-a steady state current under no load (a) 0 shorted turns (b) 9 shorted turns (c) 26 shorted turns (d) 40 shorted turns .....	118
Figure 6.2 Experimental and MATLAB extracted features at no load for 1Ω fault resistance: (a) variance (b) kurtosis (c) Maximum (d) RMS .....	120
Figure 6.3 Experimental and MATLAB extracted features at no load for 1 Ω fault resistance: (a) Fundamental current Magnitude (b) Fundamental power factor angle (c) Power factor.....	121
Figure 6.4 Experimental and MATLAB extracted features at no load for 1Ω fault resistance: (a) positive sequence component magnitude (b) negative sequence component magnitude (c) zero sequence component magnitude...	122
Figure 6.5 MATLAB extracted features at different loading condition for 1 Ω fault resistance (a) variance (b) kurtosis (c) Maximum (d) RMS .....	123

Figure 6.6 MATLAB extracted features at different loading condition for 1 $\Omega$ fault resistance (a) Fundamental current Magnitude (b) Fundamental power factor angle (c) power factor .....	124
Figure 6.7 MATLAB extracted features at different loading condition for 1 $\Omega$ fault resistance (a) positive sequence faulted current magnitude (b) negative sequence faulted current magnitude (c) zero sequence faulted current magnitude .....	125
Figure 6.8 Phase-a steady state current under no load for 26-shorter turns (a) $R_f=1.2\Omega$ (b) $R_f=1 \Omega$ (c) $R_f=0.8$ (d) $R_f=0.4 \Omega$ .....	127
Figure 6.9 MATLAB extracted features for different fault resistor values at no load (a) variance (b) kurtosis (c) Maximum (d) RMS .....	128
Figure 6.10 MATLAB extracted features for different fault resistor values at no load (a) Fundamental current Magnitude (b) Fundamental power factor angle (c) power factor .....	129
Figure 6.11 MATLAB extracted features for different fault resistor values at no load (a) positive sequence component magnitude (b) negative sequence component magnitude (c) zero sequence component magnitude .....	130
Figure 6.12 MATLAB extracted features under asymmetric condition in phase-a (a) variance (b) kurtosis (c) Maximum (d) RMS .....	131
Figure 6.13 MATLAB extracted features under asymmetric condition in phase-a (a) Fundamental current Magnitude (b) Fundamental power factor angle (c) power factor .....	132

Figure 6.14 MATLAB extracted features under asymmetric condition in phase-a (a) positive sequence component magnitude (b) negative sequence component magnitude (c) zero sequence component magnitude .....	133
Figure 6.15 Neural network topology.....	135
Figure 6.16 Diagnostic tool deployment.....	142



## LIST OF ABBREVIATIONS

$\mathbf{v}_{abc}^s, \mathbf{v}_{abc}^r$	:	<b>Stator and rotor abc-voltages</b>
$\mathbf{i}_{abc}^s, \mathbf{i}_{abc}^r$	:	<b>Stator and rotor abc-currents</b>
$\mathbf{R}_{abc}^s, \mathbf{R}_{abc}^r$	:	<b>Stator and rotor abc-phases resistances</b>
$\lambda_{abc}^s, \lambda_{abc}^r$	:	<b>Stator and rotor abc-flux linkages</b>
$\mathbf{L}_{abc}^s, \mathbf{L}_{abc}^r$	:	<b>Stator and rotor abc-inductances</b>
$\mathbf{L}_{abc}^{sr}$	:	<b>Stator and rotor abc-mutual inductances</b>
$\lambda_{mabc}^s, \lambda_{mabc}^r$	:	<b>Stator and rotor abc-PM flux linking</b>
$N_s$	:	<b>Number of turns per stator phase</b>
$\alpha_a, \alpha_b, \alpha_c$	:	<b>Phase a, b, c asymmetric turns ratio coefficients</b>
$r_s, r_r$	:	<b>Stator and rotor resistance per phase</b>
$\lambda'_m$	:	<b>PM linkage flux refer to stator side</b>
$\theta_r$	:	<b>Angle between stator phase-a and rotor phase-a.</b>
$\mathbf{K}_s$	:	<b>Stator park transformation matrix</b>
$\mathbf{K}_r$	:	<b>Rotor park transformation matrix</b>
$L_d^s$	:	<b>Stator self-inductance in d-axis</b>
$L_q^s$	:	<b>Stator self-inductance in q-axis</b>

$L_d^r$	:	Rotor self-inductance in d-axis
$L_q^r$	:	Rotor self-inductance in q-axis
$v_q^s, v_d^s, v_0^s$	:	Stator qd0 voltages
$v_q^{r'}, v_d^{r'}, v_0^{r'}$	:	Rotor qd0 voltages refer to stator side
$i_q^s, i_d^s, i_0^s$	:	Stator qd0 currents
$i_q^{r'}, i_d^{r'}, i_0^{r'}$	:	Rotor qd0 currents refer to stator side
$\lambda_q^s, \lambda_d^s, \lambda_0^s$	:	Stator qd0 linkage fluxes
$\lambda_q^{r'}, \lambda_d^{r'}, \lambda_0^{r'}$	:	Rotor qd0 linkage fluxes refer to stator side
$L'_{lrq}, L'_{lrd}, L'_{lr0}$	:	Rotor qd0 leakage inductances refer to stator side
$r'_{rq}, r'_{rd}, r'_{r0}$	:	Rotor qd0 resistances refer to stator side
$L_{ls}$	:	Leakage stator inductance
$L_{md}, L_{mq}$	:	Mutual inductances in the d- and q-axis
$T_{em}$	:	Electromagnetic torque
$T_L$	:	Load torque
$T_{damp}$	:	Damping torque
$J$	:	Motor inertia
$\omega_r$	:	Rotor speed

## ABSTRACT

Full Name : [Luqman Sulyman Faez Maraaba]  
Thesis Title : [Mathematical Modeling and Detection of Stator Abnormalities in Line Start Permanent Magnet Synchronous Motors]  
Major Field : [Electrical Engineering]  
Date of Degree : [April 2018]

In industrial applications, especially in oil and gas plants, induction motors are being gradually replaced by high efficiency permanent magnet motors, called line start permanent magnet synchronous motors (LSPMSMs). LSPMSMs have significant advantages over induction motors, which are: higher torque and power density as well as higher efficiency and operational power factor. As the number of LSPMSMs used in different fields is increasing, the maintenance scheme for these motors becomes important. In practical applications, LSPMSM can experience different types of failures such as broken bars, eccentricity, demagnetization as well as stator windings abnormalities. From the literature, it has been reported that stator winding faults in other machines represent around 36% of motors faults. Such failures threaten the normal manufacturing, interrupt the normal operation, and hence result in a significant loss of revenue. An efficient fault detection technique can reduce the maintenance expenses by preventing the high cost failures and unplanned downtimes.

Despite the importance of motors' fault detection, at the moment there is no scientific manuscript on modeling and diagnosis tool of LSPMSMs under stator winding abnormalities. Accordingly, in this dissertation, novel mathematical and finite element-based models for LSPMSMs under stator winding abnormalities (asymmetrical stator

windings and stator inter-turn fault) are developed and implemented. In addition, an experimental setup has been built for validating the developed models. The testing results of the mathematical models are in good agreement with the finite element models and experimental findings. The mathematical models are used to extract representative fault current features which are used in the development of a diagnosing tool for detecting the type and severity of stator winding abnormalities. Testing of the developed diagnosis tool shows a high accuracy of 96% in detecting the type and severity of stator winding abnormalities. Finally, the robustness of the proposed diagnostic tool against motor parameter variations has been investigated. It has been found that the abnormality detection accuracy decreases by no more than 3%. |

## ملخص الرسالة

الاسم الكامل: لقمان سليمان فايز مراعية

عنوان الرسالة: التمثيل الرياضي والكشف عن الاخطاء في ملفات العضو الثابت للمحركات التزامنية المغناطيسية حثية التشغيل

التخصص: الهندسة الكهربائية

تاريخ الدرجة العلمية: ابريل 2018

في التطبيقات الصناعية ، وخاصة في محطات النفط والغاز ، يتم استبدال المحركات الحثية بشكل تدريجي بمحركات تزامنية مغناطيسية ذات كفاءة عالية ، تسمى محركات تزامنية مغناطيسية حثية التشغيل (LSPMSM). تتمتع (LSPMSM) بميزات هامة على المحركات الحثية ، وهي: عزم دوران أعلى و طاقة أكبر وكفاءة أعلى ومعامل قدره اكبر. مع ازدياد عدد LSPMSMs المستخدمة في المجالات المختلفة ، أصبح مخطط صيانة هذه المحركات مهمًا. في التطبيقات العملية ، يمكن ل LSPMSM إختبار أنواع مختلفة من الاخطاء مثل القضبان المكسورة ، انحراف في محور دوران العضو المتحرك ، نقصان في المغناطيسية وكذلك أخطاء العضو الثابت.

تشير المراجع والابحاث أن أخطاء العضو الثابت في الآلات تمثل حوالي 36% من اخطاء المحركات. مثل هذه الاخطاء تهدد عمليات التصنيع ، وتوقف عمليات تشغيل الآلات، وبالتالي تؤدي إلى نقص كبير في الدخل. لكن وجود تقنية فعالة في الكشف عن هذه الاخطاء يمكن من تقليل عمليات الصيانة عن طريق منع حدوث الاخطاء ذات التكلفة العالية وغير المخطط لها.

على الرغم من أهمية الكشف عن الاخطاء في المحركات ، في الوقت الراهن لا يوجد اي ابحاث علمية لكشف او بناء نماذج رياضية علمية لأخطاء الاعضاء الثابتة في محركات ال LSMPSMs. وبناء على ذلك، وفي هذه الاطروحة ،تم تطوير وبناء نماذج علمية معتمدة على حقائق رياضية وعناصر محدودة للكشف عن اخطاء العضو الثابت في محركات LSMPSMs. بالإضافة إلى ذلك ، تم اثبات النماذج

المطورة عمليا في مخبر الالات. نتائج اختبار النماذج الرياضية متوافقة بشكل جيد مع نماذج العناصر المحدودة والنتائج التجريبية. يتم استخدام النماذج الرياضية لاستخلاص الخصائص المرتبطة بالخلل التمثيلي والتي تستخدم في تطوير أداة تشخيص للكشف عن نوع وشدة حالات الخطأ بالعضو الثابت. يظهر اختبار أداة التشخيص المتقدمة دقة عالية تبلغ 96% في اكتشاف نوع وشدة حالات الخلل في العضو الثابت. وأخيرا ، تم التحقيق في قوة الأداة التشخيصية المقترحة ضد التغيرات في معاملات المحرك. لقد وجد أن دقة كشف الخلل تقل بنسبة لا تزيد عن 3%.



# CHAPTER 1

## INTRODUCTION

### 1.1 Overview

High efficiency motors are being gradually exerted in many industrial applications of developed countries because of their positive impact on the environment by reducing energy consumption and CO<sub>2</sub> emission. The efficiency improvement of induction motors, which are the majority of the motors used in industry, is achieved through an optimal design of the motors. However, it is difficult to improve the induction motors efficiency significantly due to its inherent limitations. An alternative solution, which is of great interest, is to replace the induction motors with high efficiency permanent magnet (PM) motors. An important obstacle for ordinary PM motors is that these types of motor need inverter for starting. Needing an inverter is not economical for many single speed applications. To overcome this problem, the cage equipped PM motors; called Line Start Permanent Magnet Synchronous motors (LSPMSMs) have been introduced. An LSPMSM consists of a single or poly-phase stator as one of the induction motors and a hybrid rotor involving electricity conducting squirrel cage and pairs of permanent magnet poles. Line start permanent magnet synchronous motors (LSPMSMs) allow reaching super premium efficiency levels[1, 2].

In practical applications, electrical motors can experience different types of faults. In general, electrical motor failures can be categorized into electrical and mechanical faults. Motor faults/asymmetries can be also categorized into rotor and stator faults. The rotor faults are broken rotor bars, rotor eccentricity, breakage of end-rings, rotor bow and demagnetizing of permanent magnet. The stator faults include stator windings defects, stator core defects and stator frame defects. Mechanical faults include bearing damage and shaft defects. As the number of LSPMSMs used in different fields is increasing, presence of maintenance scheme based on fault detection for this type of motor becomes important and vital [3-8]. Early detection of irregularity in the motor with a proper fault diagnosis scheme will help to prevent high cost failures and hence reduces maintenance costs and more importantly prevents unscheduled downtimes that results in loss production and financial income.

The use of LSPMSMs in industry is in its infancy and no efficient scheme exists for stator windings faults detection in LSPMSMs yet. In this dissertation, two novel mathematical models for LSPMSM under stator faults (Asymmetrical stator winding and stator inter-turn fault) have been developed. In the next step, an experimental set-up has been designed and constructed in addition to a finite element analysis models which will be used to validate the developed mathematical models. The verified developed models have been used to extract and classify the stator abnormalities-related features. Finally, an intelligent neural network-based stator abnormality detection tool for LSPMSMs has been developed.

## **1.2 Thesis Motivation**

Destruction in insulation material is one of the major causes for stator winding faults in LSPMSMs. The percentage of motors failures due to problems with the winding insulation is about 36%. It is very important to detect them in time, because they can lead to the total destruction of the motor. As such, it is important to develop a diagnosis tool that will predict the type and severity of such faults. The motivation of developing such a tool can be summarized in the following points:

- Preventing catastrophic damage and reduces forced outage time by giving accurate information about the stator winding inter-turn fault.
- Enabling efficient maintenance planning and reduce maintenance costs.
- Improving the overall reliability of the electrical system.

## **1.3 Dissertation Objectives**

This dissertation aims at developing mathematical models for LSPMSMs under stator windings abnormalities (stator inter-turns fault and asymmetrical stator windings). An experimental setup will be designed and assembled to generate different faulty activities that will help in extracting current and speed signatures. Finally, an intelligent fault detection algorithm for stator inter-turn fault will be developed. The dissertation objectives can be summarized as follows:

1. Develop a mathematical model for LSPMSM under asymmetrical stator winding.
2. Develop a mathematical model for LSPMSM under stator inter-turn fault.
3. Implement the healthy and faulty LSPMSM using JMAG software.
4. Design and assemble an experimental test rig of LSPMSM.

5. Identify the electric parameters for the tested LSPMSM.
6. Collect different motor signatures from the test rig for healthy and faulty motor. Under different loading conditions.
7. Build a data bank from the extracted fault-related features using suitable condition monitoring and signal processing techniques.
8. Develop a neural network detection algorithm for detecting stator winding abnormalities in LSPMSM.

## **1.4 Dissertation Methodology**

The aim of this dissertation is to develop and implement two mathematical models for LSPMSM under stator abnormalities. The developed mathematical models will be used to develop a diagnosing tool for detecting the type and severity of stator winding abnormalities. To do so, a comprehensive theoretical investigation, experimental as well as finite element simulation validations have been conducted. The phases required for the execution of the dissertation objectives are:

### **1. Comprehensive Literature Review**

- Literature survey on construction aspects of LSPMSM, their operation principle, magnetic, steady-state and dynamic equivalent circuit.
- Literature survey on LSPMSM failures, symptoms and possible causes.
- Literature survey on condition monitoring and feature detection approaches.

- Literature survey on heuristic methods, feature selection and classification algorithm.

## 2. Modeling and Simulation

- Developing the mathematical model of LSPMSM under asymmetrical stator winding and stator inter-turn fault, and implementing the developed model using MATLAB/SIMULIK.
- Use the finite element-based software (JMAG<sup>TM</sup>) for implementing the LSPMSMs under asymmetrical stator winding and stator inter-turn fault.
- Simulating the implemented models for healthy and faulty condition as well as comparing the results of the two models.

## 3. Building the experimental set-up

- Literature survey to find technical specifications of the components and equipment's required for experimental set-up including data acquisition system.
- Implementation of the experimental set-up.
- Extracting required motor's parameters by conducting different experimental tests.
- Run the motor under healthy case as well as the stator inter-turn fault.

## 4. Data collection

- Collect experimental and simulation data from healthy LSPMSM under different loading conditions.
- Collect experimental and simulation data from LSPMSM under different stator inter-turn faults conditions and different loading levels.
- Collect simulation data from LSPMSM under different asymmetrical stator winding conditions and different loading levels.

#### 5. Building a data bank of faults representative features.

- Analyzing the mathematical models collected motor data for the healthy and faulty conditions to extract representative features.

#### 6. Fault detection algorithm design

- Designing a neural network algorithm for stator winding abnormalities detection in LSPMSM.
- Validating the proposed algorithm under unseen faults cases.

### **1.5 Findings and Contributions**

The main contribution of this dissertation is the development of two novel mathematical models for LSPMSM under stator winding abnormalities. Moreover, proposing a new efficient neural network tool for online detection of stator winding abnormalities location and severity.



The specific dissertation contributions are:

- A novel mathematical model for LSPMSM under asymmetrical stator winding has been developed.
- A novel mathematical model for LSPMSM under stator inter-turn fault has been developed.
- A two accurate finite element models for LSPMSM under asymmetrical stator winding and stator inter-turn fault have been developed using JMAG<sup>TM</sup> software.
- A comprehensive parameters identification for LSPMSM has been done.
- A laboratory experimental set-up has been implemented.
- A neural network based diagnostic tool for detecting stator abnormalities has been developed.

## **1.6 Dissertation Organization**

Besides the introduction, the dissertation contains seven chapters as follows: the second chapter presents a comprehensive literature review about construction aspects of LSPMSM, their operation principle, magnetic, steady-state and dynamic equivalent circuit. LSPMSM failures, symptoms and possible causes. Heuristic methods, feature selection and classification algorithms. The development of the mathematical and finite element models for both asymmetrical stator winding and stator inter-turn fault is presented in chapter three. A comprehensive parameter measurement for the used LSPMSM is presented in chapter 4. Chapter five presents the testing, validation for the

developed models. Chapter 6 presents the proposed neural network diagnostic tool for detecting the severity of stator winding abnormalities as well as testing results. Finally, conclusions and suggestion for future work are pointed out in chapter seven. |

## CHAPTER 2

### LITERATURE REVIEW

#### 2.1 Overview

Three phase induction motors and permanent magnet synchronous motors are widely used in the industry. Induction motors alone consume around 45% of the generated power capacity in an industrialized country [9]. However, they suffer from low power factor, relatively low operational efficiency and are larger in size compared with PMSM [10]. On the other hand, PMSM has higher operational efficiency compared with induction motor, particularly at small rated power range, since there is no current induced in the rotor (no field power losses). In addition, because the power losses of the PMSM are almost concentrated in the stator, as a result, the generated heat in the motor is easy to be dissipated. Additionally, PMSMs have a robust rotor construction, higher power density and lower rotor inertia. Unfortunately, they lack the starting capability of the induction motors. To overcome the challenges associated with these motors, researchers have been investigating and developing the LSPMSM since 1980s [11]. LSPMSM is a hybrid motor of induction and PMSM types, which has stator similar to that of an induction motor and rotor with both squirrel cage and permanent magnets. LSPMSM operates in two modes; asynchronous mode (at starting) during which the machine runs as an induction motor, and synchronous mode (at steady state) in which the motor runs at a synchronous speed

[12]. Therefore, LSPMSM has the starting capability of the induction motor, with high operational efficiency and power factor as the PMSMs.

In this chapter, a literature review of the construction aspects of LSPMSMs, their operating principle, dynamic equivalent circuit, steady state equivalent circuit, different rotor structures, general motor failures, motor failures in LSPMSM, causes of motor failures, overview about modelling of faults in motor, ways of fault modelling in motors, motors faults indicators together with the symptoms, fault analysis and feature extraction techniques, fault diagnosis as well as prognosis techniques are presented.

## **2.2 Line Start Permanent Magnet Synchronous Motors (LSPMSMs)**

The LSPMSM can be considered as a combination of a permanent magnet synchronous motor and an induction motor. It consists of three-phase winding on the stator as well as a hybrid rotor. The rotor is composed of two main parts; the squirrel cage and a permanent magnet as shown in Figure 2.1. In steady state operation, the LSPMSM differs somehow from the operation of other permanent magnet synchronous motors, whereby the rotor squirrel cage acts as a damper. At start-up, the LSPMSM is accelerated due to the asynchronous torque (cage torque) like an induction motor. However, it suffers from the braking torque due to the currents induced by the magnets (magnet opponent torque). On the other hand, at steady state, the motor runs due to synchronous torque and reluctance torque. Furthermore, the magnetic saliency, which can be quite significant, negatively affects the induction motor properties of the LSPMSM. Both effects reduce the motor starting capabilities [11, 13-15]. Figure 2.1 shows an interior-mount LSPMSM.

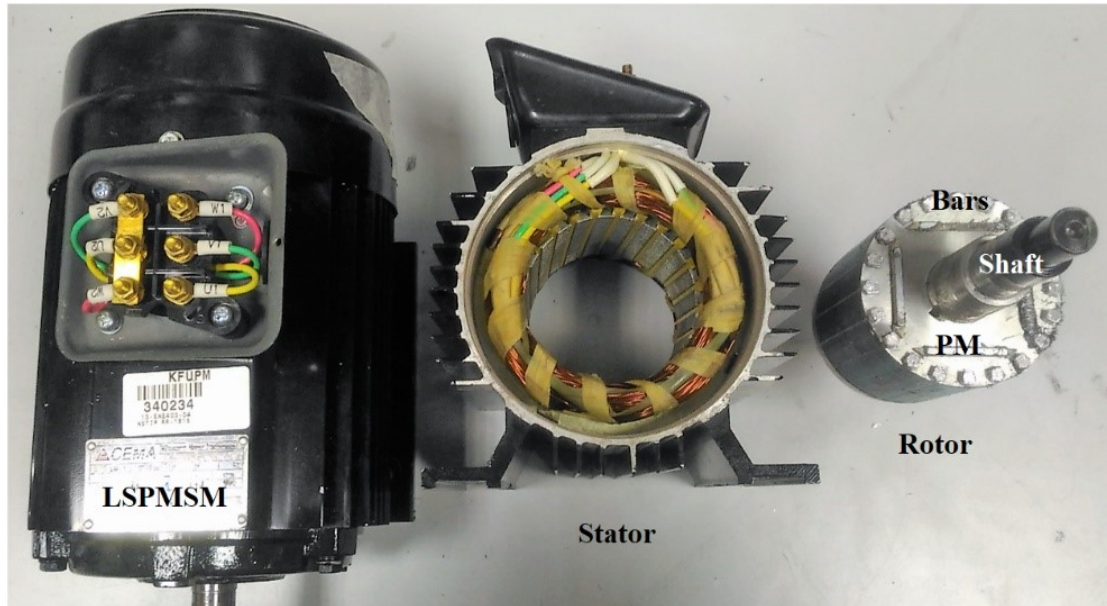


Figure 2.1 1 hp interior-mount LSPMSM

In [10], the LSPMSM has been fabricated from a small industrial induction motor with minimum time and cost. In addition, 2D finite element models have been developed to investigate the steady state and transient performance of the developed prototype motor. An experimental validation has been made for the developed model with results indicating good agreement between simulation and experimental tests. Isfahani et al.[16], developed a two axis (q-d) mathematical model for a healthy three-phase LSPMSM and implemented it using MATLAB/SIMULINK. Researchers can easily use the developed model to investigate the two modes of operation for the LSPMSM, i.e. the start-up mode and synchronous mode. The developed model was validated by the results of an experimental study. In [17] a detailed magnetic electric circuit for LSPMSM has been developed. with a design procedure for LSPMSM proposed and validated by designing a motor with high operation performance. Xiaozhuo et al. [18] studied the effect of changing the supply voltage on the performance of the LSPMSM, such as the starting current, electromagnetic torque and speed. The study was conducted using MATLAB/SIMULINK and verified

experimentally. Results demonstrated that by increasing the supply voltage, the motor draws less armature current at starting, but produces more torque. In [19], it is stated that the time to reach synchronous speed decreases as the supply voltage and the rotor resistance increase. In [20], an investigation of the LSPMSM synchronization capability with low motor saliency and high cage resistance has been conducted. It is noted that having a high rotor resistance improves the starting capability of the motor, but the synchronization capability weakens because it occurs at high slip. It was also found that using a permanent magnet with a low volume improves the motor synchronization capability. The synchronization capability of interior mount LSPMSM has been examined whereby a model for the machine and a maximum load criteria have been developed based on a Lyapunov function to investigate the effect of the electrical parameters on the synchronization capability [21]. Results show that simulation and experimental results are in good agreement.

In [22], the effect of having asymmetrical squirrel cage in LSPMSM on the developed torque has been investigated. A 2D finite element model for the motor has been used where the results reveal that both the synchronization and asynchronization torque increase by having an asymmetrical squirrel cage. In [23] the magnetization characteristics of the LSPMSM have been studied and determined experimentally as well as numerically. The investigations have been carried out based on the proposed qd-axis theory. The results were validated using the dynamic and steady state analysis of the machine with and without considering the magnetizing characteristics to assess their effects on machine performance. Both experimental and numerical results are in good agreement.

LSPMSMs suffer from cogging torque (no-current torque). Cogging torque is an undesirable torque component arising from the interaction between the stator winding slots and the permanent magnets in the rotor. These interactions cause variation in the magnetic field energy during rotation thereby introducing the cogging torque. Cogging torque introduces ripples in the speed and torque, vibration, noise and weakens the torque of the motor [24-27].

Cogging torque is also caused by the air-gap permeance variation due to slotting effects: the rotor magnet is attracted to certain positions (magnetostatics effect) where the effective permeance is maximum [25]. In [25], two methods have been adopted to reduce cogging torque in a permanent magnetic synchronous motor. The first aim is to reduce the symmetry in machine flux by introducing asymmetry in the distribution of permanent magnets whereas the second target is to use the auxiliary slots to increase the cogging torque frequencies. Finite element analysis was done to investigate the proposed method in which the results show that the cogging torque was reduced by 85%. In [28], a method for reducing cogging torque in the inset LSPMSM is proposed. The proposed method is based on the permanent magnets shifting. In this study, an analytical model for the motor is developed, and verified by finite element analysis. Also, the results are validated experimentally and correspondingly show that the shifting of the permanent magnetics reduces effectively the cogging torque and torque ripple in the machine as well as keeping the fundamental component of the back EMF unchanged, while at the same time reducing the triple harmonic components in the back EMF. The ripple torque is another torque component that introduces ripples in the machine torque. It is produced due to non-

sinusoidal distribution of magnetic flux in the air-gap. Therefore, having sinusoidal distribution of magnetic flux in the air gap will reduce the ripple torque [29].

### 2.2.1 Dynamic Model for Healthy LSPMSM

The healthy model of the LSPMSM is well-known [16, 30-35]. The equations (2.1) to (2.10) represent the transient model for the LSPMSM. Equations (2.1) to (2.4) represent the stator and rotor voltage equations while (2.5) to (2.8) represent the flux-current relationship. Equations (2.9) to (2.10) represent the electromechanical system equations.

$$V_q^s = r_s i_q^s + \omega_r \lambda_d^s + \frac{d\lambda_q^s}{dt} \quad (2.1)$$

$$V_d^s = r_s i_d^s - \omega_r \lambda_q^s + \frac{d\lambda_d^s}{dt} \quad (2.2)$$

$$V_q^{r'} = 0 = r_{rq}' i_q^{r'} + \frac{d\lambda_q^{r'}}{dt} \quad (2.3)$$

$$V_d^{r'} = 0 = r_{rd}' i_d^{r'} + \frac{d\lambda_d^{r'}}{dt} \quad (2.4)$$

$$\lambda_q^s = (L_{ls} + L_{mq}) i_q^s + L_{mq} i_q^{r'} \quad (2.5)$$

$$\lambda_q^s = (L_{ls} + L_{md}) i_d^s + L_{md} i_d^{r'} + \lambda_m' \quad (2.6)$$

$$\lambda_d^{r'} = (L_{lrq}' + L_{mq}) i_q^{r'} + L_{mq} i_q^s \quad (2.7)$$

$$\lambda_d^{r'} = (L_{lrd}' + L_{md}) i_d^{r'} + L_{md} i_d^s + \lambda_m' \quad (2.8)$$



Where  $v_q^s$  and  $v_d^s$  are stator qd voltages;  $v_q^{r'}$  and  $v_d^{r'}$  are rotor qd voltages referred to the stator side;  $i_q^s$  and  $i_d^s$  are stator qd currents;  $i_q^{r'}$  and  $i_d^{r'}$  are rotor qd currents referred to the stator side;  $\omega_r$  is the rotor speed;  $\lambda_q^s$  and  $\lambda_d^s$  are the stator qd linkage fluxes;  $\lambda_q^{r'}$  and  $\lambda_d^{r'}$  are the rotor qd linkage fluxes referred to the stator side;  $\lambda_m'$  is the flux of the permanent magnet referred to the stator side whereas  $L_{lrq}'$  and  $L_{lrd}'$  are the rotor leakage inductances in q and d-axis referred to stator side respectively;  $L_{ls}$  is the leakage stator inductance;  $L_{md}$  and  $L_{mq}$  are the mutual inductances in the d and q axis respectively.

The electromagnetic torque of LSPMSM is expressed as;

$$T_{em} = \frac{3P}{4} (i_q^s \lambda_d^s - i_d^s \lambda_q^s) \quad (2.9)$$

The mechanical equation is also expressed as;

$$\omega_r(t) = \frac{P}{2J} \int (T_{em} + T_L - T_{damp}) dt \quad (2.10)$$

Where  $T_{em}$  is the electromagnetic torque;  $T_L$  is the load torque;  $T_{damp}$  is the damping torque;

$J$  is the motor inertial;  $\omega_r$  is the rotor speed; and  $P$  is the pole's number. Figure 2.2

shows the equivalent circuit of the LSPMSM in d and q-axis.

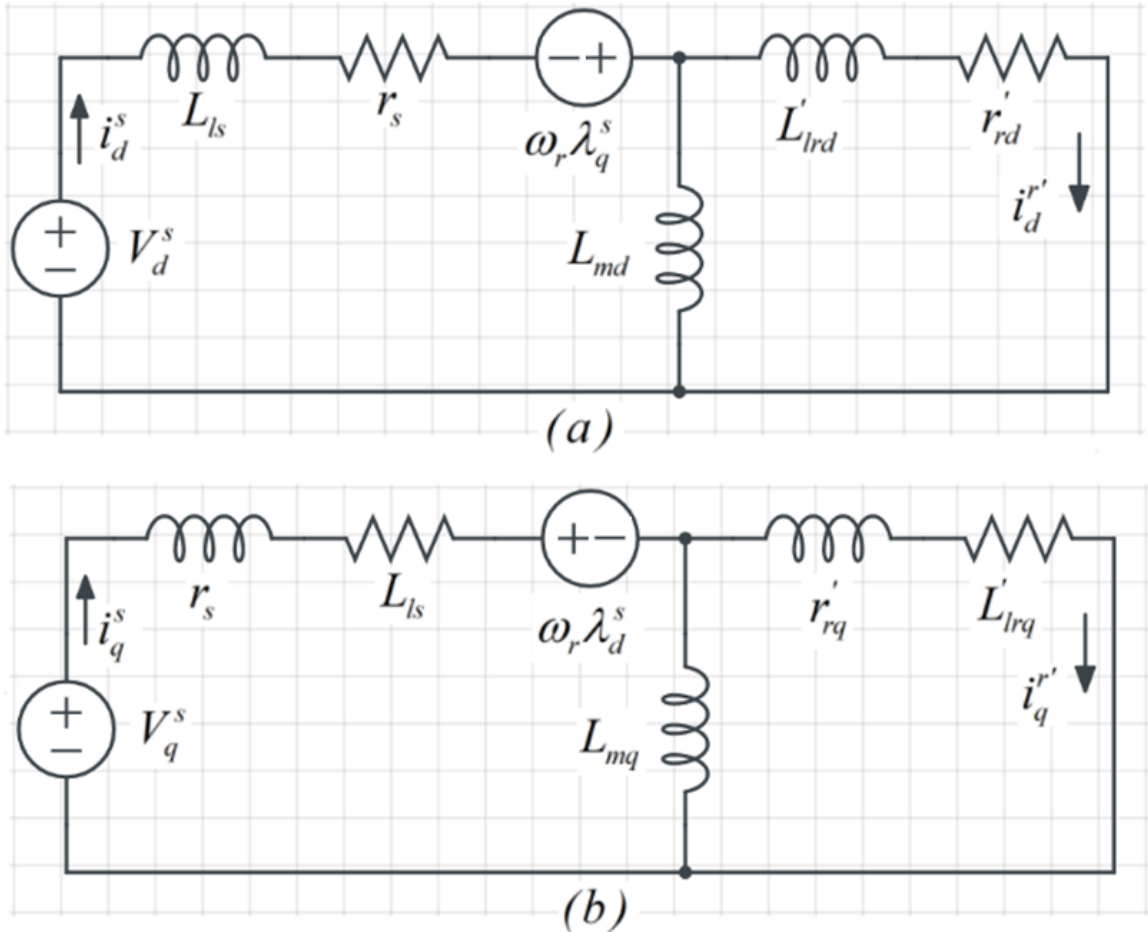
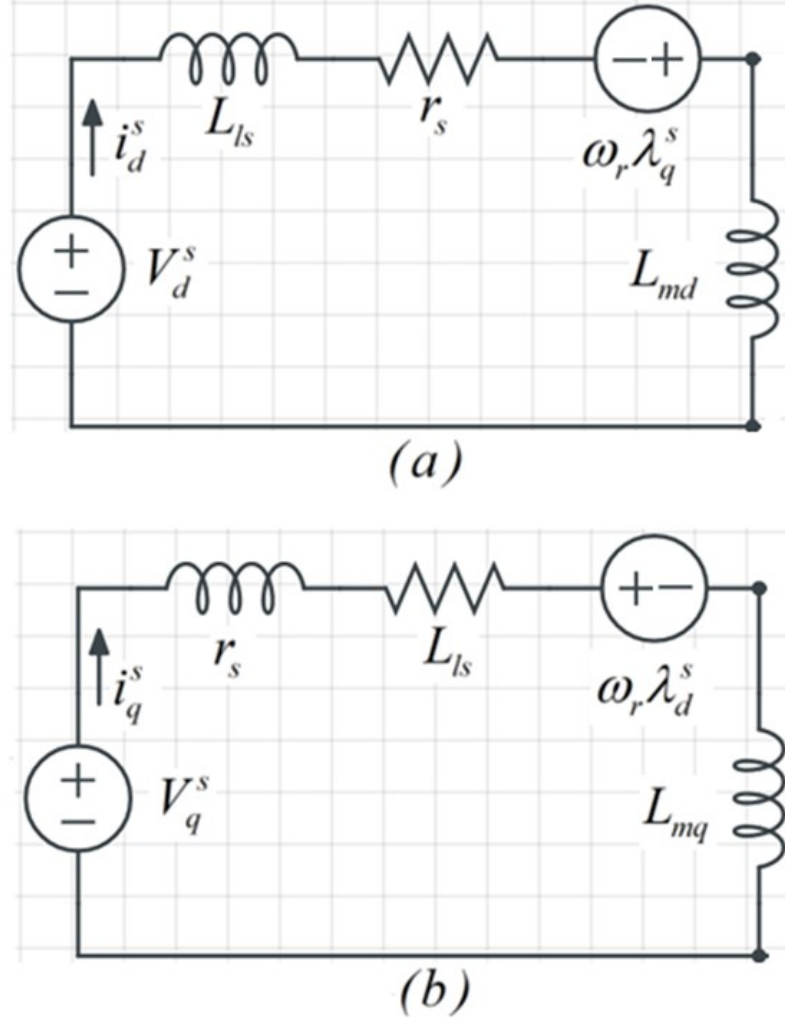


Figure 2.2 LSPMSM Equivalent circuit: (a) d-axis equivalent circuit; (b) q-axis equivalent circuit

### 2.2.2 Steady State Model for Healthy LSPMSM

In a true steady state operation of LSPMSM, there are no currents induced in the rotor cage, and thus the rotor branches need not to be included, as shown in Figure 2.3. Figure 2.3 shows a simplified equivalent circuit for a LSPMSM under steady state.



**Figure 2.3** Steady state d-q circuit diagram of LSPMSM (a) d-axis equivalent circuit (b) q-axis equivalent circuit

From Figure 2.3 the steady state model for a LSPMSM is summarized in equations (2.11) to (2.14).

$$V_q^s = r_s i_q^s + \omega_r \lambda_d^s + \frac{d\lambda_q^s}{dt} \quad (2.11)$$

$$V_d^s = r_s i_d^s - \omega_r \lambda_q^s + \frac{d\lambda_d^s}{dt} \quad (2.12)$$

$$\lambda_q^s = (L_{ls} + L_{mq}) i_q^s = L_q i_q^s \quad (2.13)$$

$$\lambda_q^s = (L_{ls} + L_{md})i_d^s + \lambda_m' = L_d i_d^s + \lambda_m' \quad (2.14)$$

### 2.2.3 Basic LSPMSMs Construction Configurations

Based on the literature, the stator and the windings of the LSPMSMs are the same as that of the induction motors of the same rating, while the rotors of both motor types differ in terms of their construction and configuration. In this section, both the stator and the rotor possible configurations for electric motors (especially LSPMSMs) are discussed. The stator winding in three-phase motors could be concentrated or distributed winding. In the concentrated winding, the turns of a coil are wound together and connected in series, i.e. all the coil-turns of a phase have the same coil axis without overlapping with the coil-turns of the other two phases. Conversely, in the distributed winding, the winding-turns are arranged in several fractional/ full pitch coils (overlapping). Thus, the coil-axis in a set of slots is different compared to the coil-axis in the adjacent set of slots [36]. Both the concentrated and distributed winding have certain characteristics. Since there is overlapping in distributed winding, the mutual inductance between the phases is higher than in concentrated windings. Furthermore, the magnetic flux in the airgap is more sinusoidal in distributed winding (harmonic component magnitude is smaller) than in concentrated winding, thus the torque ripples are smaller. In addition, heat dissipation in distributed winding is better than in concentrated since the number of conductors per slot in a concentrated winding is higher than in distributed winding. Besides, the copper losses in distributed winding motor is higher than in concentrated winding since the end coils in distributed winding are longer [37-39].

Based on the literature, there are different rotor construction of the LSPMSM which is grouped into two types, based on the location of the permanent magnets in the rotor; the

interior-mount LSPMSM and the surface-mount LSPMSM. In interior-mount LSPMSM, the permanent magnets are placed inside the rotor iron core as shown in Figure 2.4(a), while in surface-mount LSPMSM they are mounted on the surface of the rotor iron core as shown in Figure 2.4(b). In addition, the direct and quadrature inductance in surface mount LSPMSM are equal (no saliency) since the airgap reluctance in both d and q-axes are equal. on the other hand, the direct inductance is smaller than the quadrature inductance in interior-mount LSPMSM since the airgap reluctance in the d-axis is higher than in the q-axis, hence a saliency is introduced in the interior-mount LSPMSM [40, 41].

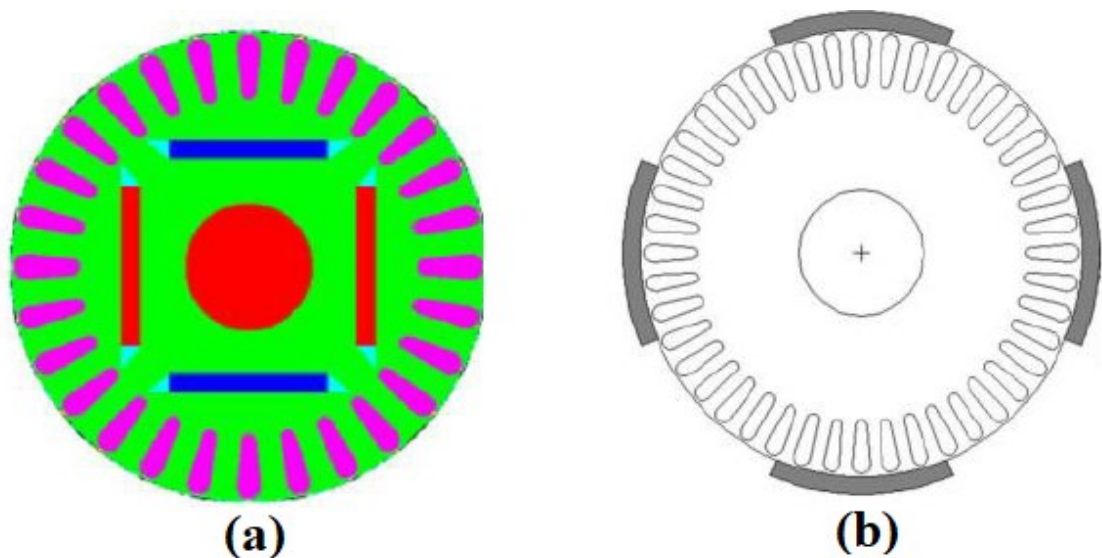


Figure 2.4 LSPMSM cross section (a) interior- mount LSPMSM (b) surface-mount LSPMSM [29]

Cosmas et al. [41] studied the transient and the steady state performance of LSPMSMs with the surface and interior rotor magnets. In the transient state, the loading capability, including the step and ramp loading as well as the synchronization capability were examined. In the steady state, the torque performance was analyzed for both motor constructions. It was found that an interior LSPMSM (ILSPMSM) attains synchronism faster than a surface-mount LSPMSM (SLSPMSM) type. Moreover, the ability of the

ILSPMSM to withstand the gradual change in the load was improved. Also, in the steady state, the electromechanical torque of the ILSPMSM was found to be better than with a SLSPMSM because it is enhanced by the reluctance torque. In [42], the performance of the ILSPMSM and SLSPMSM has been investigated and compared. For purposes of having a fair characteristics comparison between the two motors, the study has been done using the finite element analysis for two typical motors with magnets of the same dimensions and properties. Results indicated that the cogging torque developed in ILSPMSM is smaller than in SLSPMSM. Moreover, the efficiency of ILSPMSM is higher than that of SLSPMSM for the same loading conditions. Nevertheless, the loading capability of ILSPMSM in the transient state is better than for SLSPMSM. However, the SLSPMSM has a better synchronous loading capability at steady state under the same loading condition than that of ILSPMSM. Figure 2.5 shows the comparison between ILSPMSM and SLSPMSM.

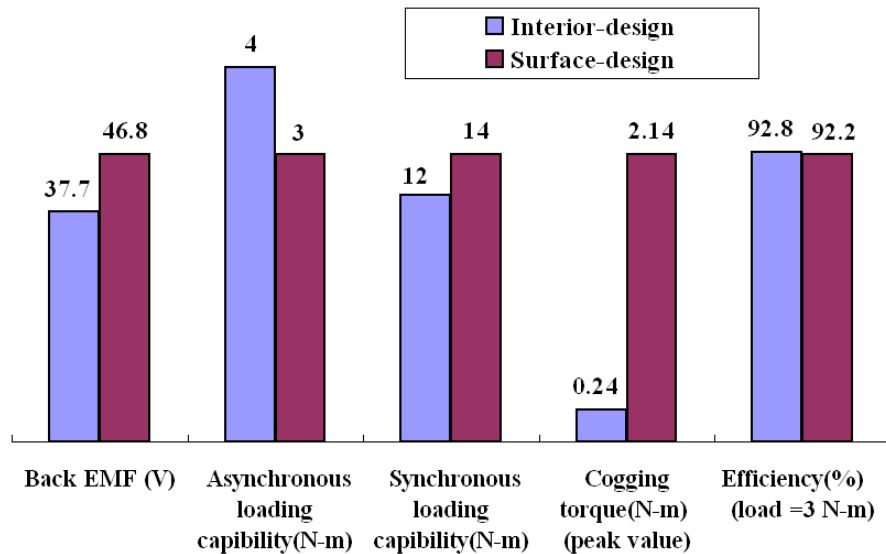


Figure 2.5 Performance comparison between two LSPMSM designs [42]

In the literature, the permanent magnets in ILSPMSM have different topologies, as shown in Figure 2.6. As observed, there are six different topology of magnet shapes. The LSPMSM with a specific rotor topology has certain characteristics such as efficiency, Power factor, starting torque and maximum torque. Figure 2.7 shows a comparison between the characteristics of LSPMSM with different rotor topologies [29].

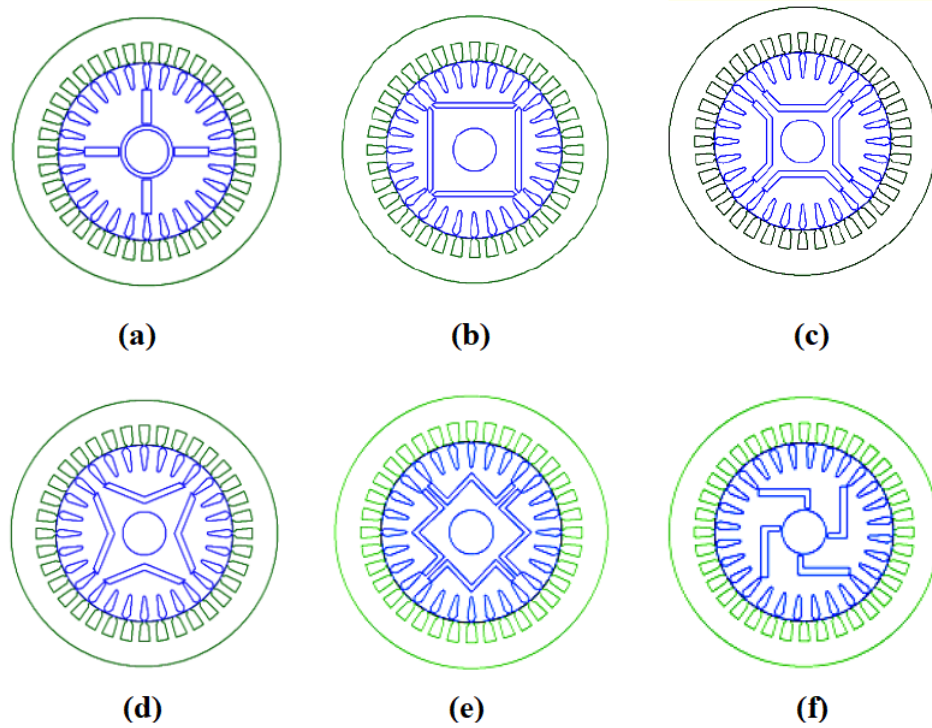


Figure 2.6 LSPMSM rotor magnets configurations (a) Spoke (b) Series (radial flux rotor) (c) U-type (d) V-type (e) W-type (f) Swastik [29]

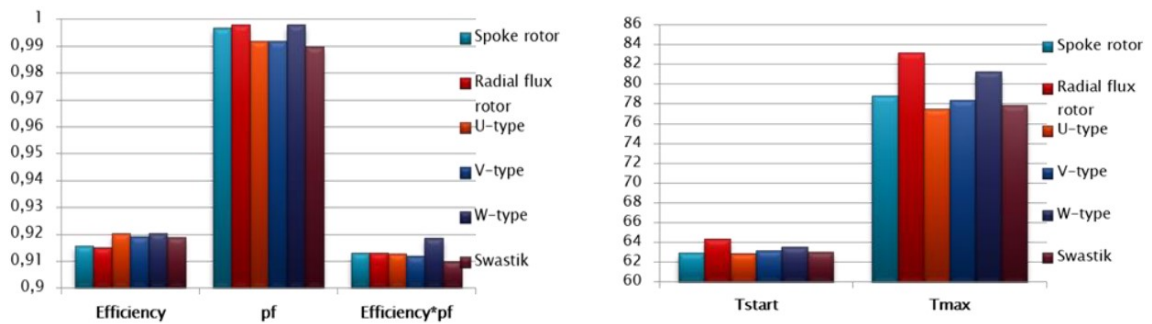


Figure 2.7 Comparison between LSPMSMs with different rotor configurations [29]

## 2.3 Electric Motors Faults

Due to the internal and external stresses acting on electric motors, they can experience several types of faults [43]. Internal stresses could be electrical, thermal, and mechanical while the external stresses are due to environmental conditions such as; high humidity, high temperature, corrosion, surrounding oil and dust. The faults in electric machines are classified into three main categories; electrical, mechanical and magnetic faults. These faults include; stator inter-turns fault, stator coil to coil fault, stator phase to phase fault, stator phase to ground fault, rotor inter-turns fault, broken bar, breakage of the end-rings, static and/or dynamic eccentricity, partial or uniform demagnetization of the permanent magnets, bearing fault, stator core defects, stator frame defects and the shaft defects [44-48]. Such failures affects the normal manufacturing processes and operation, consequently, resulting in a significant loss of revenue. In addition, some of these faults may decrease the performance, the reliability and the efficiency of the motors. Figure 2.8 summarizes the possible failures in electric motors.

In the industry, electric motors are installed in a large number. Therefore, the normal and reliable operation of electric motors is essential. However, the operation is always frustrated by the occurrences of various faults in the LSPMSM as mentioned above [49-53]. The following subsection will discuss the types of faults in electric machine in general.



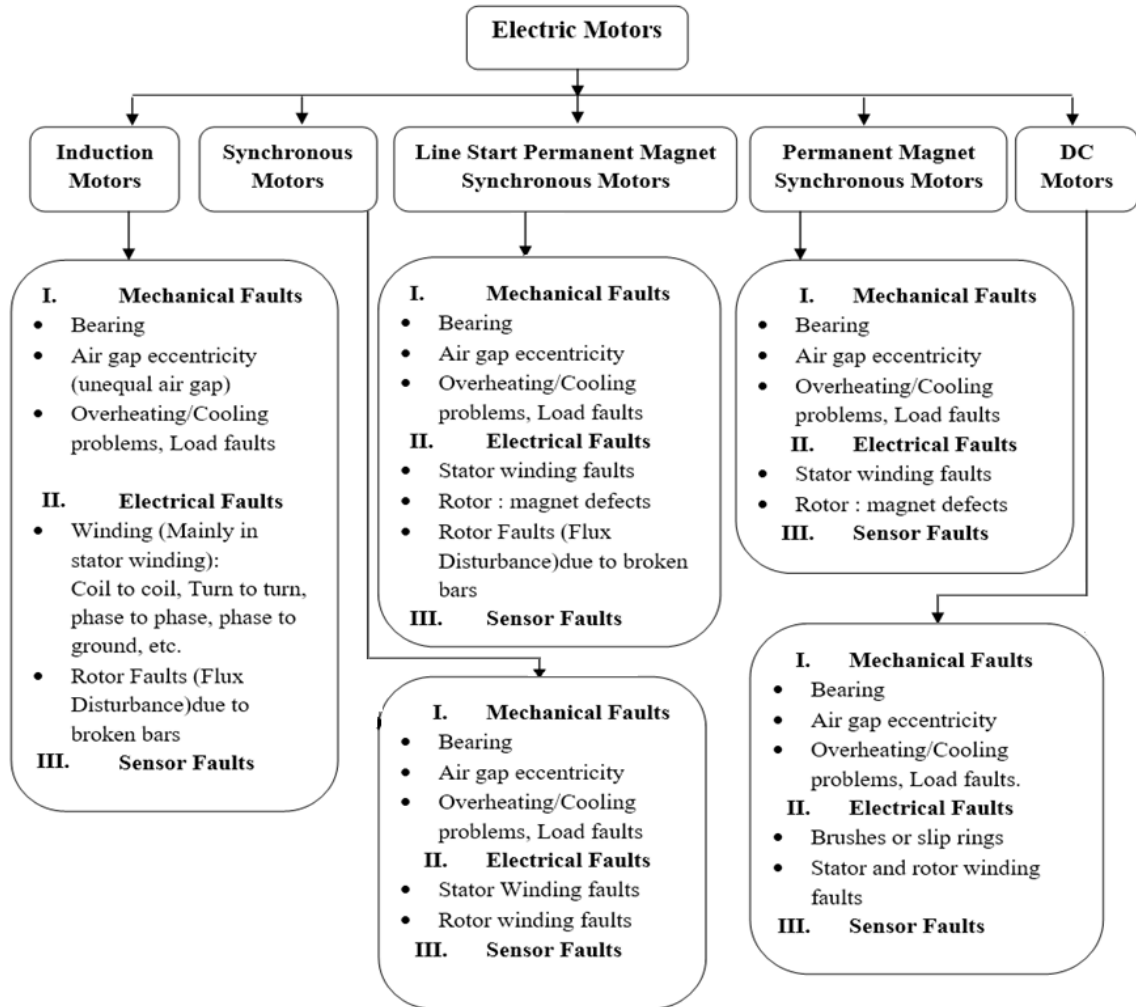
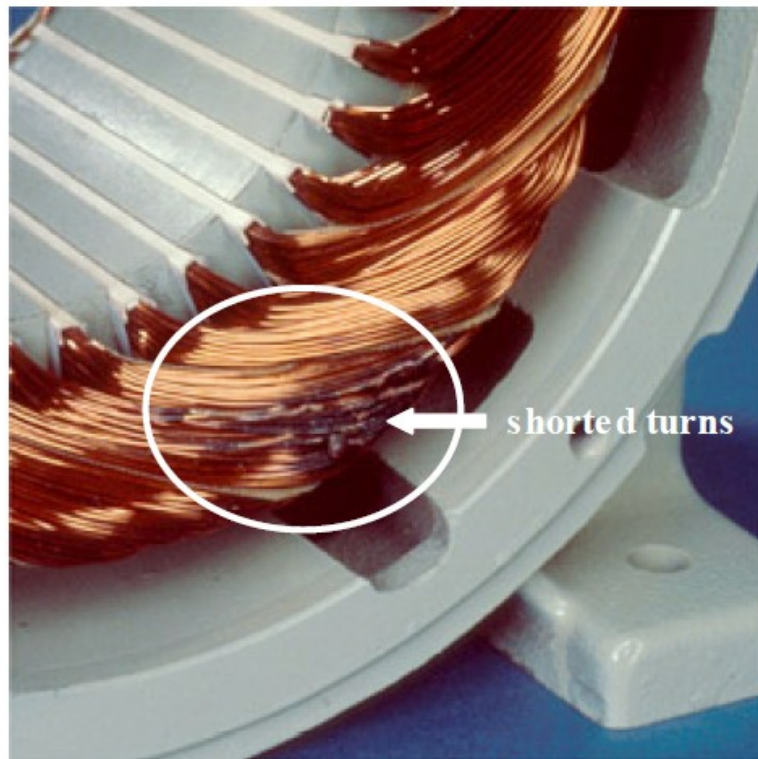


Figure 2.8. Fault types in electric motors

### 2.3.1 Stator Faults

The stator is the external group of coils which apply the electromagnetic force to the rotor and causes it to rotate. The main two parts of the stator are; the; core and windings. These parts are subjected to unavoidable stresses, whether mechanical or electrical. Bonnett and Soukup (1992) described these stresses well, and their contribution to premature failures [54, 55]. The stator windings consist of an insulated conductor, which is usually made of

copper, in larger motors and aluminium in smaller motors. Most stator abnormalities occur in the winding end parts. , It is reported that the stator winding faults in induction machines represent around 36% of the motor faults [56, 57]. The main causes of stator winding faults are; inefficient cooling system, voltage stresses, over loading, the short circuit in the winding, chemical contamination and partial discharge in the winding. In most cases the stator winding faults start as turn to turn faults, inter-turns faults, coil to coil faults, phase to ground faults and phase to phase faults but finally results into motor failures. Therefore, it is crucial to design an effective tool for detecting such faults in the initial stage since these types of faults become worse with time if not addressed [54, 58-61]. Figure 2.9 shows a stator inter-turn fault.



**Figure 2.9. Stator inter-turns fault [62]**

On the other hand, the core of the stator is made of insulated thin steel laminations which are used to reduce the eddy currents. The core is also subjected to melting due to the high ground fault current, chemical and mechanical damage during rewinding, as well as due to the damage during machine inspection. However, the stator core faults happen rarely especially in large electric machine. The stator core faults represent around 1% of the machine faults [63, 64].

### **2.3.2 Eccentricity**

The machines are assembled from two main parts; the stationary part (stator) and the rotating part (rotor). However, in normal machines both parts have the same centre axis, and the geometric centre of the stator is the same as the rotating centre of the rotor. Therefore, in the healthy case, the air gap is uniform (symmetric). Because of the inaccuracies in mechanical parts of the machine during manufacturing, incorrect bearing positioning or bearing wear and due to unavoidable stress in the machine, the rotor is sometimes displaced from its position, making the airgap to become asymmetric. This fault type is termed as eccentricity as depicted in Figure 2.10 [65-68]. Eccentricity is classified into three types; static, eccentricity and mixed eccentricity [69-72].

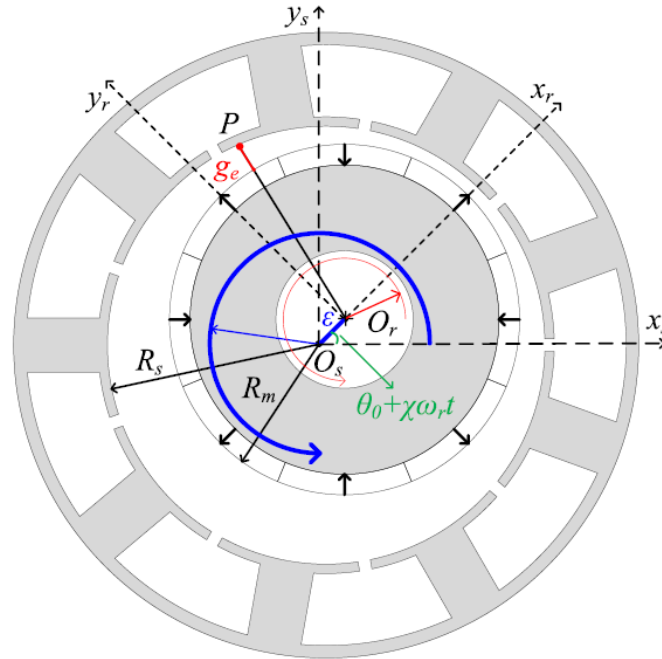


Figure 2.10. Rotor eccentricity [73]

In electric machine, an eccentricity faults are common, but the allowed percentage of eccentricity is between 5 to 10%. However, if the eccentricity percentage increases beyond these limits, there will be friction between the rotor and the stator (rotor will rub the stator), ultimately damaging the stator winding [55, 74]. According, several studies have been conducted on mathematical modeling of eccentricity faults in induction machines as well as on permanent magnet synchronous machines. [55, 75-79]. However, fewer studies are available on the LSPMSM. Mahdi et al. [52] investigated the effect of a static eccentricity fault on the performance of the LSPMSM in the synchronous period. The simulation of the faulty machine was done using finite element software

### 2.3.3 Rotor Faults

Both induction machines and LSPMSMs have a squirrel cage rotor. In general, the cage is composed of a number of bars joined together by two slip rings at both ends of the

bars. The bars of the cage and the end rings can be damaged and broken due to unavoidable stresses such as overheating and mechanical stresses etc, as well as due to inappropriate rotor design [80-83]. If a particular bar is broken, the nearby bars in the rotor will also be affected due to the generated stresses, progressively intensifying the fault. Therefore, if the broken bar fault is detected early enough, the machine can be repaired and protected before the fault is extended [84]. Sasi et al. investigated the effect of having broken bars in the machine. It was observed that having the broken bars decreases the output torque of the machine. In addition, the stator current becomes asymmetric and the output torque will have a pulsating component [85]. In the literature, the broken bar and cracked end ring faults in an induction machine is a well-defined problem, with an extensive literature survey, mathematical modelling, and fault diagnostics carried out [86-89]. However, for the LSPMSM, limited studies have been done on these types of faults [90, 91]. Figure 2.11(a), (b) and (c) show a healthy rotor, rotor with one broken bar and a rotor with three broken bars, respectively.

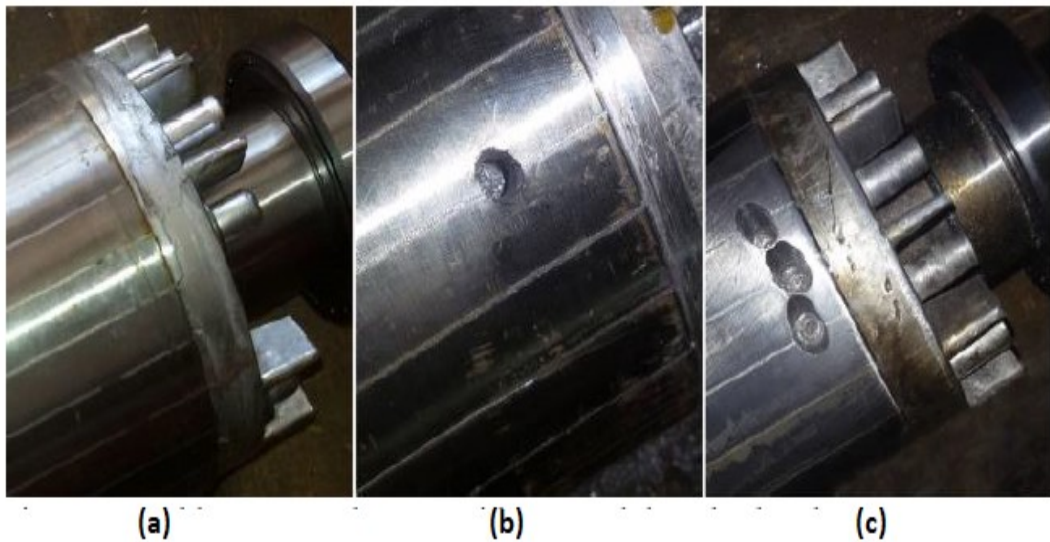


Figure 2.11. Rotor of induction motor (a) healthy (b) one broken bar (c) three broken bars [45]

### 2.3.4 Permanent Magnets Faults

Both permanent magnet synchronous motor (PMSM) and LSPMSM have permanent magnets on their rotors. In a steady state, the magnets generate the excitation torque in the machine. Under unavoidable stress such as an armature reaction, those magnets will be demagnetized. Demagnetization is defined as any reduction in the magnetic flux density of the magnet. Demagnetization occurs partially on the part of the magnets or uniformly on the full magnet area [46, 92-94]. The magnets could also be damaged due to imperfect production as shown in Figure 2.12 [65].

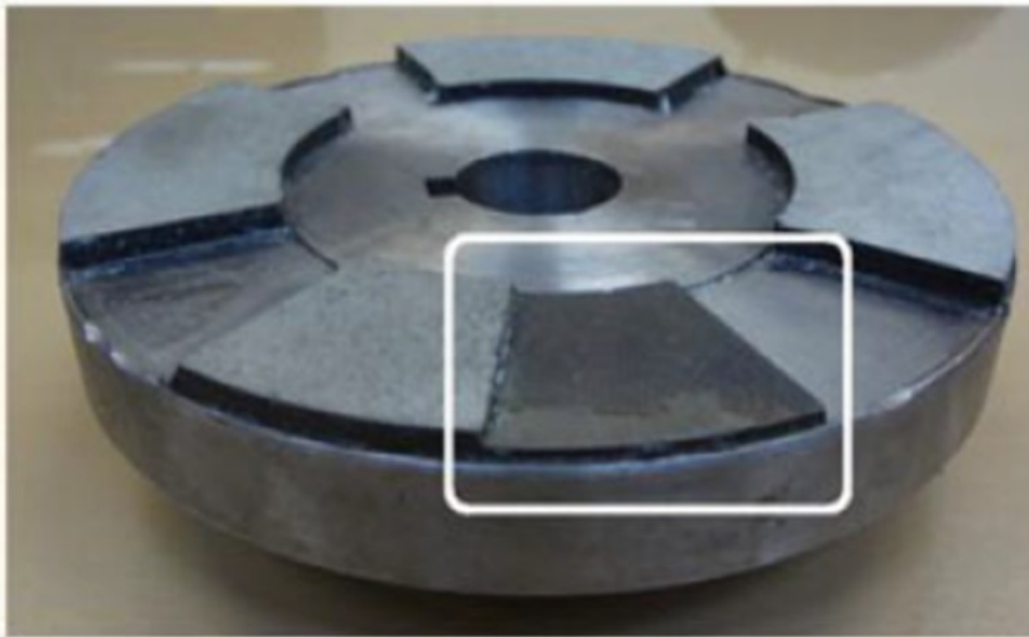


Figure 2.12. Permanent magnets damage [65]

Demagnetization of the permanent magnets occur when the machine is highly loaded, due to armature reaction, severe transient and high temperature variation [95-97]. However, permanent magnets are very sensitive to temperature variation. In [98], both the effect of temperature variation and armature reaction on the performance of LSPMSM have been investigated. The study was conducted using finite element analysis.

Under a demagnetization fault condition, the motor efficiency decreases due to the increase in the flux losses. Moreover, because of demagnetization, the generated electromotive force in the machine contains more harmonic components, which causes the motor to vibrate and heat up. In addition, the torque response of the machine also contains a pulsating torque [99].

As a conclusion, demagnetization of the rotor magnets has negative effects on the behavior of the LSPMSM and PMSM. Demagnetization of magnets result in the reduction of the residual magnetic flux density, which reduces the magnetic flux of the magnet and eventually reduces the motor torque [100]. The steady state stator current increases as the demagnetization increases to compensate for the reduction in the magnetic flux. It is also worthy to note that, deep demagnetization prevents the motor from reaching the synchronism.

## **2.4 Electric Motors Modeling Under Faults**

In industry, a large number of electric motors are installed. Therefore, the normal and reliable operation of electric motors is essential. Any failure may result in a loss of revenue, as well as the motor being regarded as out-of-service (a lengthy service outage). Thus, the early detection of abnormalities in a motor may help to avoid the expensive breakdowns. An accurate modeling of motors is considered as the initial stage in the detection and clearance of motor abnormalities [48]. The modeling of electric motors under a fault also helps in investigating the behavior and performance of motors. Based on the literature, two approaches are used for modeling the motors under faults; the

analytical approach (electrical or magnetic circuit) and the finite element analysis (FEA) approach. Although the FEA approach performs well in determining the behavior and characteristics of a machine in detail by considering the nonlinear magnetic materials of the machine, it is time-consuming and an intensive computation process. On the other hand, magnetic circuit models require less computation time compared with FEA models. However, in magnetic circuit models (reluctance model), each individual slot in the machine has its own written differential equation. Therefore, these models are considered to be high order and too complicated for electric machine control design and it is difficult to model the airgap. Finally, electric equivalent circuit models, which use the principles of magnetic coupled circuit theory, electromechanical energy conversion and reference frame theory, have been proven to be simple and effective for analyzing the performances of electric motors under faults and for design purposes [17, 101-103].

In the literature, the modelling of induction motor and PMSMs under different types of faults are extensively investigated, while few studies available on LSPMSMs because their use is still in infancy stage [56, 104-115]. Some research works have been carried out that propose the modelling of LSPMSM under fault. Abbas et al. [98] have modelled the LSPMSM using finite element analysis to investigate the performance and parameters sensitivity of the motor under temperature variation. In addition, the irreversible demagnetization due to armature reaction has been studied. In [46], the LSPMSM has been modelled using finite element analysis to examine the demagnetization of permanent magnets. Four different rotor configurations were suggested to save magnets from demagnetization where the effectiveness of the four configurations are compared. In [93], the effect of super synchronous faults on the magnets of LSPMSM has been



explored using finite element analysis. Mohammad et al. [53] proposed a new technique for detecting the broken bar faults in the LSPMSM, based on statistical analysis of the stator current envelopes in the transient state. The motor is implemented using ANSYS Maxwell® software, and analysed under four different load levels to investigate the effect of the load on the detection of the broken bars. The envelope of the stator current in the transient state is extracted using Hilbert Transform. A statistical analysis of the current envelope is done to the extract features such as the mean, energy, kurtosis, etc., which help in the detection of broken bars in a motor. In a nutshell, the effectiveness of this technique was proved because the bars of the motors carry significant current during the transient state. Mahdi et al. [52] investigated the effect of having static eccentricity fault on the performance of the LSPMSM during synchronous period. The simulation of the faulty machine was done using finite element software. The effect of the static eccentricity on the stator current harmonic components was studied. They found that the low frequency components of the stator current are good indicators for the motor under eccentricity fault, in that case, if the eccentricity is increased then the magnitude of these components increase. It is worthy to mention that in the literature no work has been done on the modeling of LSPMSM under stator inter-turn fault or asymmetric stator winding. Therefore, in the following subsection, a general introduction about the modeling of the stator faults in motors has been given.

#### **2.4.1 Modeling of Stator Inter-Turn Fault**

The stator inter-turn fault is the most common fault that occurs in electric motors. It is reported that 36% of induction motor faults are stator inter-turn faults [57, 116].

Therefore, there is need to develop the mathematical model of the motors with inter-turn faults. Different models for different types of electric motors under stator inter-turn faults have been proposed [60, 117-121]. In [57], with a mathematical model of an induction motor developed based on winding theory and simulated using MATLAB software. The simulation and experimental results show that the torque response under the stator inter-turn fault has oscillations with a double supply frequency. In [122], an improved dynamic model of the induction motor under the inter-turn fault was developed and experimentally validated. The developed model was found to be useful for inter-turn detection. In [122], a modified torque equation under fault is presented, while in [57] the torque equation is not changed. Another mathematical model of a permanent magnet synchronous motor under the stator inter-turn fault was developed [123]. The model considers the spatial harmonic in a machine, making it a novelty compared with other parametric models in the literature. Alternatively, a model of a PMSM under the inter-turn fault was developed to help in detecting the severity and the location of an inter-turn fault [58]. Likewise, a model of a PMSM with the inter-turn fault was developed and validated using FEA [124]. Despite the importance of fault detection in LSPMSMs, currently, there is a limited research on the modeling and diagnosis of LSPMSMs under the stator inter-turn fault, as the use of this type of motor in industry is still in its infancy. Accordingly, the aim of this work is to develop and implement a novel mathematical model for LSPMSM under asymmetrical stator winding and stator inter-turn fault.

## 2.5 Faults Indicators

Different kinds of signals are used as indicators for motor fault diagnosis. These indicators include; magnetic flux, vibration, stator current (negative and zero sequence or third harmonic component), zero sequence component of voltage, thermal image processing, instantaneous real power and reactive power, phase shift between stator and the supply voltage and acoustic noise [116, 125-134]. Besides, many researchers have used the instantaneous torque as a fault indicator in induction motors [129, 132, 135, 136]. It is worth mentioning that there are differences in the instantaneous torque response under the broken bar and inter-turn faults [136]. In addition, not only does the time response of torque at steady state differ under two types of fault, but also the prominent frequency components during faults are not the same [129, 132]. These differences help to distinguish between the two types of fault. The motor current is one of the promising indicators for fault detection, since it is already available from motor control services without extra design or additional hardware [116, 125-134]. The current signal inherently contains valuable information about the machine performance and operating conditions [137]. Table 2.1 summarizes some of the researches where the stator current was used as an indicator for stator inter-turn fault and their effectiveness in detecting the fault size.

**Table 2.1 Stator Current as a fault indicator [118]**

Reference	Motor Type	Current analysis	Minimum fault severity %
[138]	Induction	Positive and negative sequence components of stator current	0.43%
[139]	PMSM	Current harmonic components	4.17%
[140]	Induction	Current envelope	0.42%
[141]	Induction	Stator current-Multiple reference frames theory	2.04%
[142]	Induction	Stator current-Wavelet transform Analysis	1.5%
[143]	PMSM	Stator current-Wavelet transform Analysis	2.78%
[144]	PMSM	Empirical mode decomposition (EMD) and Quadratic time–frequency (TF) analysis of stator current	2.78%

## **2.6 Analytical Tools for Electric Motor Faults Diagnosis and Prognosis**

Preventive maintenance is always desired compared to obligatory or corrective maintenance. A lot of research efforts are being done worldwide to develop incipient fault diagnostic techniques (before the actual occurrence of faults). The neural network is a tool that plays an important role in developing online and offline diagnostic tool for motors, generators, transmission lines, cable and transformer [145-148]. A mathematical model of an induction machine with stator inter-turn fault has been derived based on winding function theory [57]. The analysis of the developed model indicated that having inter-turn faults introduces asymmetry in stator three phase currents i.e. the negative and zero sequence components increase with increase of the number of shorted turns. In

addition, the pulsating torque at double supply frequency is also introduced. Accordingly, faults consequences can help in detecting the severity of the inter-turn faults. A mathematical model for an induction motor with stator inter-turn fault has been used for detecting faults when the motor is running [149]. The stator current was used for detecting such faults based on the magnitudes of a particular frequency components in its spectrum. Both experimental and simulation analysis indicated around 8% of the phase turns are shorted. It is found that no new frequency components are introduced in the stator current because of the faults occurrence, but there is a rise in some of the existing frequency components in the healthy motor current spectrum.

A novel technique has been developed for online detection of the stator inter-turns fault in induction machine using infrared images [127]. It is revealed that the magnitude of the current in the faulty part of the stator winding is much higher than that of the rated current of the machine. This current generates excessive heat which is perceived by an infrared camera as a hot spot on the motor surface. The developed method is based on extracting several types of features from the captured infrared images, histogram-based features and structure based features, which help in detecting the severity and the location of inter-turn faults. Both experimental and simulation analysis indicated that 40% of the turns of one phase are shorted. It is also proved that the developed method is effective in detecting such faults. A fuzzy logic technique has also been implemented for detecting the status of having stator inter-turn fault in induction machine [150]. The implemented system used the magnitude of the input current for fault detection. The used data in the construction of the system was collected from simulated FEM model of the motor with

different loading and shorted turns conditions. The disadvantage of this method is that it is difficult to identify the unbalanced supply as an inter-turn fault.

To detect the location of inter-turn stator faults in the induction motors, a tool was developed by using feed forward neural network [151]. The neural network had three inputs and three outputs, with the inputs including the phase shifts between line currents and phase voltages of the machine, while each output represents the status of each stator phase (healthy or faulty). Two sets of data obtained from simulation and experiment were used in the development of two different neural networks. The data was collected under different cases of loading conditions and a number of shorted turns (up to 12.5%). The experimentally developed neural network was tested using the unseen motor with acceptable results. However, the effect of having an unbalanced supply voltage fault was not been considered. Similarly as in, the neural network to discriminate between inter-turn faults and unbalance supply voltage faults was also designed, with three inputs and four outputs [152]. The inputs comprise of the phase shifts between the line currents and the phase voltages of the machine while the first three outputs are the status of the stator phases (healthy or faulty) and the fourth output is the status of unbalanced supply voltages. The data for training and testing the neural network was acquired under different loading conditions, number of shorted turns (up to 20%) and unbalance supply conditions. The performance of the neural network is found to be accurate for fault diagnosis. However, the phase shifts between the line currents and the phase voltages are very sensitive to unbalance in supply voltages. Thus, if the phase shift is considered as an indicator for inter-turn faults, it is a difficult to detect the fault [128]. To overcome this problem, a neural network with one extra input which is the magnitude of the

negative sequence component of the voltage is compared with previously reported one was put into consideration [128]. The data used for training and testing the designed neural network was generated by simulating the mathematical model under the same conditions. The validation of the proposed scheme experimentally confirms the accuracy and efficiency of the method.

Two neural network topologies, multilayer perceptron artificial neural network (ANN) and radial basis function ANN have been designed for detecting the stator inter-turn faults under unbalanced supply voltages and different loading conditions [153]. The inputs to the neural networks are the mutual information between the motor input phase currents while the output is the status of having stator faults. Results showed that the accuracy of the implemented system was 93%-99%. In [116], both instantaneous active and reactive power spectrum were found to be good indicators for detecting stator inter-turn faults as well as discriminating between the faults and unbalance supply. Moreover, the magnitude of the real and reactive power components at double supply frequency are directly proportional to the stator inter-turn faults severity [116].

The optimal multilayer perceptron neural network has been designed for detecting two types of faults in an induction machine including the stator inter-turn faults and the dynamic eccentricity fault [154]. The inputs to the designed neural network are the set of statistical features such as the skewness, kurtosis, standard deviation, etc.. which are obtained using the input current of the machine. On the other hand, the four outputs are; the status of healthy motor, the status of inter-turn fault, the status of dynamic eccentricity fault and finally the status of having both faults. The results demonstrated good accuracy of the proposed method. In another development, a cascaded radial basis

function neural network is implemented for detecting the stator inter-turn faults and dynamic eccentricity fault in induction machine [155]. Correspondingly, an unsupervised neural network has been proposed for detecting the location of stator faults in the induction machine [156], with the Clark transformation components of the stator current as the inputs of the proposed network while the faulty location is utilized as the output. In [157], a feed forward neural network based tool for detecting inter-turn fault in permanent magnet synchronous motor was proposed. The inputs to the proposed neural network are the first, third and fifth frequency components of the motor current while the neural network has 13 binary outputs where each output represent an inter-turn fault severity level. The training and testing data are collected under different loading conditions, speed and inter-turn severity combinations. Results show a success of the tested method for fault diagnosis. , Another neural network based diagnostic tool for detecting the location of inter-turn fault for induction motor has been developed [158]. The discrete wavelet transform has been used for extracting the representative features for the fault. The developed tool is effective in detecting the faults under different loading condition, according to the results. In [159], a tool for detecting the severity of the inter-turn fault in PMSM is developed based neural network. In this study, the magnitude of the third harmonic component of the current is used as the input while the output is the inter-turn fault severity. In [160], a neural network based tool for detecting the inter-turn fault level in induction motor has been proposed which uses the sum of the absolute values of the difference in the peak values of the phase currents from each half cycle as the input while the output is the fault level.



In conclusion, many research works have been done for modelling and diagnostic of stator faults in induction and PMSM motors, while no reported work has been done on the mathematical and finite element modelling of stator winding abnormalities (stator inter-turns fault and asymmetrical stator windings) in LSPMSMs. Besides, no reported work has been done on detecting of stator winding abnormalities in LSPMSMs using ANNs or other intelligent tools. Therefore, this research work aims at developing two mathematical models for LSPMSMs under stator windings abnormalities (stator inter-turns fault and asymmetrical stator windings). In addition, developing an intelligent fault detection tool for detecting stator inter-turn fault and asymmetrical stator winding using neural network. The following chapter (chapter 3) shows in detail the steps of deriving and developing the two mathematical models for the LSPMSM under asymmetrical stator winding and inter-turn fault.

## **CHAPTER 3**

# **INTERIOR-MOUNT LSPMSM MODELING UNDER STATOR WINDING ABNORMALITIES**

### **3.1 Overview**

In order to study the machine behavior under stator winding abnormalities, the models that can express the relationship between the machine flux, voltage, current, speed, torque etc. need to be developed. This chapter details the mathematical modelling of interior-mount LSPMSM under symmetrical stator winding and stator inter-turn fault. In addition, the development of finite element models for interior-mount LSPMSM under symmetrical stator winding and stator inter-turn fault are presented. Figure 3.1 shows the steps of deriving the mathematical and finite element modeling under both abnormalities.

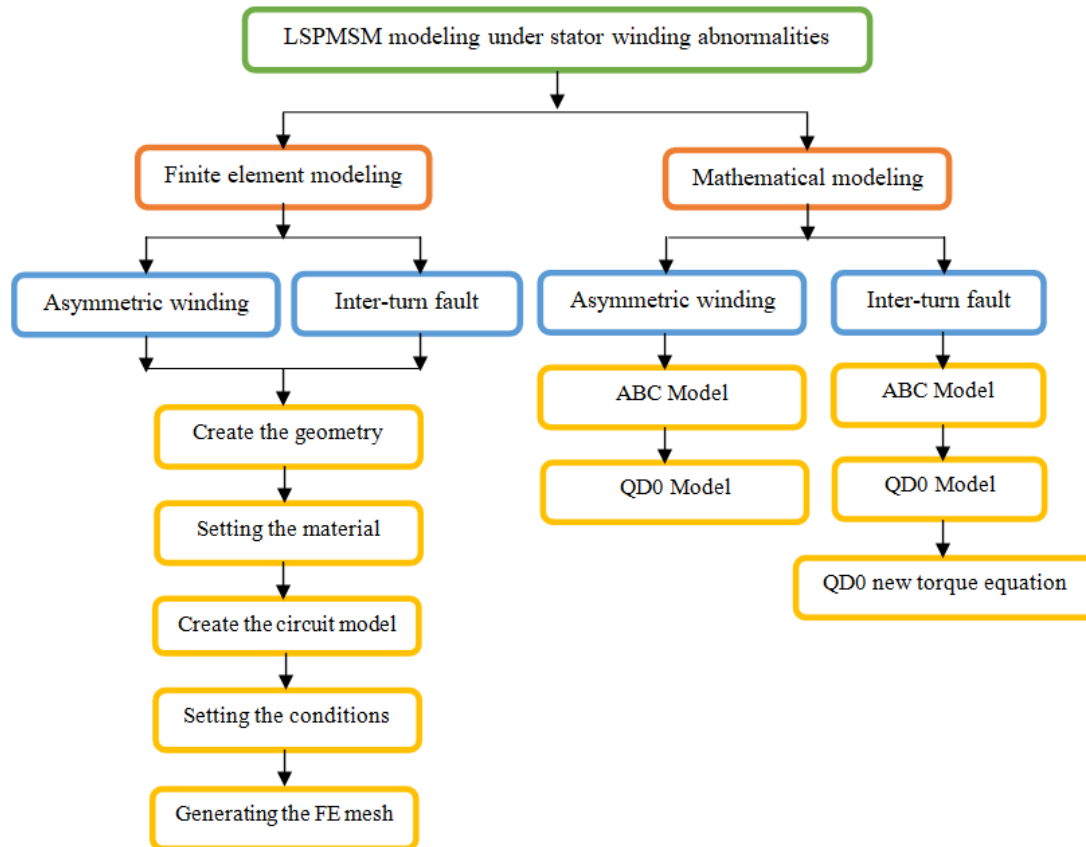


Figure 3.1 Mathematical and finite element models deriving steps

### 3.2 Mathematical Modeling of Interior-Mount LSPMSM

Reliable and safe operation of the electric motors in industry is highly needed. Accurate modeling of electric motor under faults is the first step in developing a diagnostic tool for different types of failures. In this research work, the generalized two mathematical models for interior-mount line start permanent magnet synchronous motors under asymmetrical stator windings and stator inter-turns faults have been developed. The developed mathematical models have been derived using winding theorem. They have also been implemented and simulated using MATLAB/SIMULINK software. In this section, the mathematical model of interior-mount LSPMSM under stator winding

asymmetry is developed first followed by the derivation of the model under stator inter-turns faults condition.

### **3.2.1 Mathematical Modeling of Interior-Mount LSPMSM Under Asymmetric Stator Windings**

A mathematical model of LSPMSM under asymmetrical stator windings has been developed. The next two sections show the steps for deriving the model. In the first step, an ABC-frame mathematical model for the motor is derived, considering the effect of having asymmetrical stator winding on inductances and resistances of the motor. In the second step, park transformation is used to transform the motor ABC-model into QD0-model on the rotor reference frame. Finally, the developed model will be implemented and simulated using MATLAB software.

#### **3.2.1.1 Modeling of LSPMSM with Asymmetrical Stator Winding in ABC-Phase Frame.**

The healthy model of LSPMSM is well known [16, 30-35]. Figure 3.2 shows the circuit winding diagram of the LSPMSM. To derive the ABC-model for an asymmetrical stator winding, Kirchhoff's laws are used in Figure 3.1. Moreover, four assumptions have been made, namely: no magnetic saturation, the iron magnetic permeability is infinite, the flux and magnetic motive force are sinusoidally distributed, and each stator phase has different number of turns [30].  $N_a$ ,  $N_b$  and  $N_c$  are the number of turns of the stator phase-a, phase-b and phase-c, respectively.  $N_r$  is the effective number of turns for the rotor as shown in Figure 3.2.

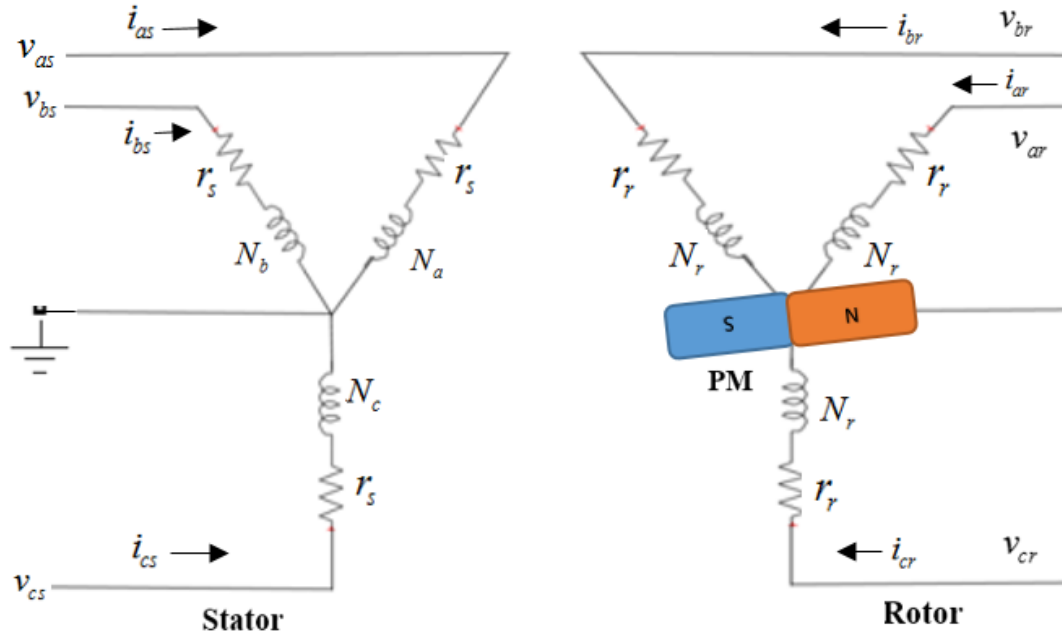


Figure 3.2 LSPMSM ABC-circuit diagram

The voltage equations of the three phase LSPMSM can be written as:

$$\begin{aligned}
 v_{abc}^s &= R_{abc}^s i_{abc}^s + \frac{d\lambda_{abc}^s}{dt} \\
 v_{abc}^r &= R_{abc}^r i_{abc}^r + \frac{d\lambda_{abc}^r}{dt}
 \end{aligned}
 \tag{3.1}$$

Where  $v_{abc}^s$  and  $v_{abc}^r$  are the terminal voltages in each phase of stator and rotor, respectively;  $i_{abc}^s$  and  $i_{abc}^r$  are the currents in each phase of stator and rotor, respectively;  $R_{abc}^s$  is the stator winding resistances for each phase;  $R_{abc}^r$  is the rotor windings resistances for each phase. It is worth mentioning that each stator phase resistance is directly proportional to its number of turns.  $\lambda_{abc}^s$  and  $\lambda_{abc}^r$  are the flux linkage on each phase of

stator and rotor windings, respectively. For conciseness, the matrix expression is used to denote three phase variables as in equation (3.2), i.e.

$$\begin{aligned}
\mathbf{v}_{abc}^s &= \begin{bmatrix} v_a^s & v_b^s & v_c^s \end{bmatrix}^T & \mathbf{v}_{abc}^r &= \begin{bmatrix} v_a^r & v_b^r & v_c^r \end{bmatrix}^T \\
\mathbf{i}_{abc}^r &= \begin{bmatrix} i_a^r & i_b^r & i_c^r \end{bmatrix}^T & \mathbf{i}_{abc}^s &= \begin{bmatrix} i_a^s & i_b^s & i_c^s \end{bmatrix}^T \\
R_{abc}^s &= \begin{bmatrix} \alpha_a r_s & 0 & 0 \\ 0 & \alpha_b r_s & 0 \\ 0 & 0 & \alpha_c r_s \end{bmatrix} & R_{abc}^r &= \begin{bmatrix} r_r & 0 & 0 \\ 0 & r_r & 0 \\ 0 & 0 & r_r \end{bmatrix} \\
\lambda_{abc}^s &= \begin{bmatrix} \lambda_a^s & \lambda_b^s & \lambda_c^s \end{bmatrix} & \lambda_{abc}^r &= \begin{bmatrix} \lambda_a^r & \lambda_b^r & \lambda_c^r \end{bmatrix}
\end{aligned} \tag{3.2}$$

Where  $r_s$  and  $r_r$  are the stator and rotor phase resistances, respectively;  $\alpha_a$ ,  $\alpha_b$  and  $\alpha_c$  are the asymmetric turns ratio coefficients of the stator phases a, b and c, respectively.

$$\alpha_a = \frac{N_a}{N_s}, \alpha_b = \frac{N_b}{N_s}, \alpha_c = \frac{N_c}{N_s} \tag{3.3}$$

For healthy motor,  $N_a = N_b = N_c = N_s \rightarrow \alpha_a = \alpha_b = \alpha_c = \frac{N_s}{N_s} = 1$

Where  $N_s$  is number of turns for stator phase at healthy condition. The magnetic fluxes  $\lambda_{abc}^s$  are generated by three different sources; one from the flux created in the stator self-inductances, the second from the flux created in the stator-rotor mutual inductances and the third is created from the flux generated by the permanent magnet (PM) on the rotor. The same analogy goes for  $\lambda_{abc}^r$ . Thus,  $\lambda_{abc}^s$  and  $\lambda_{abc}^r$  can be written as in equation (3.4).

$$\lambda_{abc}^s = L_{abc}^s i_{abc}^s + L_{abc}^{sr} i_{abc}^r + \lambda_{mabc}^s \quad (3.4)$$

$$\lambda_{abc}^r = L_{abc}^{rs} i_{abc}^s + L_{abc}^r i_{abc}^r + \lambda_{mabc}^r$$

$\lambda_{mabc}^s$  and  $\lambda_{mabc}^r$  are the PM magnetic flux linked to each phase in the stator and rotor, respectively. According to Faraday law, the flux linking the stator phases from the permanent magnet is proportional to the number of turns in each phase.

$$\lambda_{mabc}^s = \lambda_m \begin{bmatrix} \alpha_a \sin(\theta_r) \\ \alpha_b \sin(\theta_r - 120) \\ \alpha_c \sin(\theta_r + 120) \end{bmatrix} \quad \lambda_{mabc}^r = \lambda_m \begin{bmatrix} 0 \\ \frac{\sqrt{3}}{2} \\ -\frac{\sqrt{3}}{2} \end{bmatrix} \quad (3.5)$$

$\lambda_m$  is the magnitude of the magnetic flux created by the PM referred to the stator side.  $\theta_r$  is the angle of the rotor. The stator and rotor inductances are given in equation (3.6):

$$L_{abc}^{ss} = \begin{bmatrix} L_{asas} & L_{asbs} & L_{ascs} \\ L_{asbs} & L_{bsbs} & L_{csbs} \\ L_{ascs} & L_{bscs} & L_{cscs} \end{bmatrix}, \quad L_{abc}^{rr} = \begin{bmatrix} L_{arar} & L_{arbr} & L_{arcr} \\ L_{arbr} & L_{brbr} & L_{crbr} \\ L_{arcr} & L_{brcr} & L_{crcr} \end{bmatrix} \quad (3.6)$$

$$L_{abc}^{sr} = \begin{bmatrix} L_{asar} & L_{asbr} & L_{ascr} \\ L_{asbr} & L_{bsbr} & L_{csbr} \\ L_{ascr} & L_{bscr} & L_{cscr} \end{bmatrix} \quad L_{abc}^{rs} = L_{abc}^{srT}$$

The diagonal elements of  $L_{abc}^s$  are the self-inductances of the stator phases. On the other hand, the off-diagonal elements are the mutual inductances between the stator phases. They can be written as in equation (3.7) [161-163].

$$\begin{aligned}
L_{asas} &= L_{ls} + L_m - L_{\Delta m} \cos(2\theta_r) \\
L_{bsbs} &= L_{ls} + L_m - L_{\Delta m} \cos(2\theta_r - \frac{2\pi}{3}) \\
L_{csbs} &= L_{ls} + L_m - L_{\Delta m} \cos(2\theta_r + \frac{2\pi}{3}) \\
L_{asbs} &= -\frac{1}{2} L_m - L_{\Delta m} \cos(2\theta_r - \frac{\pi}{3}) \\
L_{ascs} &= -\frac{1}{2} L_m - L_{\Delta m} \cos(2\theta_r + \frac{\pi}{3}) \\
L_{bscs} &= -\frac{1}{2} L_m - L_{\Delta m} \cos(2\theta_r + \pi)
\end{aligned} \tag{3.7}$$

The same analogy goes for  $L'_{abc}$ , but  $L_{lr}$  is used in equation (3.7) instead of having  $L_{ls}$ .  $L_{ls}$  and  $L_{lr}$  are the leakage inductances of the stator and rotor phases, respectively whereas  $L_m$  is the magnetizing inductance between the stator and rotor phases.  $L_{\Delta m}$  is the fluctuation in the inductance due to saliency in the machine ( non-uniform airgap) [163]. The formula of the stator to rotor inductance in the abc-frame can be found by transforming the known qd0- stator to rotor inductance matrix ( $L_{qd0}^{sr}$ ) at healthy condition back to abc-frame [164].

$$L_{abc}^{sr} = \begin{bmatrix} L_{asar} & L_{asbr} & L_{ascr} \\ L_{bsar} & L_{bsbr} & L_{bscr} \\ L_{csar} & L_{csbr} & L_{cscr} \end{bmatrix} = K_s^{-1} L_{qd0}^{sr} K_r \tag{3.8}$$

Where  $K_s$  is the stator winding transformation matrix;  $K_r$  is the rotor winding transformation matrix. For a sinusoidal full pitched winding distribution, the self and mutual inductances can be obtained using the winding function approach [161, 165].



$$\begin{aligned}
L_m &= \frac{3}{2}(L_{mq} + L_{md}) \\
L_{\Delta m} &= \frac{3}{2}(L_{mq} - L_{md}) \\
L_{mq} &= L_q - L_{ls} \\
L_{md} &= L_d - L_{ls} \\
L_q &= 1.125\pi\mu_o \left(\frac{N_s}{P}\right)^2 \frac{DL}{g_q} \\
L_d &= 1.125\pi\mu_o \left(\frac{N_s}{P}\right)^2 \frac{DL}{g_d} \\
g_d &= \frac{l_m}{\mu_{rm}} + l_g C, g_q = l_g
\end{aligned} \tag{3.9}$$

Where  $L_{mq}$  is the mutual inductance in q-axis;  $L_{md}$  is the mutual inductance in d-axis.  $L_q$ ;  $L_d$  is the quadrature and direct axis stator self-inductances; P is the number of poles;  $\mu_o$  is the permeability of air;  $L$  is the length of the stator/rotor;  $l_g$  is the air gap length;  $D$  is the inner stator diameter;  $g_d$  is the effective air gap length in the d-axis;  $g_q$  is the effective air gap length in the q-axis;  $l_m$  is the permanent magnet length;  $\mu_{rm}$  is the relative permittivity of the permanent magnet; and  $C$  is the carter coefficient [165].

Taking into account the stator winding asymmetry explained in equation (3.3), the inductance is proportional to the square of its turn's number as proposed by the winding theory [161]. The modified inductance matrices are given in equations (3.10).

$$\left( \begin{array}{l}
L_{abc}^s = \begin{bmatrix} \alpha_a^2 L_{asas} & \alpha_a \alpha_b L_{asbs} & \alpha_a \alpha_c L_{ascs} \\ \alpha_b \alpha_a L_{bsas} & \alpha_b^2 L_{bsbs} & \alpha_b \alpha_c L_{bscs} \\ \alpha_c \alpha_a L_{csas} & \alpha_c \alpha_b L_{csbs} & \alpha_c^2 L_{cscs} \end{bmatrix} \\
L_{abc}^r = \begin{bmatrix} L_{arar} & L_{arbr} & L_{arcr} \\ L_{brar} & L_{brbr} & L_{brcr} \\ L_{crar} & L_{crbr} & L_{crcr} \end{bmatrix} \\
L_{abc}^{sr} = \begin{bmatrix} \alpha_a L_{asar} & \alpha_a L_{asbr} & \alpha_a L_{ascr} \\ \alpha_b L_{bsar} & \alpha_b L_{bsbr} & \alpha_b L_{bscr} \\ \alpha_c L_{csar} & \alpha_c L_{csbr} & \alpha_c L_{cscr} \end{bmatrix} \\
L_{abc}^{rs} = L_{abc}^{sr T}
\end{array} \right) \quad (3.10)$$

This ends the first step of deriving the ABC-model. The next step shows the transformation of the derived ABC-model to QD0-model.

### 3.2.1.2 QD0-Model of the Asymmetrical LSPMSM

With regard to Park transformation [166] with rotor reference frame, Figure 3.3 is used to transform the ABC-LSPMSM model under asymmetrical stator windings into dq0-model. Equations (3.11) to (3.13) show the transformation matrices that have been used in dq0 transform.

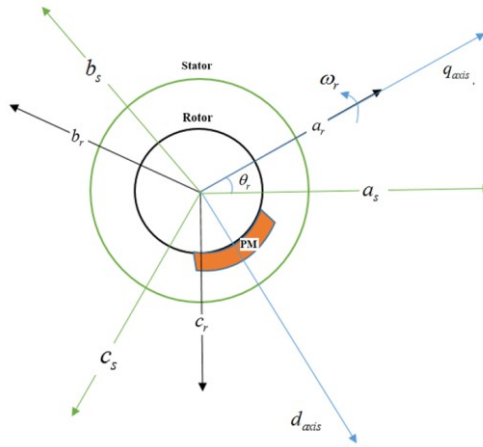


Figure 3.3 LSPMSM machine winding displacement

$$K_s = \frac{2}{3} \begin{bmatrix} \cos\theta_r & \cos(\theta_r-120) & \cos(\theta_r+120) \\ \sin\theta_r & \sin(\theta_r-120) & \sin(\theta_r+120) \\ \frac{1}{2} & \frac{1}{2} & \frac{1}{2} \end{bmatrix}, K_s^{-1} = \begin{bmatrix} \cos\theta_r & \sin\theta_r & 1 \\ \cos(\theta_r-120) & \sin(\theta_r-120) & 1 \\ \cos(\theta_r+120) & \sin(\theta_r+120) & 1 \end{bmatrix} \quad (3.11)$$

$$K_r = \frac{2}{3} \begin{bmatrix} 1 & -\frac{1}{2} & -\frac{1}{2} \\ 0 & -\frac{\sqrt{3}}{2} & \frac{\sqrt{3}}{2} \\ \frac{1}{2} & \frac{1}{2} & \frac{1}{2} \end{bmatrix}, K_r^{-1} = \begin{bmatrix} 1 & 0 & 1 \\ -\frac{1}{2} & -\frac{\sqrt{3}}{2} & 1 \\ -\frac{1}{2} & \frac{\sqrt{3}}{2} & 1 \end{bmatrix} \quad (3.12)$$

$$\theta_r = \int_0^t \omega_r(\gamma) d\gamma + \theta_r(0) \quad (3.13)$$

Where  $\omega_r$  is the rotor electrical speed. The transformation of ABC-model into QD0-model has been done in two steps. In the first step, the voltage in equation (3.1) has been transformed by first writing it in the compact form as in (3.14). Then equation (3.14) is multiply by the transformation matrix, as in equation (3.15).

$$\begin{bmatrix} v_{abc}^s \\ v_{abc}^r \end{bmatrix} = \begin{bmatrix} R_{abc}^s & 0 \\ 0 & R_{abc}^r \end{bmatrix} \begin{bmatrix} i_{abc}^s \\ i_{abc}^r \end{bmatrix} + \begin{bmatrix} \frac{d\lambda_{abc}^s}{dt} \\ \frac{d\lambda_{abc}^r}{dt} \end{bmatrix} \quad (3.14)$$

$$\underbrace{\begin{bmatrix} K_s & 0 \\ 0 & 1 \end{bmatrix}}_{\text{term 1}} \begin{bmatrix} v_{abc}^s \\ v_{abc}^r \end{bmatrix} = \underbrace{\begin{bmatrix} K_s & 0 \\ 0 & 1 \end{bmatrix} \begin{bmatrix} R_{abc}^s & 0 \\ 0 & R_{abc}^r \end{bmatrix}}_{\text{term 2}} \begin{bmatrix} i_{abc}^s \\ i_{abc}^r \end{bmatrix} + \underbrace{\begin{bmatrix} K_s & 0 \\ 0 & K_r \end{bmatrix}}_{\text{term 3}} \begin{bmatrix} \frac{d\lambda_{abc}^s}{dt} \\ \frac{d\lambda_{abc}^r}{dt} \end{bmatrix} \quad (3.15)$$

In equation (3.15) there are three terms, with each term treated separately as follow:

$$\underbrace{\begin{bmatrix} K_s & 0 \\ 0 & I \end{bmatrix}}_{\text{term 1}} \begin{bmatrix} v_{abc}^s \\ v_r^r \end{bmatrix} = \begin{bmatrix} K_s v_{abc}^s \\ v_r^r \end{bmatrix} = \begin{bmatrix} v_{qd0}^s \\ v_{qd0}^r \end{bmatrix} \quad (3.16)$$

$$\underbrace{\begin{bmatrix} K_s & 0 \\ 0 & I \end{bmatrix}}_{\text{term 2}} \begin{bmatrix} R_{abc}^s & 0 \\ 0 & R_r^r \end{bmatrix} \begin{bmatrix} i_{abc}^s \\ i_{abc}^r \end{bmatrix} = \begin{bmatrix} K_s R_{abc}^s & 0 \\ 0 & K_r R_{abc}^r \end{bmatrix} \begin{bmatrix} i_{abc}^s \\ i_{abc}^r \end{bmatrix} \quad (3.17)$$

Where:

$$\begin{bmatrix} i_{abc}^s \\ i_{abc}^r \end{bmatrix} = \begin{bmatrix} K_s^{-1} & 0 \\ 0 & K_r^{-1} \end{bmatrix} \begin{bmatrix} i_{qd0}^s \\ i_{qd0}^r \end{bmatrix} \quad (3.18)$$

Substitute (3.18) in (3.17) to get (3.19), and then manipulate (3.19) to get (3.21):

$$\underbrace{\begin{bmatrix} K_s & 0 \\ 0 & I \end{bmatrix}}_{\text{term 2}} \begin{bmatrix} R_{abc}^s & 0 \\ 0 & R_r^r \end{bmatrix} \begin{bmatrix} i_{abc}^s \\ i_{abc}^r \end{bmatrix} = \begin{bmatrix} K_s R_{abc}^s & 0 \\ 0 & K_r R_{abc}^r \end{bmatrix} \begin{bmatrix} K_s^{-1} & 0 \\ 0 & K_r^{-1} \end{bmatrix} \begin{bmatrix} i_{qd0}^s \\ i_{qd0}^r \end{bmatrix} \quad (3.19)$$

$$\underbrace{\begin{bmatrix} K_s & 0 \\ 0 & I \end{bmatrix}}_{\text{term 2}} \begin{bmatrix} R_{abc}^s & 0 \\ 0 & R_r^r \end{bmatrix} \begin{bmatrix} i_{abc}^s \\ i_{abc}^r \end{bmatrix} = \begin{bmatrix} K_s R_{abc}^s K_s^{-1} & 0 \\ 0 & K_r R_{abc}^r K_r^{-1} \end{bmatrix} \begin{bmatrix} i_{qd0}^s \\ i_{qd0}^r \end{bmatrix} \quad (3.20)$$

$$\underbrace{\begin{bmatrix} K_s & 0 \\ 0 & I \end{bmatrix}}_{\text{term 2}} \begin{bmatrix} R_{abc}^s & 0 \\ 0 & R_r^r \end{bmatrix} \begin{bmatrix} i_{abc}^s \\ i_{abc}^r \end{bmatrix} = \begin{bmatrix} K_s R_{abc}^s K_s^{-1} & 0 \\ 0 & K_r R_{abc}^r K_r^{-1} \end{bmatrix} \begin{bmatrix} i_{qd0}^s \\ i_{qd0}^r \end{bmatrix} = \begin{bmatrix} R_{qd0}^s & 0 \\ 0 & R_{qd0}^r \end{bmatrix} \begin{bmatrix} i_{qd0}^s \\ i_{qd0}^r \end{bmatrix} \quad (3.21)$$

$$R_{qd0}^s = \begin{bmatrix} r_{11}^s & r_{12}^s & r_{13}^s \\ r_{21}^s & r_{22}^s & r_{23}^s \\ r_{31}^s & r_{32}^s & r_{33}^s \end{bmatrix}, R_{qd0}^r = \begin{bmatrix} r_q & 0 & 0 \\ 0 & r_d & 0 \\ 0 & 0 & r_0 \end{bmatrix} \quad (3.22)$$

Where  $R_{qd0}^s$  is the Stator resistances matrix in dq0 axes whereby the entries of  $R_{qd0}^s$  are  $\theta_r$  dependent;  $R_{qd0}^r$  is the rotor resistance matrix in dq0 axes where the entries of  $R_{qd0}^r$  are  $\theta_r$  independent. For the third term;

$$\underbrace{\begin{bmatrix} K_s & 0 \\ 0 & K_r \end{bmatrix}}_{\text{term 3}} \begin{bmatrix} \frac{d\lambda_{abc}^s}{dt} \\ \frac{d\lambda_{abc}^r}{dt} \end{bmatrix} = \begin{bmatrix} K_s \frac{d\lambda_{abc}^s}{dt} \\ K_r \frac{d\lambda_{abc}^r}{dt} \end{bmatrix} \quad (3.23)$$

$$\begin{aligned} \lambda_{qd0}^s &= K_s \lambda_{abc}^s \\ \frac{d\lambda_{qd0}^s}{dt} &= K_s \frac{d\lambda_{abc}^s}{dt} + \frac{dK_s}{dt} \lambda_{abc}^s \\ K_s \frac{d\lambda_{abc}^s}{dt} &= \frac{d\lambda_{qd0}^s}{dt} - \frac{dK_s}{dt} \lambda_{abc}^s \\ \lambda_{abc}^s &= K_s^{-1} \lambda_{qd0}^s \\ K_s \frac{d\lambda_{abc}^s}{dt} &= \frac{d\lambda_{qd0}^s}{dt} - \frac{dK_s}{dt} K_s^{-1} \lambda_{qd0}^s \end{aligned} \quad (3.24)$$

The same analogy done in equation (3.24) goes for the rotor to get equation (3.25):

$$K_r \frac{d\lambda_{abc}^r}{dt} = \frac{d\lambda_{qd0}^r}{dt} - \frac{dK_r}{dt} K_r^{-1} \lambda_{qd0}^r \quad (3.25)$$

The term 3 will become as in equation (3.26):

$$\underbrace{\begin{bmatrix} K_s & 0 \\ 0 & K_r \end{bmatrix}}_{\text{term 3}} \begin{bmatrix} \frac{d\lambda_{abc}^s}{dt} \\ \frac{d\lambda_{abc}^r}{dt} \end{bmatrix} = \begin{bmatrix} K_s \frac{d\lambda_{abc}^s}{dt} \\ K_r \frac{d\lambda_{abc}^r}{dt} \end{bmatrix} = \begin{bmatrix} \frac{d\lambda_{qd0}^s}{dt} \\ \frac{d\lambda_{qd0}^r}{dt} \end{bmatrix} - \begin{bmatrix} \frac{dK_s}{dt} K_s^{-1} \lambda_{qd0}^s \\ \frac{dK_r}{dt} K_r^{-1} \lambda_{qd0}^r \end{bmatrix} \quad (3.26)$$

By rearranging, equation (3.26) becomes;

$$\frac{dK_r}{dt} K_r^{-1} = 0 * \begin{bmatrix} 1 & 0 & 1 \\ -\frac{1}{2} & \frac{\sqrt{3}}{2} & 1 \\ -\frac{1}{2} & -\frac{\sqrt{3}}{2} & 1 \end{bmatrix} = 0 \quad (3.27)$$

Or as in equation (3.28);

$$\begin{aligned} \frac{dK_s}{dt} K_s^{-1} &= \frac{2}{3} \omega_r \begin{bmatrix} -\sin\theta_r & -\sin(\theta_r - 120) & -\sin(\theta_r + 120) \\ \cos\theta_r & \cos(\theta_r - 120) & \cos(\theta_r + 120) \\ 0 & 0 & 0 \end{bmatrix} \begin{bmatrix} \cos\theta_r & \sin\theta_r & 1 \\ \cos(\theta_r - 120) & \sin(\theta_r - 120) & 1 \\ \cos(\theta_r + 120) & \sin(\theta_r + 120) & 1 \end{bmatrix} \\ &= \frac{2}{3} \omega_r \begin{bmatrix} 0 & -\frac{3}{2} & 0 \\ \frac{3}{2} & 0 & 0 \\ 0 & 0 & 0 \end{bmatrix} = \begin{bmatrix} 0 & \omega_r & 0 \\ -\omega_r & 0 & 0 \\ 0 & 0 & 0 \end{bmatrix} \end{aligned} \quad (3.28)$$

The final voltage equation is as in (3.29).

$$\begin{bmatrix} v_q^s \\ v_d^s \\ v_0^s \\ v_q^r \\ v_d^r \\ v_0^r \end{bmatrix} = \begin{bmatrix} r_{11}^s & r_{12}^s & r_{13}^s & 0 & 0 & 0 \\ r_{21}^s & r_{22}^s & r_{23}^s & 0 & 0 & 0 \\ r_{31}^s & r_{32}^s & r_{33}^s & 0 & 0 & 0 \\ 0 & 0 & 0 & r_r & 0 & 0 \\ 0 & 0 & 0 & 0 & r_r & 0 \\ 0 & 0 & 0 & 0 & 0 & r_r \end{bmatrix} \begin{bmatrix} i_q^s \\ i_d^s \\ i_0^s \\ i_q^r \\ i_d^r \\ i_0^r \end{bmatrix} + \begin{bmatrix} \frac{d\lambda_q^s}{dt} \\ \frac{d\lambda_d^s}{dt} \\ \frac{d\lambda_0^s}{dt} \\ \frac{d\lambda_q^r}{dt} \\ \frac{d\lambda_d^r}{dt} \\ \frac{d\lambda_0^r}{dt} \end{bmatrix} + \begin{bmatrix} \omega_r \lambda_d^s \\ -\omega_r \lambda_q^s \\ 0 \\ 0 \\ 0 \\ 0 \end{bmatrix} \quad (3.29)$$

In the second step, flux-current relations in equation (3.4) have been transformed as follows, through equations (3.30) to (3.38).

$$\begin{bmatrix} \lambda_{abc}^s \\ \lambda_{abc}^r \end{bmatrix} = \begin{bmatrix} L_{abc}^s & L_{abc}^{sr} \\ L_{abc}^{rs} & L_{abc}^r \end{bmatrix} \begin{bmatrix} i_{abc}^s \\ i_{abc}^r \end{bmatrix} + \begin{bmatrix} \lambda_{mabc}^s \\ \lambda_{mabc}^r \end{bmatrix} \quad (3.30)$$

$$\begin{bmatrix} K_s & 0 \\ 0 & K_r \end{bmatrix} \begin{bmatrix} \lambda_{abc}^s \\ \lambda_{abc}^r \end{bmatrix} = \begin{bmatrix} K_s & 0 \\ 0 & K_r \end{bmatrix} \begin{bmatrix} L_{abc}^s & L_{abc}^{sr} \\ L_{abc}^{rs} & L_{abc}^r \end{bmatrix} \begin{bmatrix} K_s^{-1} & 0 \\ 0 & K_r^{-1} \end{bmatrix} \begin{bmatrix} i_{qd0}^s \\ i_{qd0}^r \end{bmatrix} + \begin{bmatrix} K_s & 0 \\ 0 & K_r \end{bmatrix} \begin{bmatrix} \lambda_{mabc}^s \\ \lambda_{mabc}^r \end{bmatrix} \quad (3.31)$$

$$\begin{bmatrix} \lambda_{qd0}^s \\ \lambda_{qd0}^r \end{bmatrix} = \begin{bmatrix} K_s L_{abc}^s K_s^{-1} & K_s L_{abc}^{sr} K_r^{-1} \\ K_r L_{abc}^{rs} K_s^{-1} & K_r L_{abc}^r K_r^{-1} \end{bmatrix} \begin{bmatrix} i_{qd0}^s \\ i_{qd0}^r \end{bmatrix} + \begin{bmatrix} K_s \lambda_{mabc}^s \\ K_r \lambda_{mabc}^r \end{bmatrix} \quad (3.32)$$

$$K_r L_{abc}^r K_r^{-1} = \begin{bmatrix} L_{lrq} + \frac{3}{2}(L_m + L_{\Delta m}) & 0 & 0 \\ 0 & L_{lrd} + \frac{3}{2}(L_m - L_{\Delta m}) & 0 \\ 0 & 0 & L_{lr0} \end{bmatrix} \equiv L_{qd0}^r \quad (3.33)$$

$$K_s L_{abc}^s K_s^{-1} = \begin{bmatrix} L_{11}^{ss} & L_{12}^{ss} & L_{13}^{ss} \\ L_{21}^{ss} & L_{22}^{ss} & L_{23}^{ss} \\ L_{31}^{ss} & L_{32}^{ss} & L_{33}^{ss} \end{bmatrix} \equiv L_{qd0}^s \quad (3.34)$$

$$K_s L_{abc}^{sr} K_r^{-1} = \begin{bmatrix} L_{11}^{sr} & L_{12}^{sr} & 0 \\ L_{21}^{sr} & L_{22}^{sr} & 0 \\ L_{31}^{sr} & L_{32}^{sr} & 0 \end{bmatrix} \equiv L_{qd0}^{sr} \quad (3.35)$$

$$L_{qd0}^{rs} = L_{qd0}^{sr T} \quad (3.36)$$

$$\begin{bmatrix} K_s \lambda_{mabc}^s \\ K_r \lambda_{mabc}^r \end{bmatrix} = \begin{bmatrix} \lambda_{mq} \\ \lambda_{md} \\ \lambda_{m0} \\ 0 \\ \lambda_m \\ 0 \end{bmatrix} \quad (3.37)$$

The transformed current flux relation is as in equation (3.38):

$$\begin{bmatrix} \lambda_q^s \\ \lambda_d^s \\ \lambda_0^s \\ \lambda_q^r \\ \lambda_d^r \\ \lambda_0^r \end{bmatrix} = \begin{bmatrix} L_{11}^{ss} & L_{12}^{ss} & L_{13}^{ss} & L_{11}^{sr} & L_{12}^{sr} & 0 \\ L_{21}^{ss} & L_{22}^{ss} & L_{23}^{ss} & L_{21}^{sr} & L_{22}^{sr} & 0 \\ L_{31}^{ss} & L_{32}^{ss} & L_{33}^{ss} & L_{31}^{sr} & L_{32}^{sr} & 0 \\ L_{11}^{sr} & L_{21}^{sr} & L_{31}^{sr} & L_{lrq} + \frac{3}{2}(L_m + L_{\Delta m}) & 0 & 0 \\ L_{12}^{sr} & L_{22}^{sr} & L_{32}^{sr} & 0 & L_{lrd} + \frac{3}{2}(L_m - L_{\Delta m}) & 0 \\ 0 & 0 & 0 & 0 & 0 & L_{lr0} \end{bmatrix} \begin{bmatrix} i_q^s \\ i_d^s \\ i_0^s \\ i_q^r \\ i_d^r \\ i_0^r \end{bmatrix} + \begin{bmatrix} \lambda_{mq} \\ \lambda_{md} \\ \lambda_{m0} \\ 0 \\ \lambda_m \\ 0 \end{bmatrix} \quad (3.38)$$

Both the voltage equation (3.29) and the flux current relation equation (3.38) represent the LSPMSM under asymmetrical stator winding. In both equations, the rotor quantities are referred to the stator side by using equation (3.39) to obtain equations (3.40) and (3.41).

$$\begin{aligned} i_q^{r'} &= \frac{N_r}{N_s} i_q^r, \quad i_d^{r'} = \frac{N_r}{N_s} i_d^r, \quad i_0^{r'} = \frac{N_r}{N_s} i_0^r \\ v_q^{r'} &= \frac{N_s}{N_r} v_q^r, \quad v_d^{r'} = \frac{N_s}{N_r} v_d^r, \quad v_0^{r'} = \frac{N_s}{N_r} v_0^r \\ \lambda_q^{r'} &= \frac{N_s}{N_r} \lambda_q^r, \quad \lambda_d^{r'} = \frac{N_s}{N_r} \lambda_d^r, \quad \lambda_0^{r'} = \frac{N_s}{N_r} \lambda_0^r \\ L_{lrd}^{r'} &= \left(\frac{N_s}{N_r}\right)^2 L_{lrd}, \quad L_{lrq}^{r'} = \left(\frac{N_s}{N_r}\right)^2 L_{lrq} \\ r_{rd}^{r'} &= \left(\frac{N_s}{N_r}\right)^2 r_{rd}, \quad r_{rq}^{r'} = \left(\frac{N_s}{N_r}\right)^2 r_{rq} \end{aligned} \quad (3.39)$$



$$\begin{bmatrix} v_q^s \\ v_d^s \\ v_0^s \\ v_q^{r'} \\ v_d^{r'} \\ v_0^{r'} \end{bmatrix} = \begin{bmatrix} r_{11}^s & r_{12}^s & r_{13}^s & 0 & 0 & 0 \\ r_{21}^s & r_{22}^s & r_{23}^s & 0 & 0 & 0 \\ r_{31}^s & r_{32}^s & r_{33}^s & 0 & 0 & 0 \\ 0 & 0 & 0 & r_{rq}' & 0 & 0 \\ 0 & 0 & 0 & 0 & r_{rd}' & 0 \\ 0 & 0 & 0 & 0 & 0 & r_{ro}' \end{bmatrix} \begin{bmatrix} i_q^s \\ i_d^s \\ i_0^s \\ i_q^{r'} \\ i_d^{r'} \\ i_0^{r'} \end{bmatrix} + \begin{bmatrix} \frac{d\lambda_q^s}{dt} \\ \frac{d\lambda_d^s}{dt} \\ \frac{d\lambda_0^s}{dt} \\ \frac{d\lambda_q^{r'}}{dt} \\ \frac{d\lambda_d^{r'}}{dt} \\ \frac{d\lambda_0^{r'}}{dt} \end{bmatrix} + \begin{bmatrix} \omega_r \lambda_d^s \\ -\omega_r \lambda_q^s \\ 0 \\ 0 \\ 0 \\ 0 \end{bmatrix} \quad (3.40)$$

$$\begin{bmatrix} \lambda_q^s \\ \lambda_d^s \\ \lambda_0^s \\ \lambda_q^{r'} \\ \lambda_d^{r'} \\ \lambda_0^{r'} \end{bmatrix} = \begin{bmatrix} L_{11}^{ss} & L_{12}^{ss} & L_{13}^{ss} & L_{11}^{sr} & L_{12}^{sr} & 0 \\ L_{21}^{ss} & L_{22}^{ss} & L_{23}^{ss} & L_{21}^{sr} & L_{22}^{sr} & 0 \\ L_{31}^{ss} & L_{32}^{ss} & L_{33}^{ss} & L_{31}^{sr} & L_{32}^{sr} & 0 \\ L_{11}^{sr} & L_{21}^{sr} & L_{31}^{sr} & L_{lrq}' + \frac{3}{2}(L_m + L_{\Delta m}) & 0 & 0 \\ L_{12}^{sr} & L_{22}^{sr} & L_{32}^{sr} & 0 & L_{lrd}' + \frac{3}{2}(L_m - L_{\Delta m}) & 0 \\ 0 & 0 & 0 & 0 & 0 & L_{lr0}' \end{bmatrix} \begin{bmatrix} i_q^s \\ i_d^s \\ i_0^s \\ i_q^{r'} \\ i_d^{r'} \\ i_0^{r'} \end{bmatrix} + \begin{bmatrix} \lambda_{mq} \\ \lambda_{md} \\ \lambda_{m0} \\ 0 \\ \lambda_m' \\ 0 \end{bmatrix} \quad (3.41)$$

Equations (3.40), (3.41), (2.9) and (2.10) represent the final QD0-model that will be used for simulation purposes. For completeness, equation (2.9) and (2.10) are repeated as follow;

The electromagnetic torque is expressed as;

$$T_{em} = \frac{3P}{4} (i_q^s \lambda_d^s - i_d^s \lambda_q^s) \quad (2.9)$$

The mechanical equation is also expressed as;

$$\omega_r(t) = \frac{P}{2J} \int (T_{em} + T_L - T_{damp}) dt \quad (2.10)$$

### 3.2.2 Mathematical Modeling of Interior-Mount LSPMSM Under Stator Inter-Turn Fault

This section presents in detail the steps for deriving the mathematical model of the interior-mount LSPMSM with the stator inter-turn fault. The subsequent sub-sections show the steps for deriving the mathematical model.

#### 3.2.2.1 ABC-Model of stator inter-turn fault in LSPMSM

There is no work on the modeling of an interior-mount LSPMSM under the stator inter-turn fault existing in the literature. Figure 3.4 shows the stator circuit diagram of an LSPMSM under the inter-turn fault in phase-a. To derive the mathematical model of the motor under the stator inter-turn fault, Kirchhoff's laws are used.

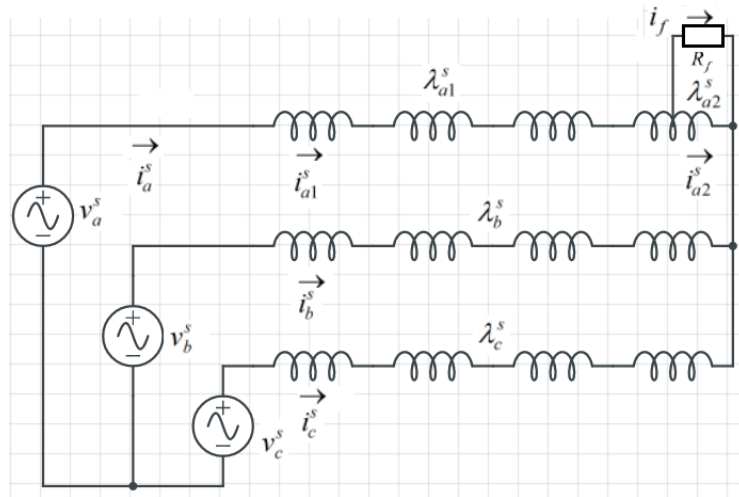


Figure 3.4 The stator of the LSPMSM under inter-turn fault in phase-a

It should be noted that the resistance of the stator phases is directly proportional to the number of turns per phase, while the inductance is proportional to the square of the number of turns, based on the winding theory. In addition, according to Faraday's law,

the flux linking the stator phases from the permanent magnet is proportional to the number of turns in each phase. In this section, the mathematical ABC-model of an LSPMSM with the inter-turn fault in phase-a is derived. Phase-a is divided into two parts: part-a<sub>1</sub> (healthy part) and part-a<sub>2</sub> (faulty part), as shown in Figure 3.4. Using Kirchhoff's voltage law, the voltage equations are as follows:

$$\begin{aligned} v_{a_1 a_2 bc}^s &= R_{a_1 a_2 bc}^s i_{a_1 a_2 bc}^s + \frac{d\lambda_{a_1 a_2 bc}^s}{dt} \\ v_{abc}^r &= R_{abc}^r i_{abc}^r + \frac{d\lambda_{abc}^r}{dt} \end{aligned} \quad (3.42)$$

Where  $R_{a_1 a_2 bc}^s$  is the resistance matrix for the stator.

Equations (3.43) and (3.44) represent equation (3.42) in matrix form, where the stator is represented by four differential equation (3.43) while the rotor by three differential equations (3.44) as follows:

$$\begin{bmatrix} v_{a_1}^s \\ v_{a_2}^s \\ v_b^s \\ v_c^s \end{bmatrix} = r_s \begin{bmatrix} 1-\mu & 0 & 0 & 0 \\ 0 & \mu & 0 & 0 \\ 0 & 0 & 1 & 0 \\ 0 & 0 & 0 & 1 \end{bmatrix} \begin{bmatrix} i_{a_1}^s \\ i_{a_2}^s \\ i_b^s \\ i_c^s \end{bmatrix} + \frac{d}{dt} \begin{bmatrix} \lambda_{a_1}^s \\ \lambda_{a_2}^s \\ \lambda_b^s \\ \lambda_c^s \end{bmatrix} \quad (3.43)$$

$$\begin{bmatrix} v_a^r \\ v_b^r \\ v_c^r \end{bmatrix} = r_r \begin{bmatrix} 1 & 0 & 0 \\ 0 & 1 & 0 \\ 0 & 0 & 1 \end{bmatrix} \begin{bmatrix} i_a^r \\ i_b^r \\ i_c^r \end{bmatrix} + \frac{d}{dt} \begin{bmatrix} \lambda_a^r \\ \lambda_b^r \\ \lambda_c^r \end{bmatrix} \quad (3.44)$$

Where the fault current  $i_f = i_{a_1}^s - i_{a_2}^s = i_a^s - i_{a_2}^s$  based on Figure 3.3;  $\mu$  is the shorted turns

ratio i.e  $\mu = \frac{N_{sh}}{N_s}$ ; and  $N_{sh}$  is the number of shorted turns.

By adding the first two rows of equation (3.43) and rearranging the terms, the machine voltage equations can be expressed as in equations (3.45) and (3.46)

$$\begin{bmatrix} v_{abc}^s \\ v_{abc}^r \end{bmatrix} = \begin{bmatrix} R_{abc}^s & 0 \\ 0 & R_{abc}^r \end{bmatrix} \begin{bmatrix} i_{abc}^s \\ i_{abc}^r \end{bmatrix} + \frac{d}{dt} \begin{bmatrix} \lambda_{abc}^s \\ \lambda_{abc}^r \end{bmatrix} + \mu \begin{bmatrix} A_1 \\ 0 \end{bmatrix} i_f \quad (3.45)$$

$$v_{a_2}^s = \mu r_s (i_a^s - i_f) + \frac{d}{dt} \lambda_{a_2}^s = R_f i_f \quad (3.46)$$

Where  $A_1 = [-r_s \ 0 \ 0]^T$  and  $v_a^s = v_{a_1}^s + v_{a_2}^s$ . Equation (3.46) represent the voltage across the shorted turns.  $R_{abc}^s$  and  $R_{abc}^r$  are the stator and rotor resistance matrix under healthy conditions.

$$R_{abc}^s = \begin{bmatrix} r_s & 0 & 0 \\ 0 & r_s & 0 \\ 0 & 0 & r_s \end{bmatrix}, \quad R_{abc}^r = \begin{bmatrix} r_r & 0 & 0 \\ 0 & r_r & 0 \\ 0 & 0 & r_r \end{bmatrix} \quad (3.47)$$

The flux current relation equations of the three-phase faulted LSPMSM shown in Figure 3 can be written as;

$$\begin{aligned} \lambda_{a_1 a_2 bc}^s &= L_{a_1 a_2 bc}^s i_{a_1 a_2 bc}^s + L_{a_1 a_2 bc}^{sr} i_{a_1 a_2 bc}^r + \lambda_{m a_1 a_2 bc}^s \\ \lambda_{abc}^r &= L_{a_1 a_2 bc}^{rs} i_{a_1 a_2 bc}^s + L_{abc}^r i_{abc}^r + \lambda_{m abc}^r \end{aligned} \quad (3.48)$$

Where  $\lambda_{a_1 a_2 bc}^s$  and  $\lambda_{abc}^r$  are the flux linkage vectors;  $L_{a_1 a_2 bc}^s$  and  $L_{abc}^r$  are the inductance matrices for the stator and rotor circuit, respectively;  $L_{a_1 a_2 bc}^{sr}$  and  $L_{a_1 a_2 bc}^{rs}$  are the mutual inductance matrices between the stator and rotor; and  $\lambda_{m a_1 a_2 bc}^s$  is the linkage flux on the stator due to the permeant magnets. Equations (3.49 and 3.50) represent the flux current relation of equation (3.48) in matrix form.

$$\begin{bmatrix} \lambda_{a_1}^s \\ \lambda_{a_2}^s \\ \lambda_b^s \\ \lambda_c^s \end{bmatrix} = \begin{bmatrix} (1-\mu^2)L_{asas} & \mu(1-\mu)(L_{asas}-L_{ls}) & (1-\mu)L_{asbs} & (1-\mu)L_{ascs} \\ \mu(1-\mu)(L_{asas}-L_{ls}) & \mu^2L_{asas} & \mu L_{asbs} & \mu L_{ascs} \\ (1-\mu)L_{bsas} & \mu L_{bsas} & L_{bsbs} & L_{bscs} \\ (1-\mu)L_{csas} & \mu L_{csas} & L_{csbs} & L_{cscs} \end{bmatrix} \begin{bmatrix} i_{a_1}^s \\ i_{a_2}^s \\ i_b^s \\ i_c^s \end{bmatrix} \quad (3.49)$$

$$+ \begin{bmatrix} (1-\mu)L_{asar} & (1-\mu)L_{asbr} & (1-\mu)L_{ascr} \\ \mu L_{asar} & \mu L_{asbr} & \mu L_{ascr} \\ L_{bsar} & L_{bsbr} & L_{bscr} \\ L_{csar} & L_{csbr} & L_{cscr} \end{bmatrix} \begin{bmatrix} i_a^r \\ i_b^r \\ i_c^r \end{bmatrix} + \lambda_m \begin{bmatrix} (1-\mu)\sin\theta_r \\ \mu\sin\theta_r \\ \sin(\theta_r-120^\circ) \\ \sin(\theta_r+120^\circ) \end{bmatrix}$$

$$\begin{bmatrix} \lambda_a^r \\ \lambda_b^r \\ \lambda_c^r \end{bmatrix} = \begin{bmatrix} (1-\mu)L_{asar} & \mu L_{asar} & L_{bsar} & L_{csar} \\ (1-\mu)L_{asbr} & \mu L_{asbr} & L_{bsbr} & L_{csbr} \\ (1-\mu)L_{ascr} & \mu L_{ascr} & L_{bscr} & L_{cscr} \end{bmatrix} \begin{bmatrix} i_{a_1}^s \\ i_{a_2}^s \\ i_b^s \\ i_c^s \end{bmatrix} + \begin{bmatrix} L_{arar} & L_{arbr} & L_{arcr} \\ L_{brar} & L_{brbr} & L_{brcr} \\ L_{crar} & L_{crbr} & L_{cr cr} \end{bmatrix} \begin{bmatrix} i_a^r \\ i_b^r \\ i_c^r \end{bmatrix} + \lambda_m \begin{bmatrix} 0 \\ -\frac{\sqrt{3}}{2} \\ \frac{\sqrt{3}}{2} \end{bmatrix} \quad (3.50)$$

Writing equation (3.49) and (3.50) in terms of the healthy and the faulty machines, by adding the first two rows of equation (3.49) since  $\lambda_a^s = \lambda_{a_1}^s + \lambda_{a_2}^s$ , yields the following:

$$\begin{bmatrix} \lambda_{abc}^s \\ \lambda_{abc}^r \end{bmatrix} = \begin{bmatrix} L_{abc}^{ss} & L_{abc}^{sr} \\ L_{abc}^{rs} & L_{abc}^{rr} \end{bmatrix} \begin{bmatrix} i_{abc}^s \\ i_{abc}^r \end{bmatrix} + \begin{bmatrix} \lambda_{mabc}^s \\ \lambda_{mabc}^r \end{bmatrix} + \mu \begin{bmatrix} A_2 \\ A_3 \end{bmatrix} i_f \quad (3.51)$$

$$\lambda_{a_2}^s = -\mu A_2^T i_{abc}^s - \mu A_3^T i_{abc}^r - \mu^2 L_{asas} i_f + \mu \lambda_m \sin\theta_r \quad (3.52)$$

Where  $A_2 = -[L_{asas} \quad L_{asbs} \quad L_{ascs}]^T$  and  $A_3 = -[L_{asar} \quad L_{asbr} \quad L_{ascr}]^T$ .

Equations (3.45, 3.46) and (3.51, 3.52) represent the final ABC-mathematical model (voltages and flux-current relation equations) of the LSPMSM under stator inter-turn fault.

### 3.2.2.2 QD0-Model of stator inter-turn fault in LSPMSM

Based on Park transformation [166] with rotor reference frame, Figure 3.2 is used to transform the ABC-LSPMSM model under inter-turn fault into QD0-model. Transformation matrices in equations (3.11) and (3.12) are used to transform the voltage and flux current relation equation for the model. The voltage equation (3.45) is multiplied by the transformation matrices with some matrix computations to arrive at the qd0 voltage equation as follow.

$$\begin{bmatrix} K_s v_{abc}^s \\ K_r v_{abc}^r \end{bmatrix} = \begin{bmatrix} K_s R_{abc}^s & 0 \\ 0 & K_r R_{abc}^r \end{bmatrix} \begin{bmatrix} K_s^{-1} i_{qd0}^s \\ K_r^{-1} i_{qd0}^r \end{bmatrix} + \begin{bmatrix} K_s \frac{d}{dt} \lambda_{abc}^s \\ K_r \frac{d}{dt} \lambda_{abc}^r \end{bmatrix} + \mu \begin{bmatrix} K_s A_1 \\ K_r 0 \end{bmatrix} i_f \quad (3.53)$$

After some matrix computation, equation (3.53) becomes;

$$\begin{bmatrix} v_{qd0}^s \\ v_{qd0}^r \end{bmatrix} = \begin{bmatrix} R_{qd0}^s & 0 \\ 0 & R_{qd0}^r \end{bmatrix} \begin{bmatrix} i_{qd0}^s \\ i_{qd0}^r \end{bmatrix} + \begin{bmatrix} K_s \frac{d}{dt} \lambda_{abc}^s \\ K_r \frac{d}{dt} \lambda_{abc}^r \end{bmatrix} + \mu \begin{bmatrix} K_s A_1 \\ 0 \end{bmatrix} i_f \quad (3.54)$$

To transform the second term of equation (3.54) the following has been done.

$$\begin{aligned} \lambda_{qd0}^s &= K_s \lambda_{abc}^s \\ \frac{d\lambda_{qd0}^s}{dt} &= K_s \frac{d\lambda_{abc}^s}{dt} + \frac{dK_s}{dt} \lambda_{abc}^s \\ K_s \frac{d\lambda_{abc}^s}{dt} &= \frac{d\lambda_{qd0}^s}{dt} - \frac{dK_s}{dt} \lambda_{abc}^s \\ \lambda_{abc}^s &= K_s^{-1} \lambda_{qd0}^s \\ K_s \frac{d\lambda_{abc}^s}{dt} &= \frac{d\lambda_{qd0}^s}{dt} - \frac{dK_s}{dt} K_s^{-1} \lambda_{qd0}^s \end{aligned} \quad (3.55)$$

by using the same analogy as in equation (3.55) for the rotor, the following equations (3.56) to (3.58) are obtained.

$$K_r \frac{d\lambda_{abc}^r}{dt} = \frac{d\lambda_{qd0}^r}{dt} - \frac{dK_r}{dt} K_r^{-1} \lambda_{qd0}^r \quad (3.56)$$

$$\frac{dK_r}{dt} K_r^{-1} = 0 \quad (3.57)$$

$$\frac{dK_s}{dt} K_s^{-1} = \begin{bmatrix} 0 & \omega_r & 0 \\ -\omega_r & 0 & 0 \\ 0 & 0 & 0 \end{bmatrix} \quad (3.58)$$

To transform the last term of equation (3.54), the following has been done.

$$K_s \begin{bmatrix} -r_s \mu \\ 0 \\ 0 \end{bmatrix} = \begin{bmatrix} -\frac{2}{3} \mu r_s \cos \theta_r \\ -\frac{2}{3} \mu r_s \sin \theta_r \\ -\frac{1}{3} \mu r_s \end{bmatrix} \quad (3.59)$$

The final voltage equation becomes;

$$\begin{bmatrix} v_q^s \\ v_d^s \\ v_0^s \\ v_q^{r'} \\ v_d^{r'} \\ v_0^{r'} \end{bmatrix} = \begin{bmatrix} r_s & 0 & 0 & 0 & 0 & 0 \\ 0 & r_s & 0 & 0 & 0 & 0 \\ 0 & 0 & r_s & 0 & 0 & 0 \\ 0 & 0 & 0 & r_{rq}' & 0 & 0 \\ 0 & 0 & 0 & 0 & r_{rd}' & 0 \\ 0 & 0 & 0 & 0 & 0 & r_{ro}' \end{bmatrix} \begin{bmatrix} i_q^s \\ i_d^s \\ i_0^s \\ i_q^{r'} \\ i_d^{r'} \\ i_0^{r'} \end{bmatrix} + \begin{bmatrix} \frac{d\lambda_q^s}{dt} \\ \frac{d\lambda_d^s}{dt} \\ \frac{d\lambda_0^s}{dt} \\ \frac{d\lambda_q^{r'}}{dt} \\ \frac{d\lambda_d^{r'}}{dt} \\ \frac{d\lambda_0^{r'}}{dt} \end{bmatrix} + \begin{bmatrix} \omega_r \lambda_d^s \\ -\omega_r \lambda_q^s \\ 0 \\ 0 \\ 0 \\ 0 \end{bmatrix} + \begin{bmatrix} -\frac{2}{3} \mu r_s i_f \cos \theta_r \\ -\frac{2}{3} \mu r_s i_f \sin \theta \\ -\frac{1}{3} \mu r_s i_f \\ 0 \\ 0 \\ 0 \end{bmatrix} \quad (3.60)$$

To get the qd0-transformation of equation (3.46), the voltages are represented as;

$$\begin{aligned}
v_{a_2}^s &= \mu r_s i_a^s - \mu r_s i_f + \frac{d}{dt} \lambda_{a_2}^s = R_f i_f \\
v_{a_2}^s &= [\mu r_s \quad 0 \quad 0] K_s^{-1} i_{qd0}^s - \mu r_s i_f + \frac{d}{dt} \lambda_{a_2}^s = R_f i_f \\
v_{a_2}^s &= [\mu r_s \cos \theta_r \quad \mu r_s \sin \theta_r \quad \mu r_s] \begin{bmatrix} i_q^s \\ i_d^s \\ i_0^s \end{bmatrix} - \mu r_s i_f + \frac{d}{dt} \lambda_{a_2}^s = R_f i_f
\end{aligned} \tag{3.61}$$

The final qd0 voltage equation becomes;

$$v_{a_2}^s = \mu r_s (i_q^s \cos \theta_r + i_d^s \sin \theta_r + i_0^s - i_f) + \frac{d}{dt} \lambda_{a_2}^s = R_f i_f \tag{3.62}$$

On the other hand, the transformation of the flux current relation in equations (3.51) and (3.52) is done in the following steps. First, equation (3.51) is multiplied by the transformation matrices in addition to some matrix computation as follows:

$$\begin{bmatrix} K_s \lambda_{abc}^s \\ K_r \lambda_{abc}^r \end{bmatrix} = \begin{bmatrix} K_s L_{abc}^{ss} K_s^{-1} & K_s L_{abc}^{sr} K_r^{-1} \\ K_r L_{abc}^{rs} K_s^{-1} & K_r L_{abc}^{rr} K_r^{-1} \end{bmatrix} \begin{bmatrix} i_{qd0}^s \\ i_{qd0}^r \end{bmatrix} + \begin{bmatrix} K_s \lambda_{mabc}^s \\ K_r \lambda_{mabc}^r \end{bmatrix} + \mu \begin{bmatrix} K_s A_2 \\ K_r A_3 \end{bmatrix} i_f \tag{3.63}$$

In matrix form

$$\begin{bmatrix} \lambda_q^s \\ \lambda_d^s \\ \lambda_0^s \\ \lambda_q^{r'} \\ \lambda_d^{r'} \\ \lambda_0^{r'} \end{bmatrix} = \begin{bmatrix} L_{is} + L_{mq} & 0 & 0 & L_{mq} & 0 & 0 \\ 0 & L_{is} + L_{md} & 0 & 0 & 0 & L_{22}^{sr} \\ 0 & 0 & L_{is} & 0 & 0 & 0 \\ L_{mq} & 0 & 0 & L_{lrq}' + L_{mq} & 0 & 0 \\ 0 & L_{md} & 0 & 0 & L_{lrd}' + L_{md} & 0 \\ 0 & 0 & 0 & 0 & 0 & L_{lr0}' \end{bmatrix} \begin{bmatrix} i_q^s \\ i_d^s \\ i_0^s \\ i_q^{r'} \\ i_d^{r'} \\ i_0^{r'} \end{bmatrix} + \begin{bmatrix} 0 \\ \lambda_m^s \\ 0 \\ 0 \\ \lambda_m^{r'} \\ 0 \end{bmatrix} + \mu \begin{bmatrix} K_s \begin{bmatrix} L_{asas} \\ L_{asbs} \\ L_{ascs} \end{bmatrix} \\ K_r \begin{bmatrix} L_{asar} \\ L_{asbr} \\ L_{ascr} \end{bmatrix} \end{bmatrix} i_f \tag{3.64}$$



$$\begin{bmatrix} \lambda_q^s \\ \lambda_d^s \\ \lambda_0^s \\ \lambda_q^{r'} \\ \lambda_d^{r'} \\ \lambda_0^{r'} \end{bmatrix} = \begin{bmatrix} L_{ls} + L_{mq} & 0 & 0 & L_{mq} & 0 & 0 \\ 0 & L_{ls} + L_{md} & 0 & 0 & 0 & L_{22}^{sr} \\ 0 & 0 & L_{ls} & 0 & 0 & 0 \\ L_{mq} & 0 & 0 & L_{lrq}' + L_{mq} & 0 & 0 \\ 0 & L_{md} & 0 & 0 & L_{lrd}' + L_{md} & 0 \\ 0 & 0 & 0 & 0 & 0 & L_{lr0}' \end{bmatrix} \begin{bmatrix} i_q^s \\ i_d^s \\ i_0^s \\ i_q^{r'} \\ i_d^{r'} \\ i_0^{r'} \end{bmatrix} + \begin{bmatrix} 0 \\ \lambda_m' \\ 0 \\ 0 \\ \lambda_m' \\ 0 \end{bmatrix} - \begin{bmatrix} \mu(L_{\Delta m} + L_m + \frac{2}{3}L_{ls}) \cos \theta_r \\ \mu(L_m - L_{\Delta m} + \frac{2}{3}L_{ls}) \sin \theta_r \\ \mu \frac{1}{3}L_{ls} \\ \mu(L_{\Delta m} + L_m) \cos \theta_r \\ \mu(L_m - L_{\Delta m}) \sin \theta_r \\ 0 \end{bmatrix} \quad (3.65)$$

To get the qd0 transformation of equation (3.52), the following has been done.

$$\lambda_{a_2}^s = -\mu A_2^T K_s^{-1} i_{qd0}^s - \mu A_3^T K_r^{-1} i_{qd0}^{r'} - \mu^2 L_{asas} i_f + \mu \lambda_m \sin \theta_r \quad (3.66)$$

$$\mu A_2^T K_s^{-1} = [X_1 \quad X_2 \quad X_3] = \left[ \mu \left( \frac{3}{2}(L_{\Delta m} + L_m) + L_{ls} \right) \cos \theta_r \quad \mu \left( \frac{3}{2}(L_m - L_{\Delta m}) + L_{ls} \right) \sin \theta_r \quad \mu L_{ls} \right] \quad (3.67)$$

$$\mu A_3^T K_r^{-1} = [X_{11} \quad X_{12} \quad X_{13}] = \left[ \mu \left( \frac{3}{2}(L_{\Delta m} + L_m) \right) \cos \theta_r \quad \mu \left( \frac{3}{2}(L_m - L_{\Delta m}) \right) \sin \theta_r \quad 0 \right] \quad (3.68)$$

The final equation is

$$\lambda_{a_2}^s = X_1 i_q^s + X_2 i_d^s + X_3 i_0^s + X_{11} i_q^{r'} + X_{12} i_d^{r'} + X_{13} i_0^{r'} - \mu^2 L_{asas} i_f + \mu \lambda_m \sin \theta_r \quad (3.69)$$

The final voltage and flux-current relation of the QD0-model is represented by equations (3.60), (3.62), (3.65) and (3.69).to complete the model, the torque equation is derived as in the next section.

### 3.2.2.3 Electromagnetic Torque under Stator Inter-Turn Fault.

In addition to the modification in the voltages and flux current relations under stator inter-turns fault, the electromagnetic torque formula need to be modified [124, 167-173]. This section shows the steps for deriving the electromagnetic torque under fault in the abc model and its transformation to the qdo-model. The electromagnetic torque,  $T_{em}$ , generated by the LSPMSM can be derived from the coenergy,  $W_c$ , of the magnetic system as represented in equation (3.70) [174-176].

$$T_{em} = \frac{P}{2} \frac{\partial W_c}{\partial \theta_r} \quad (3.70)$$

$$\text{Where } W_c = \frac{1}{2} i_{a_1 a_2 bc}^{sT} L_{a_1 a_2 bc}^S i_{a_1 a_2 bc}^s + i_{a_1 a_2 bc}^{sT} L_{a_1 a_2 bc}^{sr} i_{abc}^r + \frac{1}{2} i_{abc}^{rT} L_{abc}^r i_{abc}^r + i_{a_1 a_2 bc}^{sT} \lambda_{a_1 a_2 bc} + W_{PM} \quad (3.71)$$

$W_{PM}$  is a constant representing the energy stored in the permanent magnet rotor of the LSPMSM. By substituting equation (3.71) into (3.70), the torque can be expressed in terms of the phase currents and the rotor angular position as in equation (3.72).

$$T_{em} = \frac{P}{2} \left( \underbrace{\frac{1}{2} i_{a_1 a_2 bc}^{sT} \frac{\partial L_{a_1 a_2 bc}^S}{\partial \theta_r} i_{a_1 a_2 bc}^s}_{\text{term 1}} + \underbrace{i_{a_1 a_2 bc}^{sT} \frac{\partial L_{a_1 a_2 bc}^{sr}}{\partial \theta_r} i_{abc}^r}_{\text{term 2}} + \underbrace{\frac{1}{2} i_{abc}^{rT} \frac{\partial L_{abc}^r}{\partial \theta_r} i_{abc}^r}_{\text{term 3}} + \underbrace{i_{a_1 a_2 bc}^{sT} \frac{\partial \lambda_{a_1 a_2 bc}}{\partial \theta_r}}_{\text{term 4}} \right) \quad (3.72)$$

By separating equation (3.72) into its terms and subsequently transforming them;

#### Term 1

$$\frac{1}{2} i_{a_1 a_2 bc}^{sT} \frac{\partial L_{a_1 a_2 bc}^S}{\partial \theta_r} i_{a_1 a_2 bc}^s = \frac{1}{2} \left( i_{abc}^{sT} \frac{\partial L_{abc}^S}{\partial \theta_r} i_{abc}^s + \mu i_f \frac{\partial A_2^T}{\partial \theta_r} i_{abc}^s \right) \quad (3.73)$$

### abc to qd0 transformation

$$\begin{aligned}
\frac{1}{2} \left( i_{abc}^{sT} \frac{\partial L_{abc}^s}{\partial \theta_r} i_{abc}^s + \mu i_f \frac{\partial A_2^T}{\partial \theta_r} i_{abc}^s \right) &= \frac{1}{2} \left( \left\{ K_s^{-1} i_{qd0}^s \right\}^T \frac{\partial L_{abc}^s}{\partial \theta_r} K_s^{-1} i_{qd0}^s + \mu i_f \frac{\partial A_2^T}{\partial \theta_r} K_s^{-1} i_{qd0}^s \right) \\
&= \frac{1}{2} \left( i_{qd0}^{sT} K_s^{-1T} \frac{\partial L_{abc}^s}{\partial \theta_r} K_s^{-1} i_{qd0}^s + \mu i_f \frac{\partial A_2^T}{\partial \theta_r} K_s^{-1} i_{qd0}^s \right) \\
&= \frac{1}{2} \left( \frac{9}{2} L_{\Delta m} i_{qd0}^{sT} \begin{bmatrix} 0 & -1 & 0 \\ -1 & 0 & 0 \\ 0 & 0 & 0 \end{bmatrix} i_{qd0}^s + 3 \mu i_f L_{\Delta m} [\sin \theta_r \quad \cos \theta_r \quad 0] i_{qd0}^s \right) \\
&= \frac{9}{4} L_{\Delta m} \begin{bmatrix} -i_q^s & -i_d^s & 0 \end{bmatrix} \begin{bmatrix} i_q^s \\ i_d^s \\ i_0^s \end{bmatrix} + \frac{3}{2} \mu i_f L_{\Delta m} (i_q^s \sin \theta_r + i_d^s \cos \theta_r) \\
&= -\frac{9}{2} L_{\Delta m} i_q^s i_d^s + \frac{3}{2} \mu i_f L_{\Delta m} (i_q^s \sin \theta_r + i_d^s \cos \theta_r)
\end{aligned} \tag{3.74}$$

### Term 2

$$i_{a_1 a_2 bc}^{sT} \frac{\partial L_{a_1 a_2 bc}^{sr}}{\partial \theta_r} i_{abc}^r = \left( i_{abc}^{sT} \frac{\partial L_{abc}^{sr}}{\partial \theta_r} i_{abc}^r + \mu i_f \frac{\partial A_3^T}{\partial \theta_r} i_{abc}^r \right) \tag{3.75}$$

### abc to qd0 transformation

$$\begin{aligned}
\left( i_{abc}^{sT} \frac{\partial L_{abc}^{sr}}{\partial \theta_r} i_{abc}^r + \mu i_f \frac{\partial A_3^T}{\partial \theta_r} i_{abc}^r \right) &= \frac{1}{2} \left( \left\{ K_s^{-1} i_{qd0}^s \right\}^T \frac{\partial L_{abc}^{sr}}{\partial \theta_r} K_r^{-1} i_{qd0}^r + \mu i_f \frac{\partial A_3^T}{\partial \theta_r} K_r^{-1} i_{qd0}^r \right) \\
&= \frac{1}{2} \left( i_{qd0}^{sT} K_s^{-1T} \frac{\partial L_{abc}^{sr}}{\partial \theta_r} K_r^{-1} i_{qd0}^r + \mu i_f \frac{\partial A_3^T}{\partial \theta_r} K_r^{-1} i_{qd0}^r \right) \\
&= \frac{9}{4} i_{qd0}^{sT} \begin{bmatrix} 0 & L_m - L_{\Delta m} & 0 \\ -(L_m + L_{\Delta m}) & 0 & 0 \\ 0 & 0 & 0 \end{bmatrix} i_{qd0}^r + \frac{3}{2} \mu i_f [(L_m + L_{\Delta m}) \sin \theta_r \quad -(L_m - L_{\Delta m}) \cos \theta_r \quad 0] i_{qd0}^r \\
&= \frac{9}{4} L_{\Delta m} \begin{bmatrix} -(L_m + L_{\Delta m}) i_d^s & (L_m - L_{\Delta m}) i_q^s & 0 \end{bmatrix} \begin{bmatrix} i_q^r \\ i_d^r \\ i_0^r \end{bmatrix} + \frac{3}{2} \mu i_f ((L_m + L_{\Delta m}) i_q^r \sin \theta_r - (L_m - L_{\Delta m}) i_d^r \cos \theta_r) \\
&= \frac{9}{4} (-(L_m + L_{\Delta m}) i_d^s i_q^r + (L_m - L_{\Delta m}) i_d^r i_q^s) + \frac{3}{2} \mu i_f ((L_m + L_{\Delta m}) i_q^r \sin \theta_r - (L_m - L_{\Delta m}) i_d^r \cos \theta_r)
\end{aligned} \tag{3.76}$$

### Term 3

$$\frac{1}{2} i_{abc}^{rT} \frac{\partial L_{abc}^r}{\partial \theta_r} i_{abc}^r \quad (3.77)$$

### abc to qd0 transformation

$$\begin{aligned} \frac{1}{2} i_{abc}^{rT} \frac{\partial L_{abc}^r}{\partial \theta_r} i_{abc}^r &= \frac{1}{2} \left( \{K_r^{-1} i_{qd0}^r\}^T \frac{\partial L_{abc}^r}{\partial \theta_r} K_r^{-1} i_{qd0}^r \right) \\ &= \frac{1}{2} \left( i_{qd0}^{rT} K_r^{-1T} \frac{\partial L_{abc}^r}{\partial \theta_r} K_r^{-1} i_{qd0}^r \right) \\ &= \frac{1}{2} \left( \frac{9}{2} L_{\Delta m} \begin{bmatrix} i_q^r & i_d^r & i_0^r \end{bmatrix} \begin{bmatrix} -\sin 2\theta_r & -\cos 2\theta_r & 0 \\ -\cos 2\theta_r & \sin 2\theta_r & 0 \\ 0 & 0 & 0 \end{bmatrix} \begin{bmatrix} i_q^r \\ i_d^r \\ i_0^r \end{bmatrix} \right) \\ &= \frac{9}{4} L_{\Delta m} \begin{bmatrix} -i_q^r \sin 2\theta_r - i_d^r \cos 2\theta_r & -i_q^r \cos 2\theta_r + i_d^r \sin 2\theta_r & 0 \end{bmatrix} \begin{bmatrix} i_q^r \\ i_d^r \\ i_0^r \end{bmatrix} \\ &= \frac{9}{4} L_{\Delta m} \left( -i_q^2 \sin 2\theta_r - 2i_d^r i_q^r \cos 2\theta_r + i_d^2 \sin 2\theta_r \right) \end{aligned} \quad (3.78)$$

### Term 4

$$i_{a_1 a_2 bc}^{sT} \frac{\partial \lambda_{m a_1 a_2 bc}}{\partial \theta_r} = i_{abc}^{sT} \frac{\partial \lambda_{m abc}}{\partial \theta_r} - \mu i_f \lambda_m \frac{\partial \sin \theta_r}{\partial \theta_r} = \lambda_m i_{abc}^{sT} \begin{bmatrix} \cos \theta_r \\ \cos(\theta_r - 120^\circ) \\ \cos(\theta_r + 120^\circ) \end{bmatrix} - \mu i_f \lambda_m \frac{\partial \sin \theta_r}{\partial \theta_r} \quad (3.79)$$

### ABC to QD0 transformation

$$\begin{aligned} \lambda_m i_{abc}^{sT} \begin{bmatrix} \cos \theta_r \\ \cos(\theta_r - 120^\circ) \\ \cos(\theta_r + 120^\circ) \end{bmatrix} - \mu i_f \lambda_m \frac{\partial \sin \theta_r}{\partial \theta_r} &= \lambda_m \{K_s^{-1} i_{qd0}^s\}^T \begin{bmatrix} \cos \theta_r \\ \cos(\theta_r - 120^\circ) \\ \cos(\theta_r + 120^\circ) \end{bmatrix} - \mu i_f \lambda_m \cos \theta_r \\ &= \lambda_m i_{qd0}^{sT} \begin{bmatrix} \frac{3}{2} \\ \frac{2}{2} \\ 0 \\ 0 \end{bmatrix} - \mu i_f \lambda_m \cos \theta_r = \frac{3}{2} \lambda_m i_q^s - \mu i_f \lambda_m \cos \theta_r \end{aligned} \quad (3.80)$$

The final electromagnetic torque formula is given as;

$$T_{em} = \frac{P}{2} \left\{ \begin{array}{l} -\frac{9}{2} L_{\Delta m} i_q^s i_d^s + \frac{3}{2} \mu i_f L_{\Delta m} (i_q^s \sin \theta_r + i_d^s \cos \theta_r) \\ + \frac{9}{4} (-(L_m + L_{\Delta m}) i_d^s i_q^r + (L_m - L_{\Delta m}) i_d^r i_q^s) + \frac{3}{2} \mu i_f ((L_m + L_{\Delta m}) i_q^r \sin \theta_r - (L_m - L_{\Delta m}) i_d^r \cos \theta_r) \\ + \frac{9}{4} L_{\Delta m} (-i_q^{r2} \sin 2\theta_r - 2i_d^r i_q^r \cos 2\theta_r + i_d^{r2} \sin 2\theta_r) \\ + \frac{3}{2} \lambda_m i_q^s - \mu i_f \lambda_m \cos \theta_r \end{array} \right\} \quad (3.81)$$

Hence, the equations that represent the LSPMSM under stator inter-turn fault condition are represented by equations (3.60), (3.62), (3.65), (3.69) and (3.81).

### 3.3 JMAG<sup>TM</sup> Finite Element Modeling

In this section, both the asymmetrical stator winding and stator inter-turn finite element model have been developed using JMAG<sup>TM</sup>. JMAG<sup>TM</sup> is an electromagnetic simulation program developed by JSOL Corporation. JMAG provides a 2D/3D platform to construct motor models. Material properties can be assigned to each part of the model. JMAG<sup>TM</sup> includes a material library based on commercial and industrial materials. The material properties and names are obtained from the manufacturer's data sheets and brochures. Additional materials can be easily added, along with their complete mechanical, electrical and magnetic properties. Moreover, the available material can be customized based on the application.

#### 3.3.1 JMAG Modeling under Asymmetrical Stator Winding Condition

This section summarizes the steps for creating the Finite element model of the motor under asymmetrical stator windings using JMAG<sup>TM</sup> Software, figure 3.5. As a first step, the motor geometry is created and in the second step, the material for each part of the

motor is selected. The circuit models for the stator and the rotor are implemented in the third step. Finally, the simulation conditions are set to generate the Finite element (FE) mesh. Figure 3.6 shows the motor used in this study. Table 3.1 shows the used motor parameters.

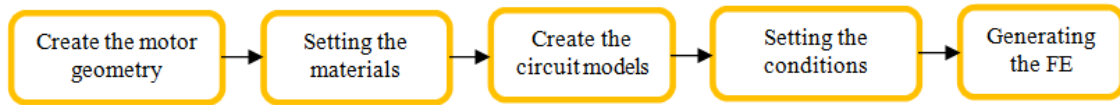


Figure 3.5 The steps for JMAG motor modeling

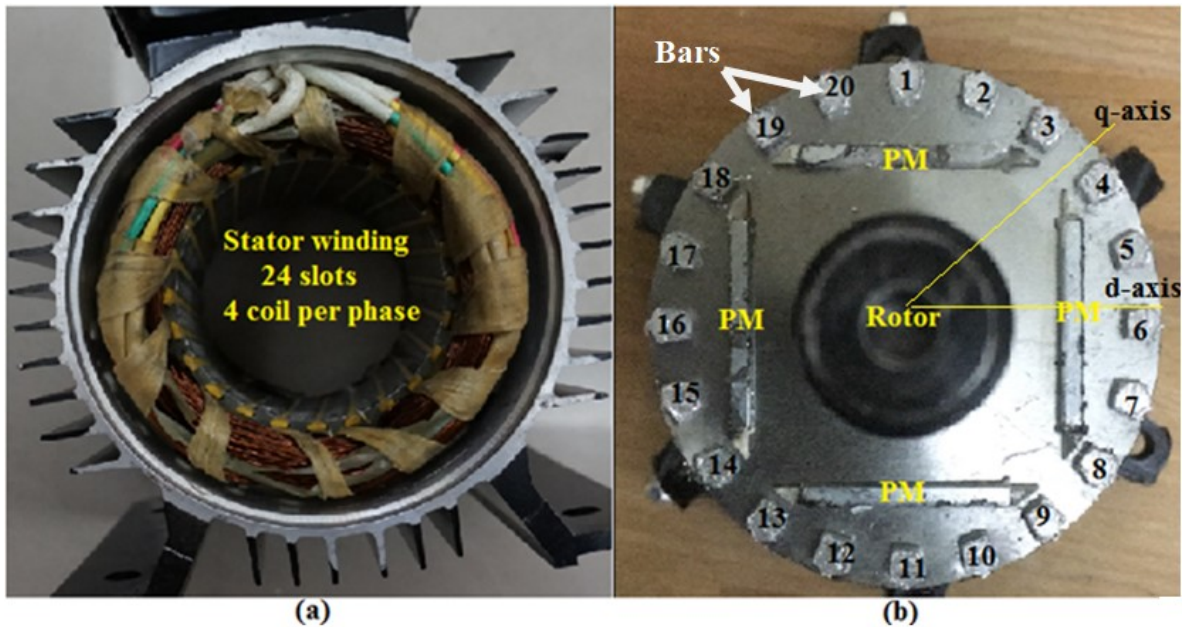


Figure 3.6 1 HP LSPMSM: (a) stator (b) rotor

Based on the literature, a 2D FEM is sufficient to investigate the motor's performance during a symmetrical stator winding and stator inter-turn fault [117, 124, 177]. Therefore, in the current research, a 2D geometry of the motor is created using AUTOCAD™. The created model has been imported to JMAG™ software from AUTOCAD™. Figure 3.7 shows the created 2D geometric model of the motor. After that, the material type for each part in the model is set as given in Table 3.2

**Table 3.1 LSPMSM Parameters**

Parameters	Value
Mean air gab radius	37.35 mm
Number of poles	4
Air gab length	0.3 mm
Permanent magnetic thickness	3 mm
Stack length	80
Number of turns per stator phase	86 *4
Rotor bar resistivity	$2.655 \cdot 10^{-8} \Omega \cdot m$
Rotor end ring resistance	$1 \cdot 10^{-5} \Omega$
Angle between two adjacent rotor bars	18
Number of bars	20
Permanent magnet flux Density	1.25T
Machine rated power	1hp
Moment of inertia	0.00158608 kg.m <sup>2</sup>
Rated voltage	400 Vrms
Rated frequency	60 Hz
Rated speed	1800 rpm
Bar length	80mm
Bar cross sectional area	27mm <sup>2</sup>

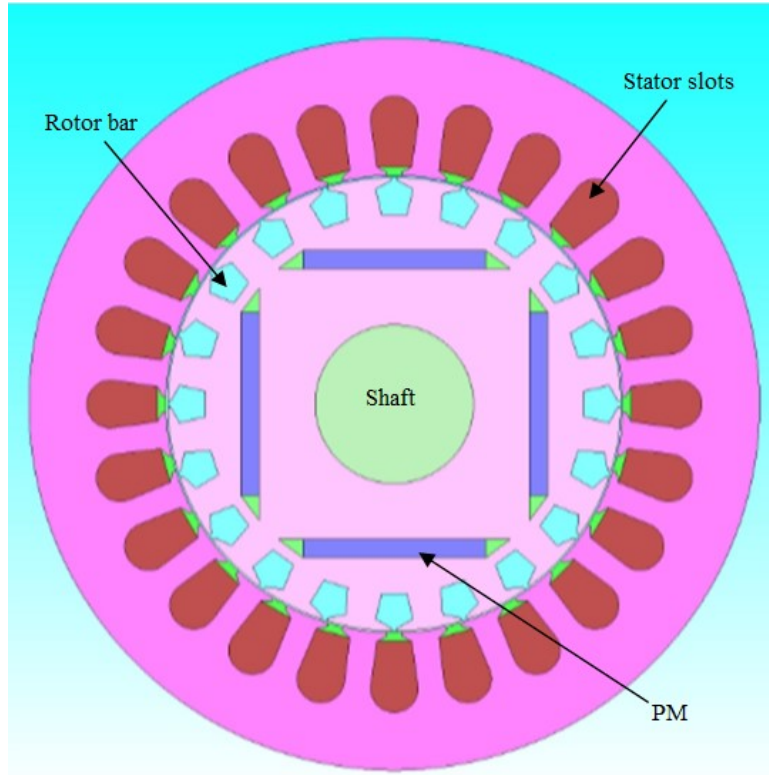


Figure 3.7 The 2-D geometry model parts of LSPMSM in JMAG™.

Table 3.2 The Materials assigned to each motor part.

Component	Material
Stator Core	Stainless Steel
Stator lamination	50JN600 - Silicon Steel
Stator Coils	Copper
Rotor Magnets	Recoma-24HE
Rotor bars	Aluminum Al99.7
Rotor lamination	50JN600 - Silicon Steel
Shaft	Steel
Air gap	Air



Each part of the geometric model should be linked to a circuit model to implement the electrical function. Figure 3.8 shows the circuit of the stator part. Each phase shown in the figure has 344 turns. It is that phase u (phase a) is composed of four coils, with each coil span two slot, while for the other two phases, each coil span 8 slots. Therefore, it is easy to introduce asymmetry in the stator winding of the motor by changing the number of turns in one of the coils of phase a.

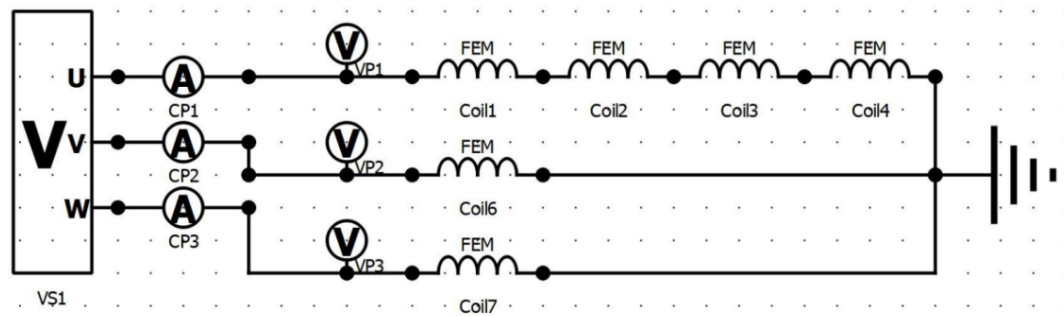


Figure 3.8 Stator winding circuit.

The third step in the modeling is to set up the conditions and rules of the analysis, which includes setting the step time for the simulation, stator and rotor circuit topologies, setting the rotation condition, and choosing the motor static parameters. The last step in modeling is to generate the mesh as shown in figure 3.9. Finally, the analysis is performed, and results are obtained.

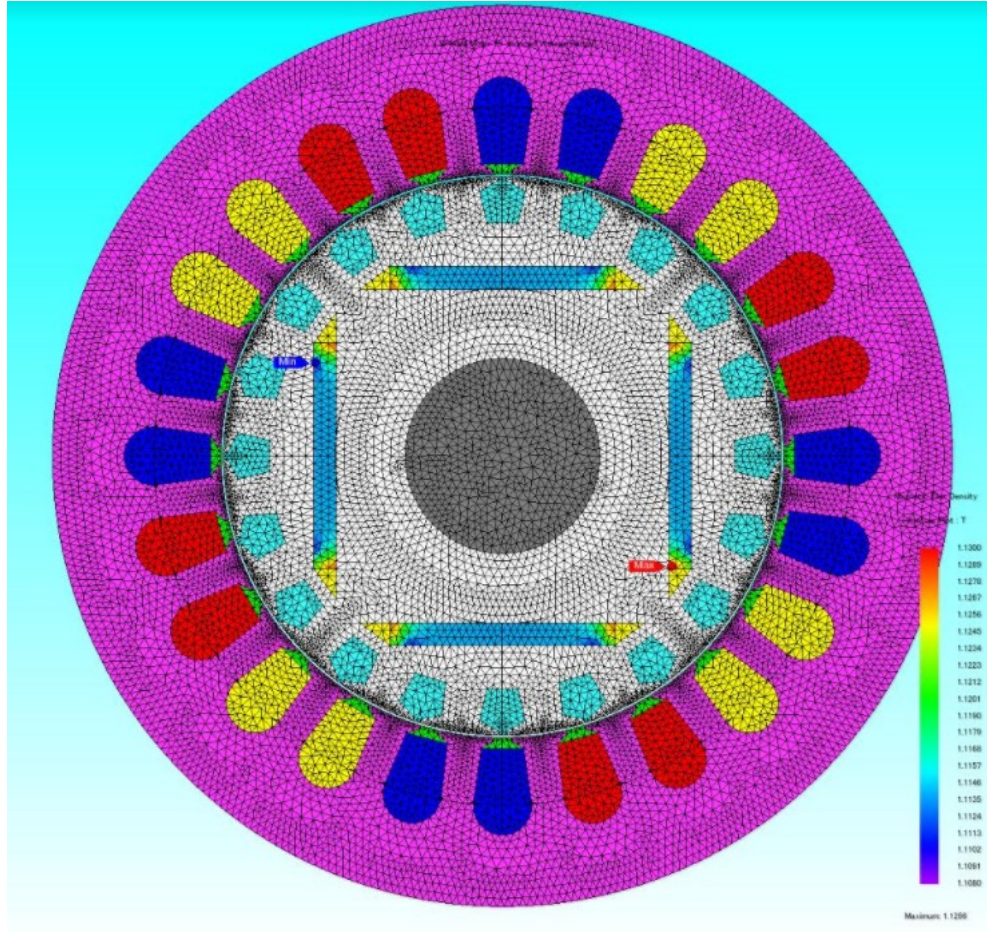
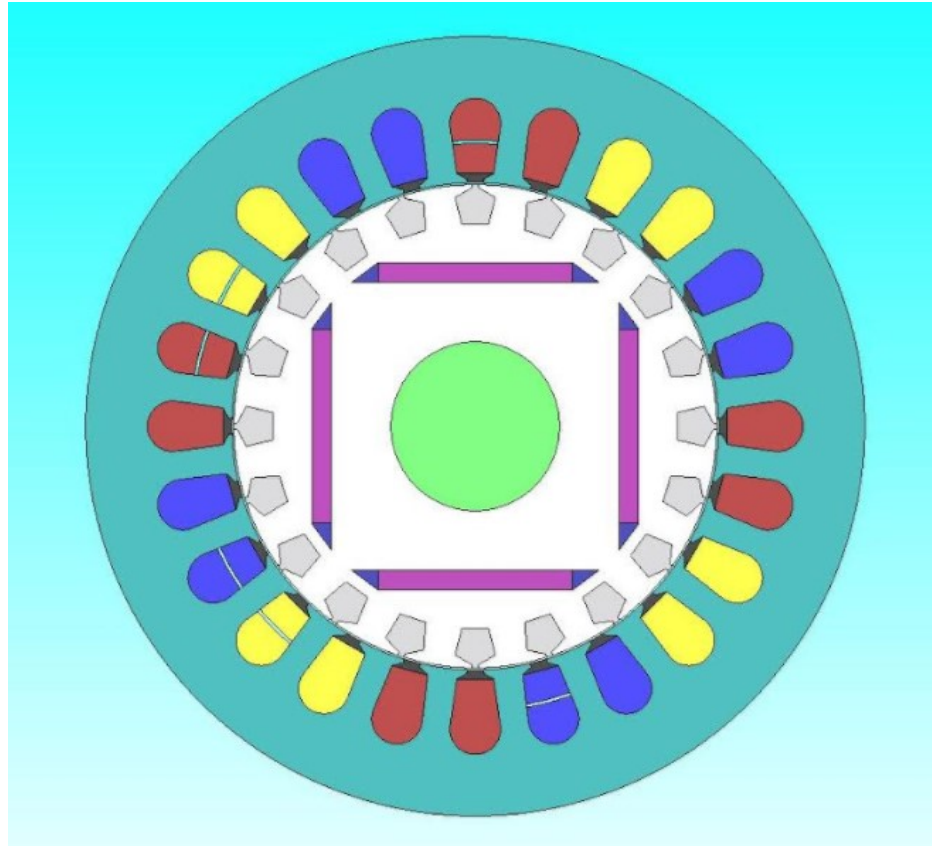


Figure 3.9 Finite element mesh

### 3.3.2 JMAG Modeling under Stator Inter-Turns Fault

In this study, FEM based model of an interior-mount LSPMSM with stator inter-turn fault was developed. In the developed model, the fault could occur in any of the phases. To create the FEM, the motor geometry was drawn using AUTOCAD™ and then imported into JMAG™. Figure 3.10 shows the 2D model's geometry. Each of the stator's phases occupies 8 slots (phase-a occupies the red slots, phase-b occupies the yellow slots, and phase-c occupies the blue slots). The figure clearly shows that one pair of each of the phases slots is split into two parts: the inner part contains the healthy turns of the faulty

phase coil, and the outer part contains the faulty turns of the same coil. After the geometry has been created, the material for each part of the motor is selected.



**Figure 3.10. 2D JMag™ geometry under stator inter-turn fault**

To implement the electrical functionality in the 2D geometric model, the rotor and stator are linked to a circuit model. The bars and end rings are linked to the rotor circuit, and the stator slots are linked to the stator circuit. Figure 3.11 shows the stator circuit. The figure clearly shows that phase-a has four coils (coil 1 to coil 4). Coils 1, 2 and 3 are linked to the unsplit red slots of figure 3.10; the healthy part of coil 4 is linked to the inner part of the split red slots; and the faulty part of coil 4 is linked to the outer part of the split red slots. The total number of turns in coil 4 (comprising both parts) is 86; therefore, it is easy to vary the number of shorted turns by changing the number of turns in the faulty

part of coil 4. In order to limit the current in the shorted turns, an external resistance ( $R_{short\_a}$ ) is used. The same analogy goes for phase-b and -c.

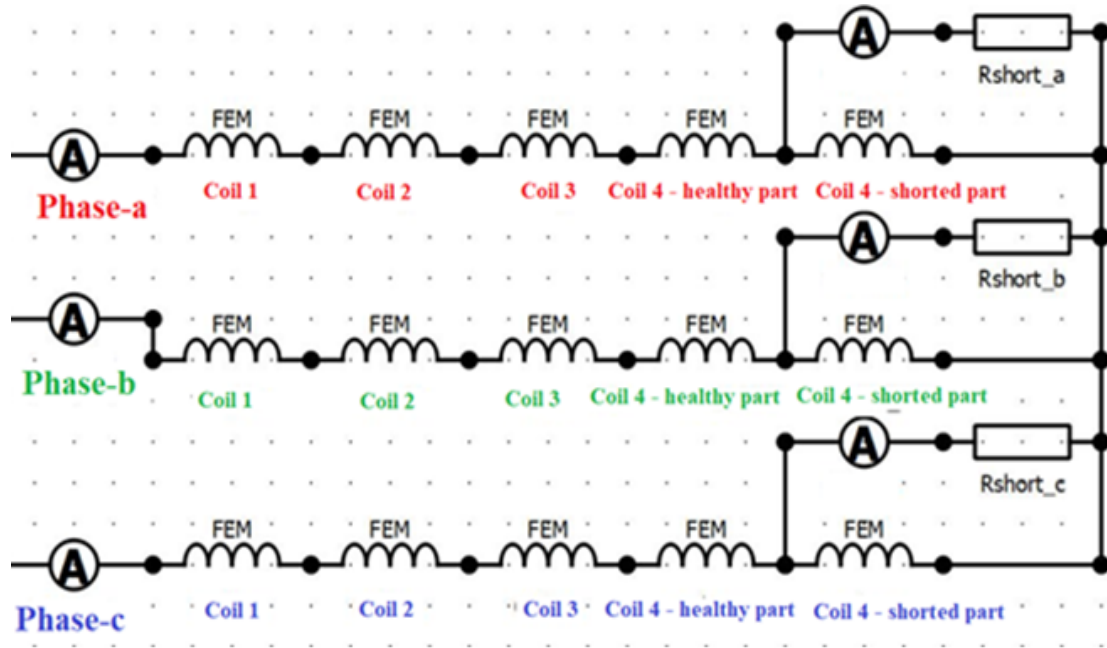


Figure 3.11 Stator winding circuit

The unknown motor parameters which needed to simulate the developed MATLAB and JMAG models have been measured for 1hp LSPMSM motors. The following chapter (chapter 4) show all experimental test which have been used in parameters identification.

## CHAPTER 4

### LSPMSM PARAMETERS IDENTIFICATION

#### 4.1 Overview

Manufactures of such commercially available machines provide the main machine parameters. Other detailed parameters which are very important for implementing various types of models and controllers are usually not given. Thus, parameter estimation is extremely important for the operators of modern drives to implement high performance models and controllers. It is also invaluable for the machine designer and manufacturers wishing to do various simulation and analysis before the prototypes are made [178-181].

There are a lot of models which describe the motor behavior such as FEM [22, 179, 182-185], qd0 reference frame [178-181, 186-189] and magnetic equation [17, 190]. Among of the models, d-q reference frame model provides optimum combination of analysis time and parameter requirements along with acceptable analysis results. Utilizing the d-q reference frame in the development process and in optimizing the LSPMSM design gives the required results in case adequate parameter measurements are obtained.

To investigate, analyze and predict the performance of LSPMSM using the derived mathematical models, an accurate equivalent circuit parameters measurement of the motor is needed. Measuring the parameters of interior-mount LSPMSM is a challenging task because the rotor configuration of the motor is very complicated since it consists of a

squirrel cage and interior mount permanent magnets. Accordingly, in this chapter, a brief description of the experimental tests conducted in the machine laboratory at KFUPM on a 1hp Interior-mount LSPMSM to measure the electric circuit parameters are given. These test include; DC test to measure the stator DC resistance, AC single phase (rotor not included) test to measure stator AC resistance and leakage inductance, block rotor test to measure rotor resistance and leakage inductance in both d and q-axis, DC step test to measure the magnetizing inductance in d and q-axis, and the open circuit test to measure the flux linkage from the permanent magnets [191-194]. The next sections give details of each test show in figure 4.1.



Figure 4.1 Laboratory tests

## 4.2 DC Test

The aim of this test is to find the dc resistance of the stator winding [195, 196], which is defined as the resistance of the winding between a phase terminal and the center of the windings (neutral point in star connected stator winding). To perform this test, two digital multimeters are needed, in addition to a variable DC power supply as shown in figure 4.2.





Figure 4.2 DC test setup

A variable DC voltage is applied between the terminals of two phases, as shown in Figure 4.3 and the voltage and the corresponding current are recorded. It is worth to mention that the effect of the inductance in the winding is neglected since the applied voltage is DC (zero frequency). Based on Kirchhoff voltage law, the formula for calculating the stator resistance is given as;

$$R_s = \frac{V_{DC}}{2I_{DC}} \quad (4.1)$$

Where  $V_{DC}$  and  $I_{DC}$  are the measured DC voltage and current, respectively.

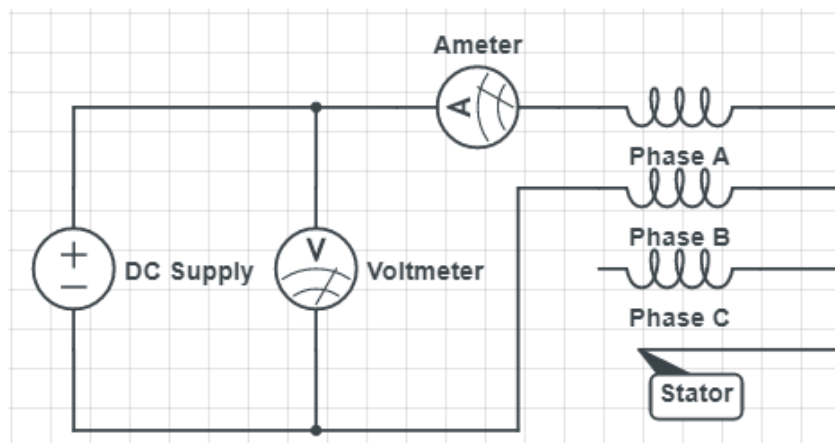


Figure 4.3 DC test circuit diagram

Table 4.1 shows the DC test result for the tested motor. Table 4.1 presents ten sets of test results, which were used to find the average value of DC stator resistance.

**Table 4.1 DC test results**

$V_{DC}$ (V)	$I_{DC}$ (A)	$R_s$ ( $\Omega$ )
5.3	0.495	5.35
6.61	0.62	5.33
7.56	0.71	5.32
8.443	0.8	5.28
9.53	0.89	5.35
10.96	1.03	5.32
11.94	1.14	5.24
12.72	1.19	5.34
13.91	1.293	5.38
14.93	1.394	5.36
Average Value		5.33

It should be noted that the value of the stator resistance in the DC test is not the same value used in AC simulation. Hence in DC test, the skin effect that occurs when an AC voltage is applied to the windings is neglected [196, 197]. Therefore, more details concerning the correction of stator resistance can be found in the single-phase without rotor test proposed further in this study. Stator resistance value of DC test is used later in the step DC test (section 4.5).



### 4.3 Single Phase AC Test (Rotor not Included)

The goal of this test is to measure the stator phase AC resistance ( $r_s$ ) and leakage inductance ( $L_{ls}$ ) [198]. In this test, a variable AC voltage is applied to a phase of the stator, when the rotor is pulled out. Figure 4.4 shows the circuit diagram of the test. Based on circuit analysis, the resistance  $r_s$  and the inductance  $L_{ls}$  can be calculated by using equation (4.2) and (4.3) respectively as follow:

$$r_s = \frac{V_\phi}{I_\phi} \cos \theta \quad (4.2)$$

$$L_{ls} = \left(\frac{1}{2\pi f}\right) * \left(\frac{V_\phi}{I_\phi} \sin \theta\right) \quad (4.3)$$

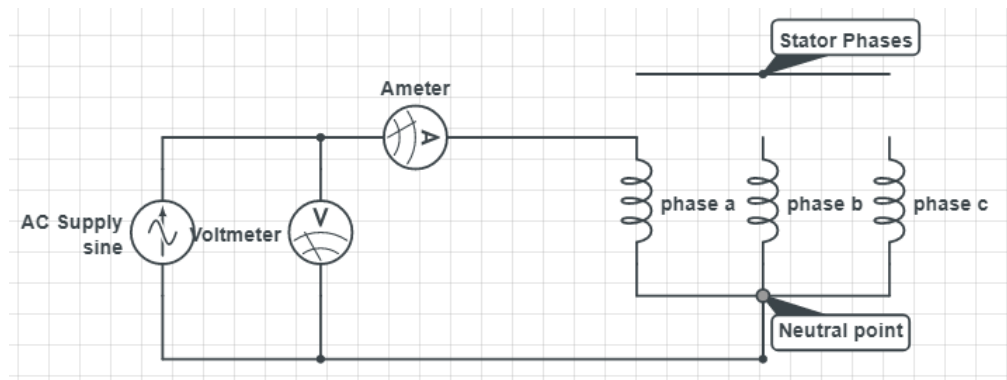


Figure 4.4 circuit diagram of single phase AC without rotor test

Using equation (4.2) and (4.3), the applied phase voltage ( $V_\phi$ ), the corresponding current ( $I_\phi$ ) and the phase shift ( $\theta$ ) between them are required to calculate stator resistance and leakage inductance. Therefore, an AC power supply, ammeter, voltmeter, CASSY unit and a computer were used to perform the test as shown in Figure 4.5. Figure 4.6 shows a

sample of the voltage and current waveforms acquired with a CASSY and from which the angle between the voltage and current is measured.

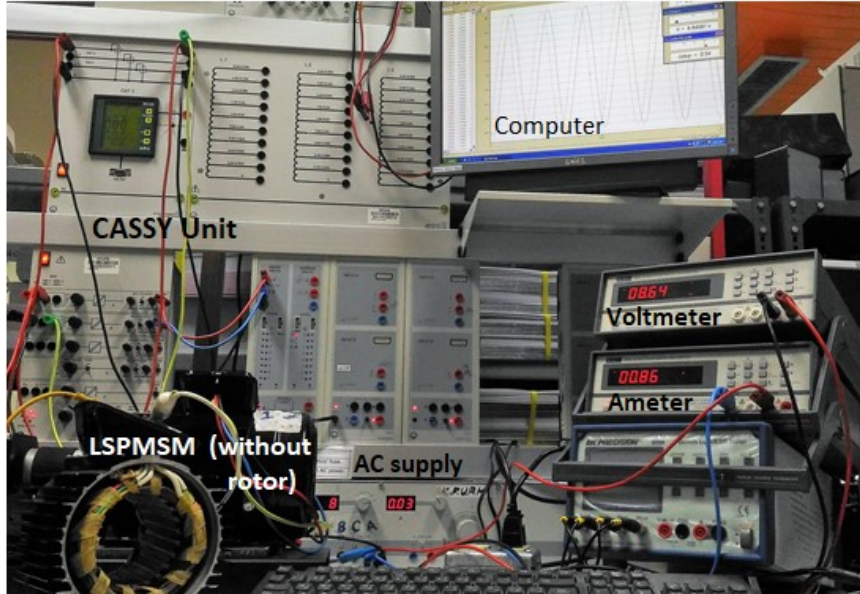


Figure 4.5 Experimental set-up for single phase AC test without rotor

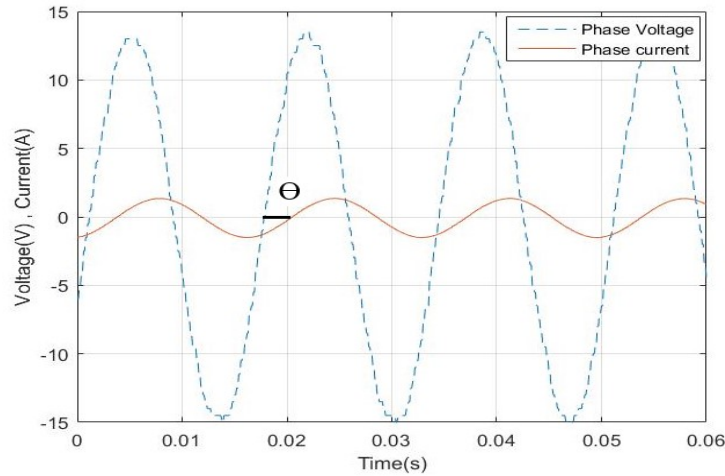


Figure 4.6 Voltage and current waveforms using CASSY unit

The results of the test are listed in Table 4.2. The values of AC stator resistance and leakage inductance are  $5.55\Omega$  and  $22.27\text{mH}$ , respectively. It is worth mentioning that these values are close to the measured by the CPC 100 device (Multi function primary test system for power transformers, current transformers, voltage transformers, rotating

machines, grounding systems, lines and cables, and circuit breakers) when the rotor was pulled out ( $r_s=5.46 \Omega$  and  $L_{ls}=22.55$  mH).

**Table 4.2 Single phase AC without rotor test Results**

$V_\phi$ (V)	$I_\phi$ (A)	$\theta$ (Deg)	$r_s$ ( $\Omega$ )	$L_{ls}$ (H)
15.31	1.529	56.63	5.51	0.022
17.71	1.7687	56.63	5.51	0.022
21.154	2.108	56.63	5.52	0.022
23.811	2.363	56.63	5.54	0.022
26.98	2.671	56.63	5.56	0.022
29.44	2.9	55.94	5.68	0.022
Average Value			5.55	0.022

#### 4.4 Blocked Rotor Test

In the blocked rotor test, both resistance and leakage inductance of the rotor can be measured [199, 200]. To perform the test on a LSPMSM, a set of low three-phase voltages are applied at the stator phases, while the rotor is blocked ( $\omega_r = 0$ ), Figure 4.7. Under the condition that the three-phase voltages applied to the tested machine are much lower compared to the rated voltages, the magnetizing branches ( $L_{mq}$  and  $L_{md}$ ) can be considered as open circuit. In addition, because the rotor is blocked ( $\omega_r = 0$ ), all dependent sources are shorted. Therefore, the q-axis equivalent circuit of LSPMSM is reduced to a series circuit that consists of stator resistance, stator leakage inductance, rotor resistance in q-axis ( $r'_{rq}$ ) and rotor leakage reactance in q-axis ( $L'_{lrq}$ ), as shown in Figure 4.8.a. Also, the d-axis circuit is reduced to a series circuit which consists of four

elements: stator resistance, stator leakage inductance, rotor resistance in d-axis ( $r'_{rd}$ ) and rotor leakage reactance in d-axis ( $L'_{lrd}$ ), as shown in Figure 4.8.b.

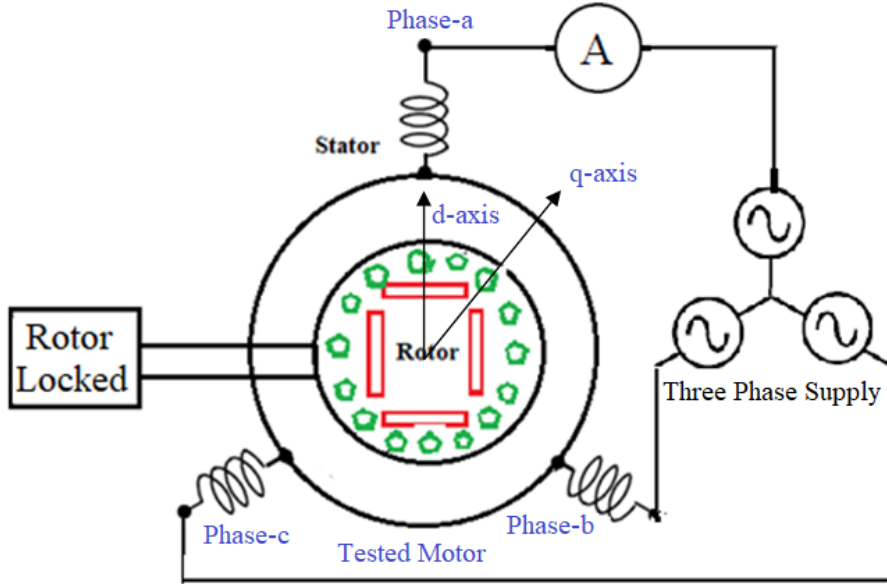


Figure 4.7 schematic diagram of locked rotor test

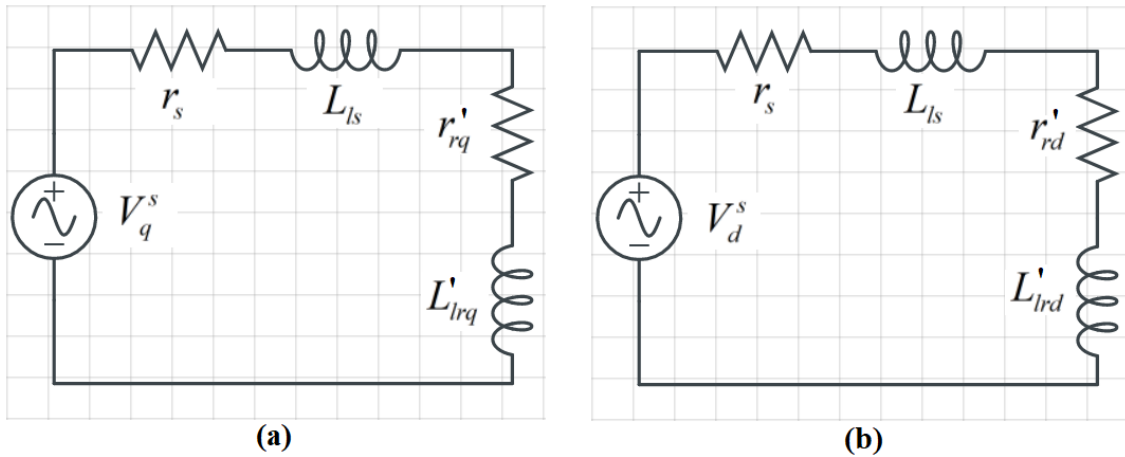


Figure 4.8 LSPMSM circuit under blocked rotor conditions (a) q-circuit (b) d-circuit

To calculate the d and q axis rotor parameters, the test is done for two different locked rotor positions; first the  $d$ -axis is aligned with phase a, and secondly the  $q$ -axis is aligned with phase a. The motor d-axis parameters ( $r'_{rd}$  and  $L'_{lrd}$ ) can be calculated when the rotor d-axis is aligned with phase-a. To place the rotor in the first locked rotor position, phase

$a$  of the motor is connected to the positive terminal of a DC supply while phases  $b$  and  $c$  are connected to the negative terminal of that supply. A three-phase low voltage is subsequently applied at the stator phases, where the phase voltage ( $V_\phi$ ), phase current ( $I_\phi$ ) and the angle ( $\theta$ ) between them are measured. Figure 4.9 shows the laboratory experimental setup of the blocked rotor test. The results of the test are displayed in Table 4.3. By using these results, the d-axis equivalent resistance ( $R_{id}$ ) and reactance ( $X_{id}$ ) referred to the stator side are calculated using equation (4.4) and (4.5). The results are shown in Table 4.3.

$$R_{id} = \frac{V_\phi}{I_\phi} \cos \theta = r_s + r'_{rd} \quad (4.4)$$

$$X_{id} = \frac{V_\phi}{I_\phi} \sin \theta = X_{ls} + X'_{lrd} \quad (4.5)$$

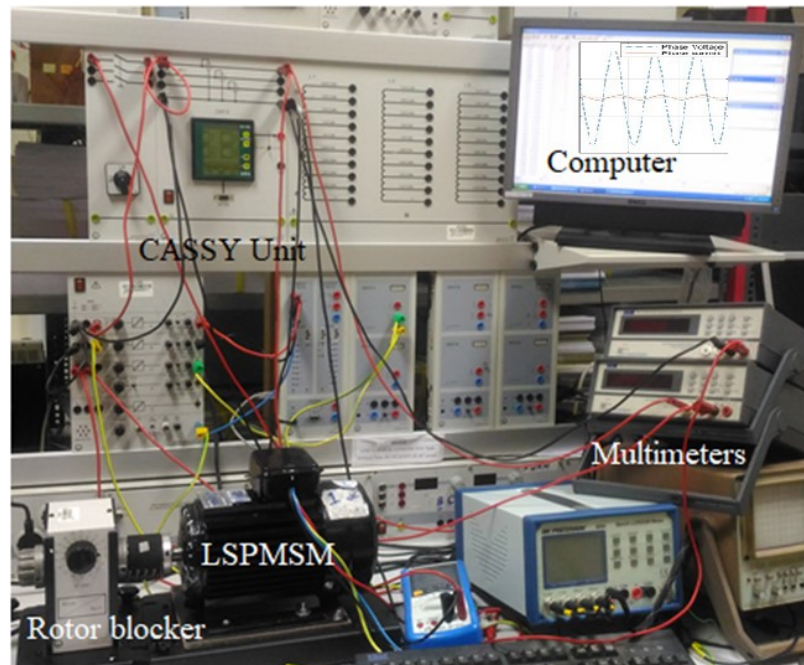


Figure 4.9 Blocked rotor test experimental set-up

**Table 4.3 locked rotor test result (rotor d-axis aligned with phase a)**

$I_{\phi}$ (A)	$V_{\phi}$ (V)	$\theta$ (deg)	$R_{id}$ ( $\Omega$ )	$X_{id}$ ( $\Omega$ )	$r'_{rd}$ ( $\Omega$ )	$L'_{lrd}$ (H)
0.72	13.59	50.21	12.05	14.47	6.50	0.016
1.04	20.19	50.21	12.46	14.96	6.91	0.017
1.49	29.17	50.21	12.50	15.01	6.95	0.018
1.79	36.18	50.21	12.92	15.51	7.36	0.019
2.56	45.00	50.21	12.27	14.74	6.72	0.017
Average value					6.89	0.017

To place the rotor in the second locked rotor position (rotor q-axis aligned with phase-a), phase *b* of the motor is connected to the positive terminal of a DC supply while phase *c* is connected to the negative terminal of that supply but phase-*a* is kept floating. The same measurements done for the first locked rotor position are repeated. The voltage and current wave forms for the both locked rotor positions are plotted as shown in Figure 4.10. Where figure 4.10-a corresponds to d-axis alignment and figure 4.10-b corresponds to q-axis alignment. The results of this test are given in Table 4.4. Equations (4.4) and (4.5) are modified by replacing subscript “d” with “q” to calculate the q-axis equivalent resistance ( $R_{iq}$ ) and reactance ( $X_{iq}$ ) referred to the stator side. It is clear from these results that the q and d rotor leakage inductances are very close to each other.

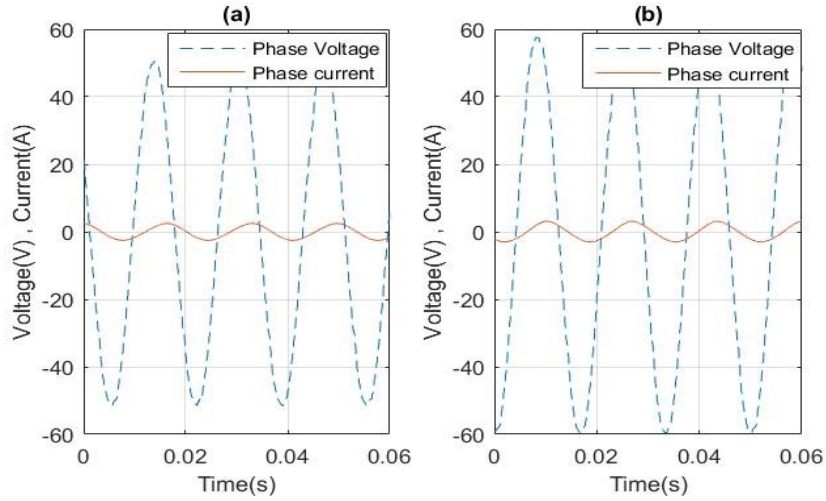


Figure 4.10 Locked rotor test current and voltage wave form (a) d-axis (b) q-axis

Table 4.4 locked rotor test result (rotor q-axis aligned with phase a)

$I_{\phi}$ (A)	$V_{\phi}$ (V)	$\theta$ (deg)	$R_{iq}$ ( $\Omega$ )	$X_{iq}$ ( $\Omega$ )	$r'_{rq}$ ( $\Omega$ )	$L'_{lrq}$ (H)
0.748	15.98	45.41	14.99	15.21	9.44	0.018
1.055	22.52	45.41	14.98	15.20	9.43	0.018
1.5	33.38	45.41	15.62	15.85	10.07	0.020
2.11	41.86	45.41	13.93	14.13	8.37	0.015
2.51	50.69	45.41	14.18	14.38	8.62	0.016
Average value					9.19	0.017

It is worth mentioning that the result obtained from the blocked rotor test are close to the those measured by CPC100 ( $r'_{rd} = 7.12\Omega$ ,  $L'_{lrd} = 16.71mH$ ,  $r'_{rq} = 8.92\Omega$  and  $L'_{lrq} = 18.12mH$ ).

## 4.5 DC Step Test

The goal of DC step response test is to measure the  $d$ - and  $q$ -axis synchronous inductances ( $L_d$  and  $L_q$ ) [201, 202]. In this test, the rotor of tested machine is locked in two distinct positions, where in the first the  $d$ -axis is aligned with phase-a to measure  $L_d$ , and in the second the  $q$ -axis is aligned with phase-a to measure  $L_q$ . Figure 4.11 shows the schematic diagram of the DC step test conducted for the case when  $d$ -axis is aligned with stator phase-a.

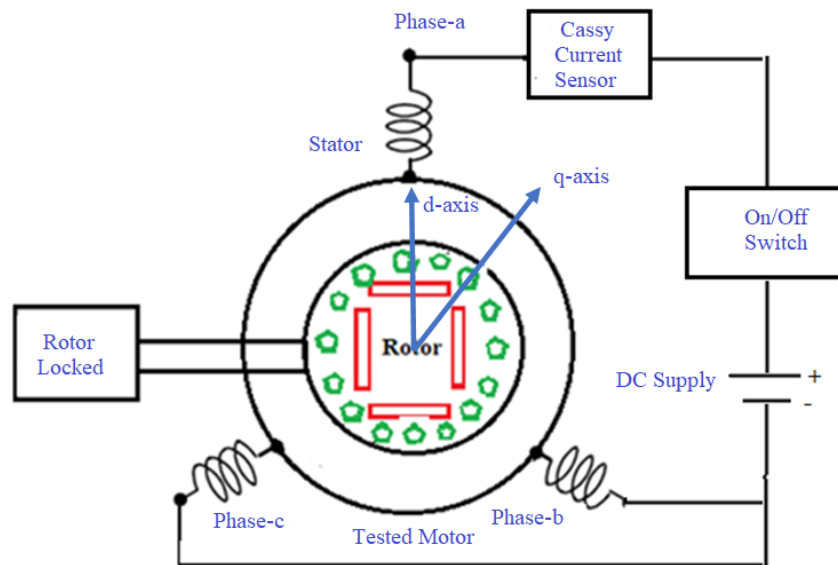


Figure 4.11 Schematic diagram of step DC test

Based on circuit theory, the equivalent circuit of the tested motor during the test is a resistance- inductance circuit, as shown in Figure 4.12. Therefore, the current in the circuit can be described by equation (4.6):

$$i(t) = \frac{V}{R} (1 - e^{-\frac{t}{\tau}}) \quad t \geq 0$$

$$\tau = \frac{L_t}{R}$$
(4.6)



Where  $V$  is the DC source voltage,  $\tau$  is the time constant,  $R$  is the equivalent resistance seen by the source which is equal to  $1.5R_s$ ,  $L_t$  is the equivalent inductance seen by the source which is equal to  $1.5L$ ,  $R_s$  is the DC resistance value measured in section 4.2.  $L$  is the inductance of the motor which is a function of the rotor position.  $L$  can be replaced by  $L_d$  if the rotor  $d$ -axis is aligned with phase-a, or  $L_q$  if the rotor  $d$ -axis is aligned with phase-a.

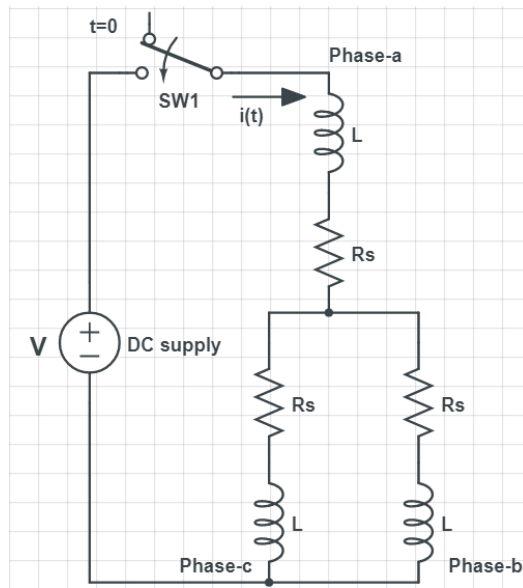


Figure 4.12 Equivalent circuit of tested machine under step DC test

Figure 4.13 shows the step response of the tested machine for the two locked rotor positions. The test was repeated for a set of DC voltages, whereby the time constant was calculated from the plots. The calculated values of  $L_d$  and  $L_q$  are listed in Table 4.5 and 4.6.

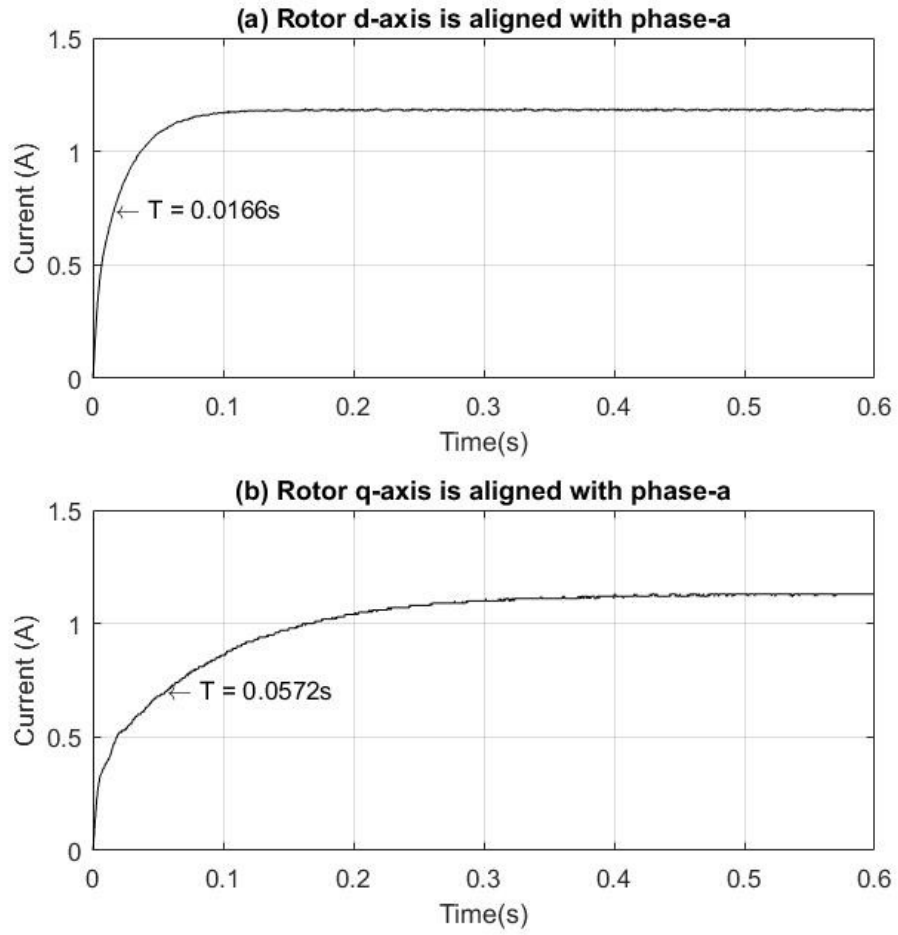


Figure 4.13 Step response of the tested motor

Table 4.5 Step DC test result- rotor d-axis aligned with phase-a

V (volt)	$\tau$ (s)	R( $\Omega$ )	$L_d$ (H)
1.4	0.0163	7.99	0.0868
3.2	0.0171		0.0911
5.07	0.0188		0.1002
7.15	0.0172		0.0916
9.43	0.0166		0.0884
10	0.0178		0.0948
10.5	0.0181		0.0965
11	0.0189		0.1006
Average value			0.0937

**Table 4.6 Step DC test result- rotor q-axis aligned with phase-a**

V (volt)	$\tau$ (s)	R( $\Omega$ )	$L_q$ (H)	
1.76	0.0524	7.99	0.2792	
3.44	0.0515		0.2743	
5.6	0.0513		0.2733	
7.2	0.0529		0.2818	
9.02	0.0572		0.3047	
9.7	0.056		0.2983	
10.3	0.0501		0.2669	
10.8	0.053		0.2823	
Average value			0.2826	

The magnetizing inductances ( $L_{md}$  and  $L_{mq}$ ) can be calculated using equation (4.7) as follows:

$$\begin{aligned} L_{md} &= L_d - L_{ls} = 0.0938 - 0.0223 = 71.5mH \\ L_{mq} &= L_q - L_{ls} = 0.2826 - 0.0223 = 260.3mH \end{aligned} \quad (4.7)$$

## 4.6 Open Circuit Test

The flux linkage ( $\lambda'_m$ ) created by the permanent magnets (PMs) on the stator side can be measured by using the open circuit test [163, 203]. In this test, the tested motor is driven by a DC motor as a prime mover, whereby the tested motor phases are kept open (no supply is connected to the motor). Figures 4.14 and 4.15 show the schematic and experimental setup, respectively.

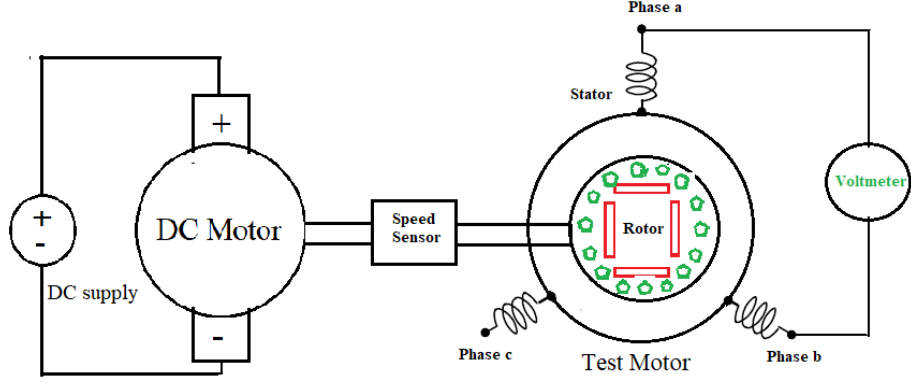


Figure 4.14 Open circuit test diagram

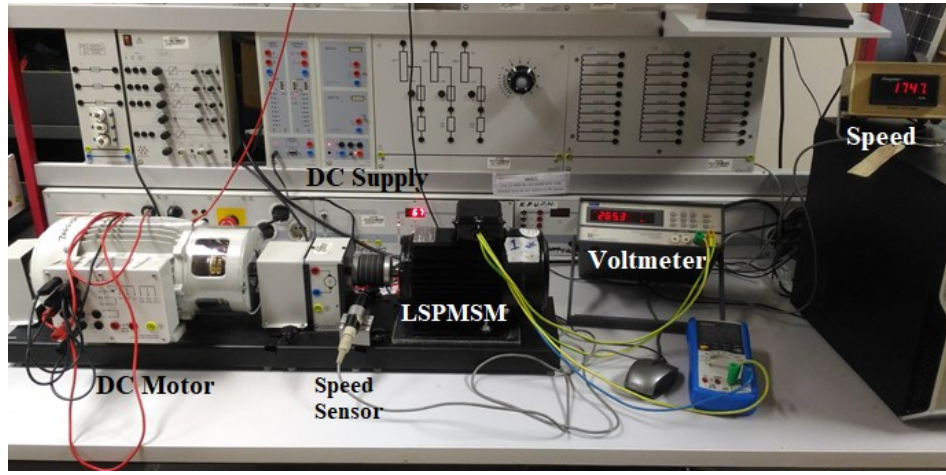


Figure 4.15 Experimental set-up of the open circuit test

Since the stator is kept open, there is no current through the stator windings. Besides, an induced voltage is generated in the stator of the tested machine. Therefore, there is no induced current through the rotor bars. Accordingly, under these conditions the  $d$ - and  $q$ -axis stator voltages and flux-current are represented in equations (4.8) and (4.9):

$$\begin{aligned}\lambda_q^s &= (L_{ls} + L_{mq})i_q^s + L_{mq}i_q^r & \rightarrow & \lambda_q^s = (L_{ls} + L_{mq})0 + L_{mq}0 \\ \lambda_d^s &= (L_{ls} + L_{md})i_d^s + L_{md}i_d^r + \lambda_m' & \rightarrow & \lambda_d^s = (L_{ls} + L_{md})0 + L_{md}0 + \lambda_m'\end{aligned}\quad (4.8)$$

$$\begin{aligned}v_q^s &= \frac{d}{dt}\lambda_q^s + r_s i_q^s + \omega_r \lambda_d^s & \rightarrow & v_q^s = 0 + r_s 0 + \omega_r \lambda_m' \\ v_d^s &= \frac{d}{dt}\lambda_d^s + r_s i_d^s - \omega_r \lambda_q^s & \rightarrow & v_d^s = 0 + r_s 0 - \omega_r 0 = 0\end{aligned}\quad (4.9)$$

Therefore, from equation 4.9

$$\lambda'_m = \frac{v_q^s}{\omega_r} = \frac{\sqrt{2}V_{ab}}{\sqrt{3}\omega_r} = \frac{\sqrt{2}V_{ab}}{\sqrt{3}\omega_m \frac{P}{2}} = \frac{\sqrt{2}V_{ab}}{\sqrt{3} \frac{P}{2} \left(\frac{2\pi n_m}{60}\right)} = \frac{60\sqrt{2} V_{ab}}{\sqrt{3} P \pi n_m} \quad (4.10)$$

The test has been done for a set of different rotor speeds ( $n_m$ ), from which the line voltage  $V_{ab}$  was measured and the results are listed in Table 4.7. Equation 4.10 is used to calculate the flux. Also, Figure 4.17 (a) shows the induced voltage waveform in stator winding at 1060 rpm rotor speed, while Figure 4.17 (b) shows the relationship between the rotor speed and the induced voltage in the stator during open circuit. It is clear from the figure that the relation between the speed and induced voltage almost linear.

**Table 4.7 Open circuit test results**

$n_m(\text{rpm})$	$V_{ab}(\text{V})$	$\lambda'_m(\text{Wb})$
418	63.1	0.5885
494	74.5	0.5879
536	81.2	0.5905
630	95.7	0.5921
697	106	0.5928
1308	199	0.5931
1404	213.4	0.5925
1506	228.8	0.5922
1601	243.4	0.5926
1701	258.3	0.5919
1800	272.8	0.5908
1847	280.9	0.5928
Average value		0.5915

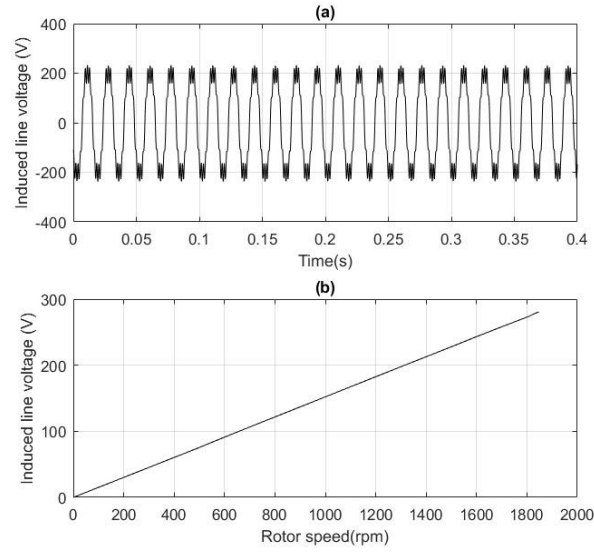


Figure 4.16 (a). Induced line voltage at 1060rpm rotor speed (b) relation between rotor speed and induced line voltage

## 4.7 Parameters Identification Summary

Using the above described experimental tests, the measured values are listed in Table 4.8. However, the listed parameters are approximate values due to human errors, instrumentation errors and environmental condition. The measured parameters are used in the simulation of the developed mathematical model in the following chapters.

Table 4.8 Tested motor measured parameters

Parameters	value	Parameters	value
$r_s$ ( $\Omega$ )	5.55	$L'_{lrq}$ (H)	0.0174
$L_{ls}$ (H)	0.0223	$L_{md}$ (mH)	71.5
$r'_{rd}$ ( $\Omega$ )	6.89	$L_{mq}$ (mH)	260.36
$L'_{lrd}$ (H)	0.0174	$\lambda'_m$ (Wb)	0.5915
$r'_{rq}$ ( $\Omega$ )	9.19		

# CHAPTER 5

## TESTING AND VALIDATION OF THE DEVELOPED MODELS

### 5.1 Overview

The aim of the work presented in this chapter is to test and validate the developed Mathematical models of LSPMSM under healthy, asymmetric stator winding and inter-turn fault. MATLAB and finite element simulation analysis as well as experimental tests are done. The simulation and experimental tests are carried out for the 1 hp interior-mount LSPMSM with parameters given in table 5.1. The implemented model has been simulated under different loading conditions for balanced three phase source. The Cassy system (Software, sensor and Profi-Cassy) and the isolation amplifier are used for acquiring motor speed, voltage and the current response as displayed in the experimental setup of Figure 5.1. It is worth mentioning that the resolution of the analog to digital converter in cassy system is 12 bits.

**Table 5.1 Tested motor parameters**

<i>Parameter</i>	<i>Value</i>	<i>Parameter</i>	<i>Value</i>	<i>Parameter</i>	<i>Value</i>	<i>Parameter</i>	<i>Value</i>
$N$ (rpm)	1800	$r'_{rd}(\Omega)$	6.887	$L'_{lrq}(mH)$	17	$L'_d(mH)$	88.796
$F$ (Hz)	60	$\lambda'_m$ (Wb)	0.591	$L'_{lrd}(mH)$	17.3	power	1 hp
$N_s$ (turns)	344	$L_{md}(mH)$	71.496	$r'_{rq}(\Omega)$	9.187	$P$	4
$r_s$ ( $\Omega$ )	5.55	$L_{mq}(mH)$	260.355	$L_d^s(mH)$	93.496	PF	0.94
$L_{ls}$ (mH)	22	$L_q^s(mH)$	282.355	$L'_q(mH)$	277.355	Torque	4 N.m

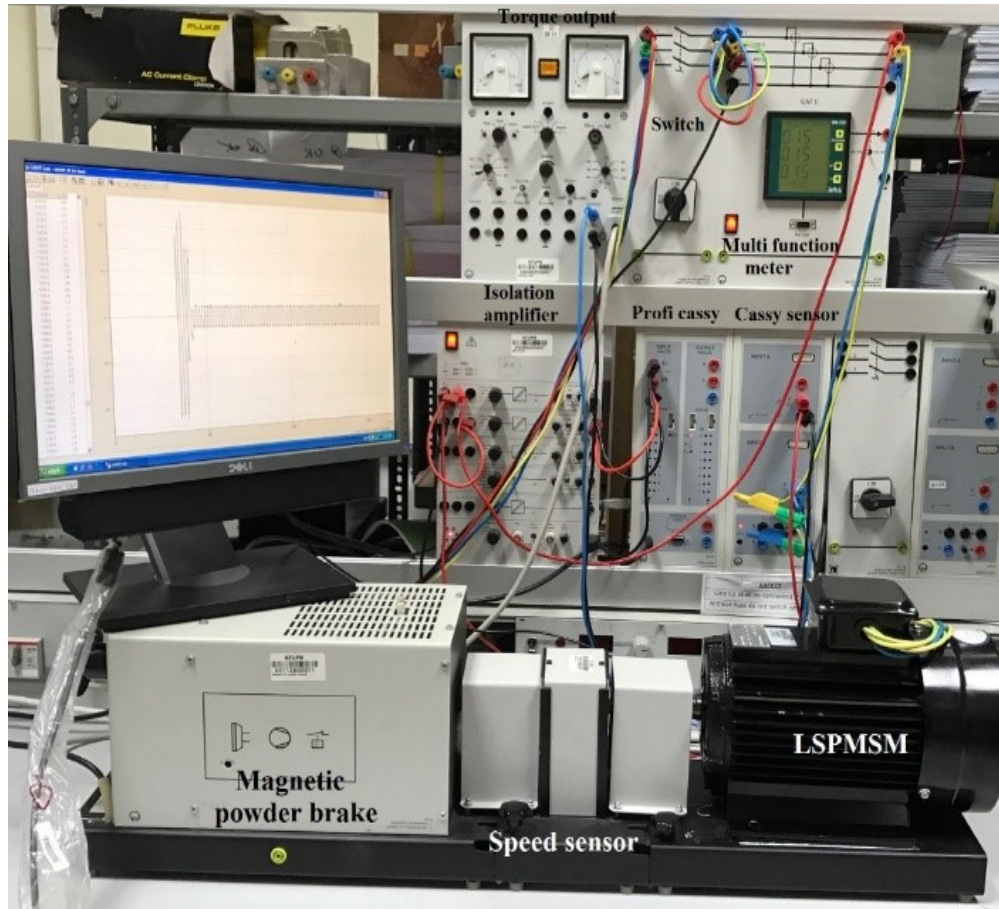


Figure 5.1 Experimental set-up

## 5.2 Testing of the Healthy LSPMSM

To test the principle of operation of the LSPMSM, the developed MATLAB and JMAG models have been simulated under the healthy condition of the motor with different loading levels. The stator current and the motor speed obtained from MATLAB model, JMAG software and the experimental setup, under no load, 2 N.m load and full load conditions are shown in Figures 5.2 to 5.4, respectively. It is clear that the MATLAB simulation results obtained from the derived mathematical model are in good agreement with the results obtained using JMAG software and experimental set-up.



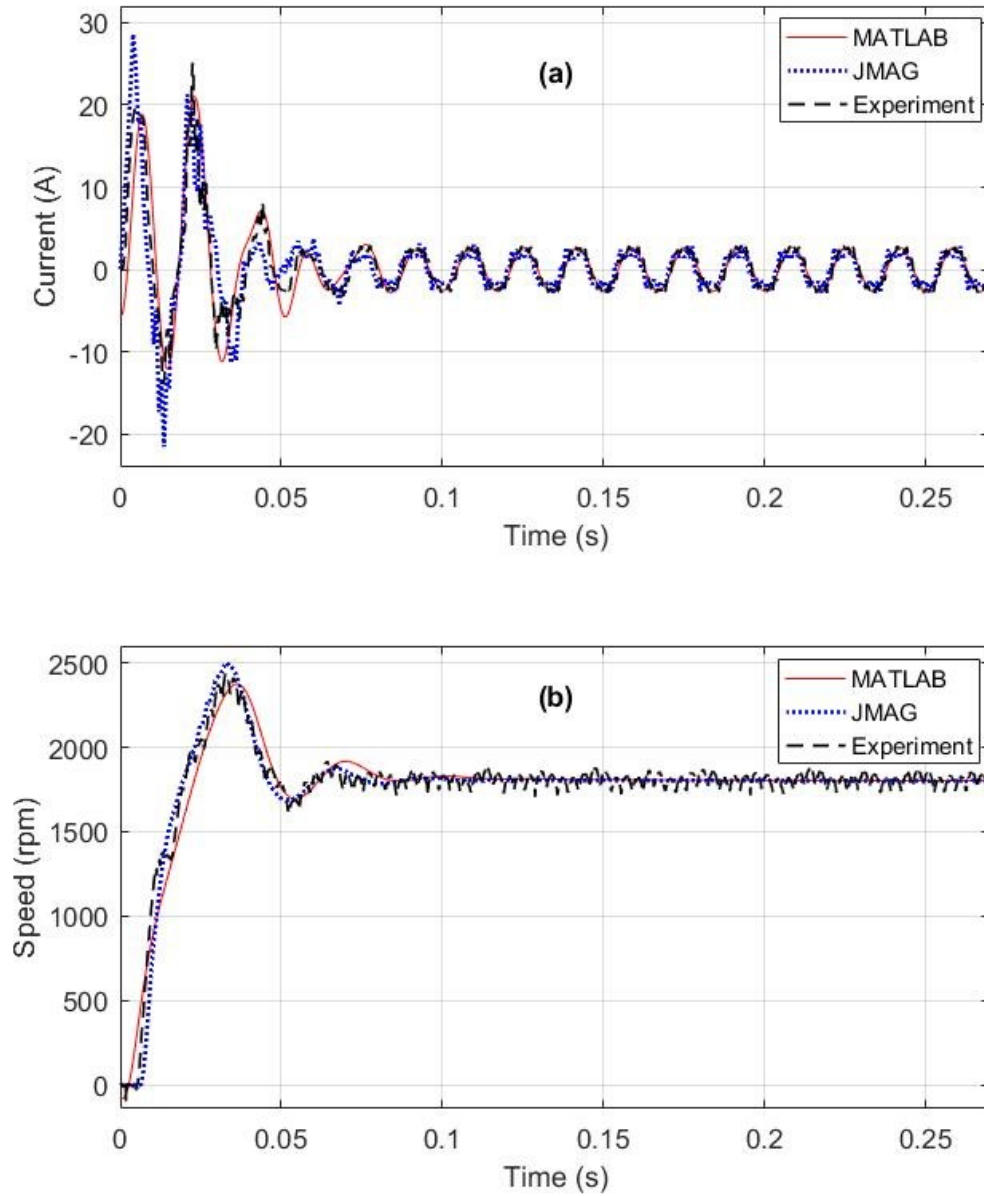


Figure 5.2 Healthy motor at no load (a) Stator phase-a current (b) speed

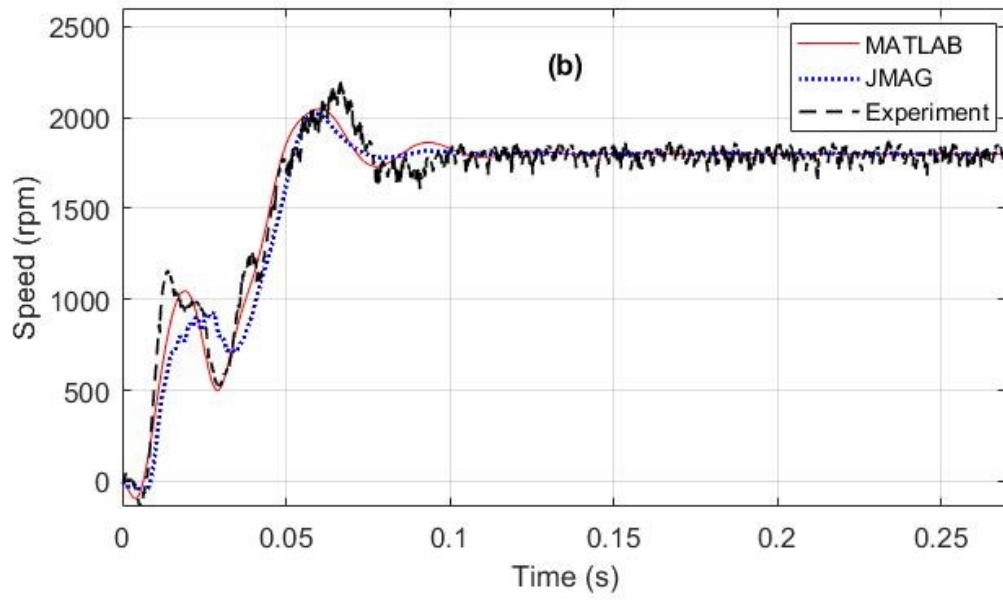
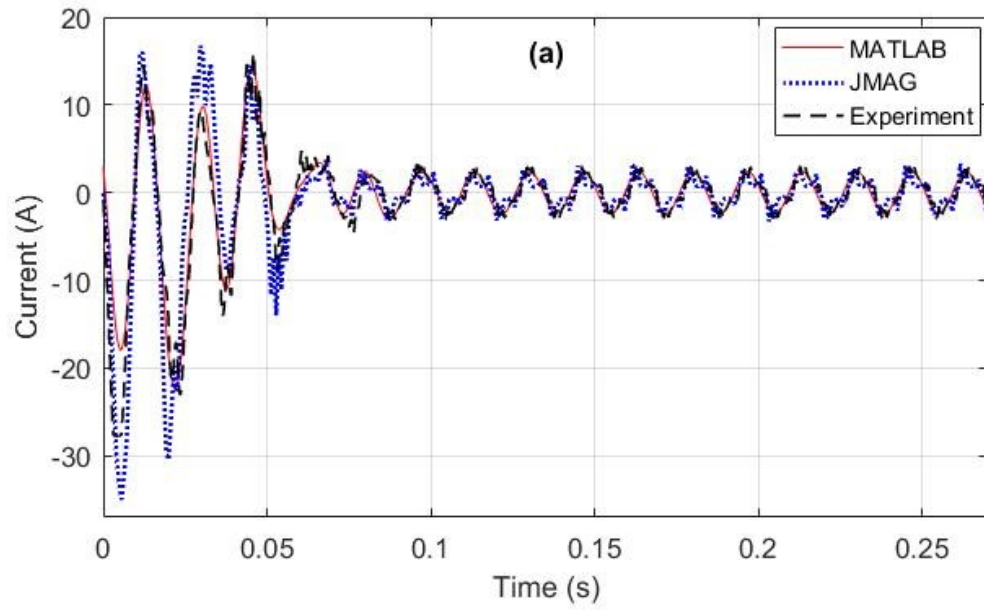
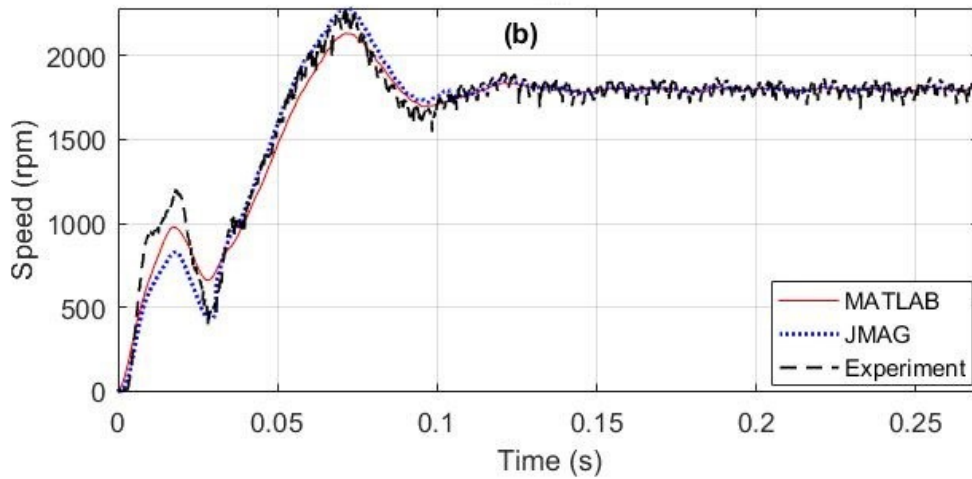
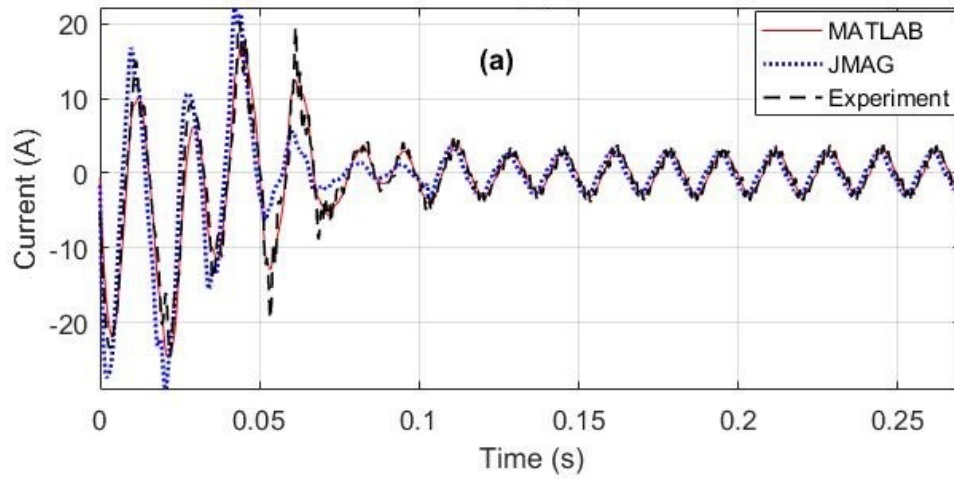
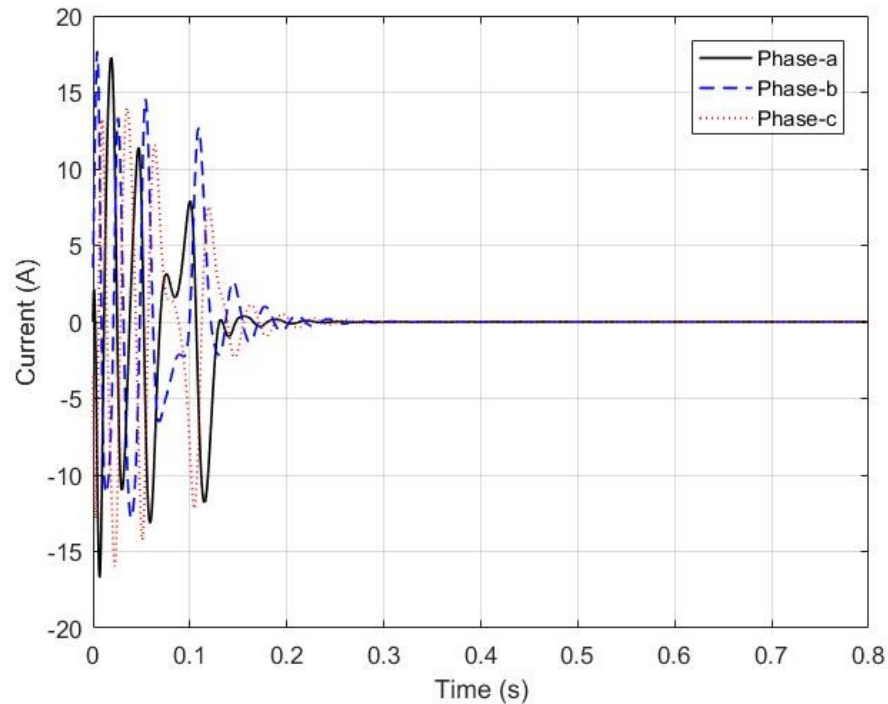


Figure 5.3 Healthy motor at 2 N.m load (a) Stator phase-a current (b) speed



**Figure 5.4 Healthy motor at full load (a) Stator phase-a current (b) speed**

In addition, the figures show that the starting current of LSPMSM is similar to that of an induction motor, which is around 5 to 7 times the steady state current. It is worth mentioning that at the starting of the motor, the current is the sum of both the stator and rotor winding currents while at steady state it is only the current in the stator winding. Hence, no current will be induced in the rotor bars. Figure 5.5 shows three phase rotor current at full load for MATLAB.



**Figure 5.5 Rotor three phase current at full load**

Additionally, it is clear from the figures 5.2-5.4 that at steady state, the motor runs at a synchronous speed (1800 rpm). Therefore, there is no relative speed between the rotational magnetic field of the stator and the rotor. Hence, there is no induction torque during this state. Both the excitation torque and reluctance torque (in salient pole machine) are driving the motor shaft at steady state. At starting, the main torque component which forces the motor to rotate is the induction torque whereas the excitation torque is considered as a braking torque. Although the excitation torque (braking torque) is out of phase of the induction torque during starting, the induction torque is larger and hence the machine is self-starting. Figure 5.6 shows the electromechanical torque of the motor and its components at full load for MATLAB simulation.

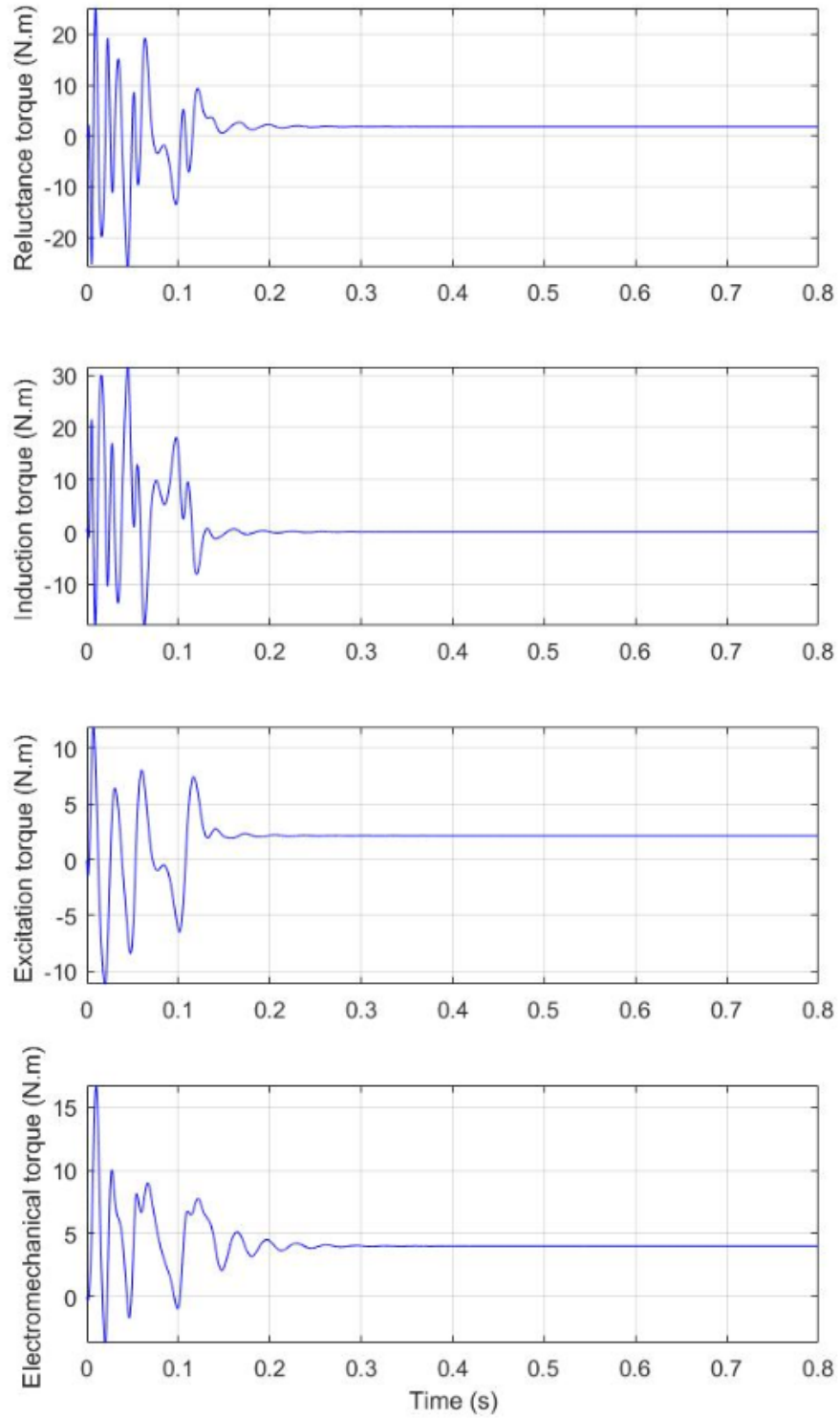


Figure 5.6 Motor torque components at full load (a) reluctance torque (b) induction torque (c) excitation torque (d) electromechanical torque

Based on the presented experimental and simulation results for both no load and loading cases, the discrepancy between the experimental and simulation responses is acceptable for the following reasons: First, the motor used in the experimental test has small differences in the stator resistance. Secondly, the three-phase power source used in the simulation test is exactly balanced while that the one in the experimental test some slight differences between phase voltages exist. Thirdly, in the simulation test, the starting angle of the rotor can be exactly adjusted while in the experimental test, the starting angle can be approximately adjusted. Fourthly, the positions of the bars, permanent magnets and windings in the slots were not considered in the mathematical modeling. Finally, the four assumptions previously mentioned were considered when the mathematical model was derived. Moreover, the oscillatory nature of the speed response at steady state is due to the interaction between the rotor magnets and the stator supply current as well as the cogging torque [26-28].

### **5.3 Testing of LSPMSM under Asymmetrical Stator Winding**

The performance of the motor under asymmetrical stator winding conditions, with specifications listed in **Table 5.1**, is investigated by using the implemented MATLAB mathematical model which is based on the derived equations (3.40), (3.41), (2.9) and (2.10). In order to validate the results of the developed mathematical model, the performance of the motor has been simulated using the developed finite element model with the help of the JMAG<sup>TM</sup> software. Both models have been simulated and analyzed for the three different asymmetrical cases listed in Table 5.2. Simulation results obtained for current, speed and torque from MATLAB and JMAG are in very good agreement.

Figure 5.7 indicates the stator phase-a current under full load condition for the three asymmetric cases. It is demonstrated that the current response of phase-a is affected by having a different number of turns for phase-a compared to the number of turns in phases-b and c. Additionally, the amplitude of the current increases with the increase of asymmetry in turns number among the phases.

**Table 5.2 The simulated asymmetrical cases**

<i>Case#</i>	<i>Asymmetric coefficient values</i>
<i>Case I</i>	$\alpha_a = \alpha_b = \alpha_c = 1$
<i>Case II</i>	$\alpha_a = 0.971, \alpha_b = \alpha_c = 1$
<i>Case III</i>	$\alpha_a = 0.9128, \alpha_b = \alpha_c = 1$

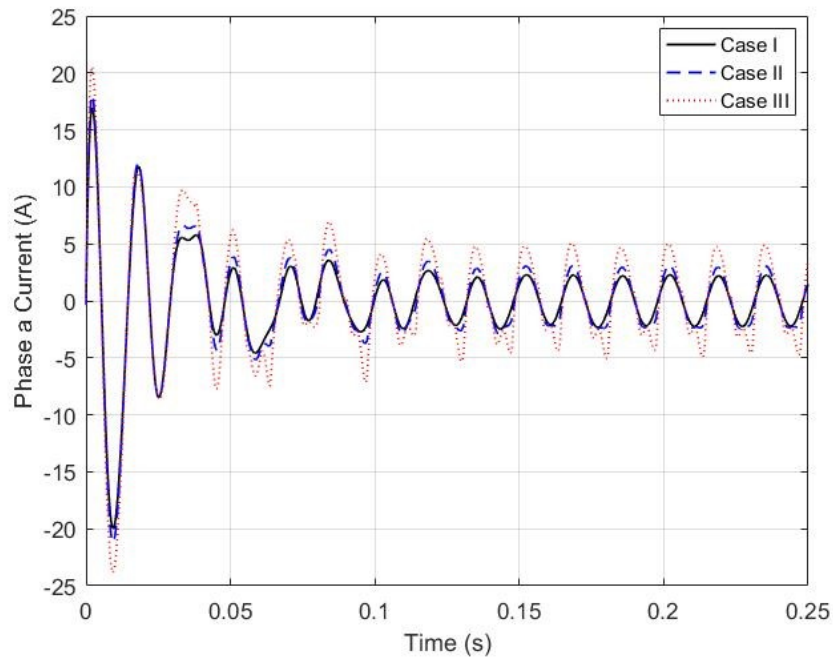


**Figure 5.7 Stator phase-a current at full load**

Figures 5.8 to 5.10 show the current, speed and torque responses of MATLAB and JMAG for the three simulation cases of the tested motor at full load, respectively. Figure 5.8 illustrates that the current for both models increases during steady state as the asymmetry between phases is increased. Also, it is clear from the figures 5.9 and 5.10 that the asymmetric condition affects the speed and torque. Based on the above results, it is confirmed that the asymmetric fault in stator winding introduces oscillation components in the speed and torque response of the motor during steady state as shown in Figure 5.7 and Figure 5.8. The oscillation increases as the asymmetry between phases increases.

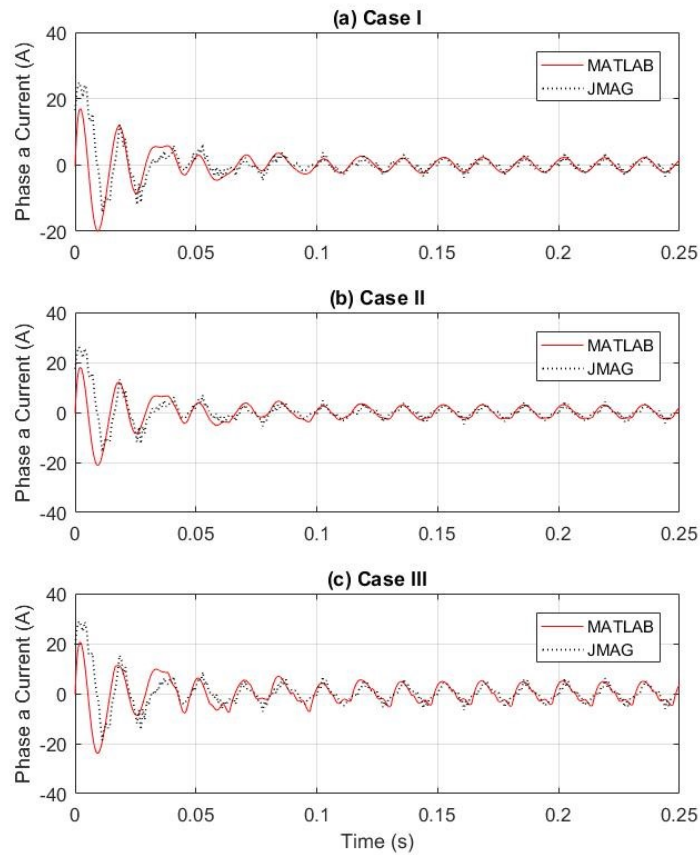


**Figure 5.8 Stator phase-a current at full load (a) Case I (b) Case II (c) Case III**



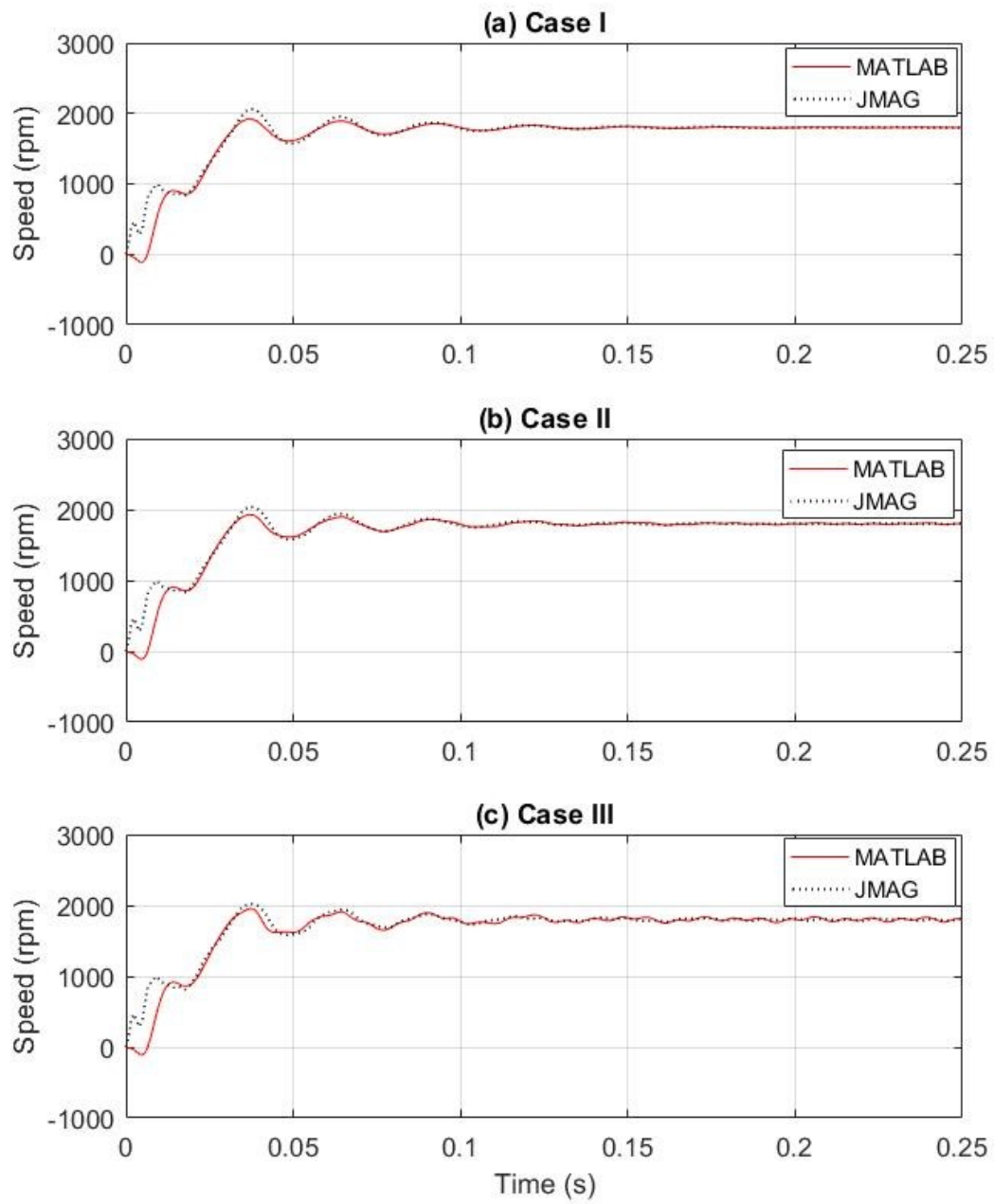


Figure 5.9 Rotor speed at full load (a) Case I (b) Case II (c) Case III

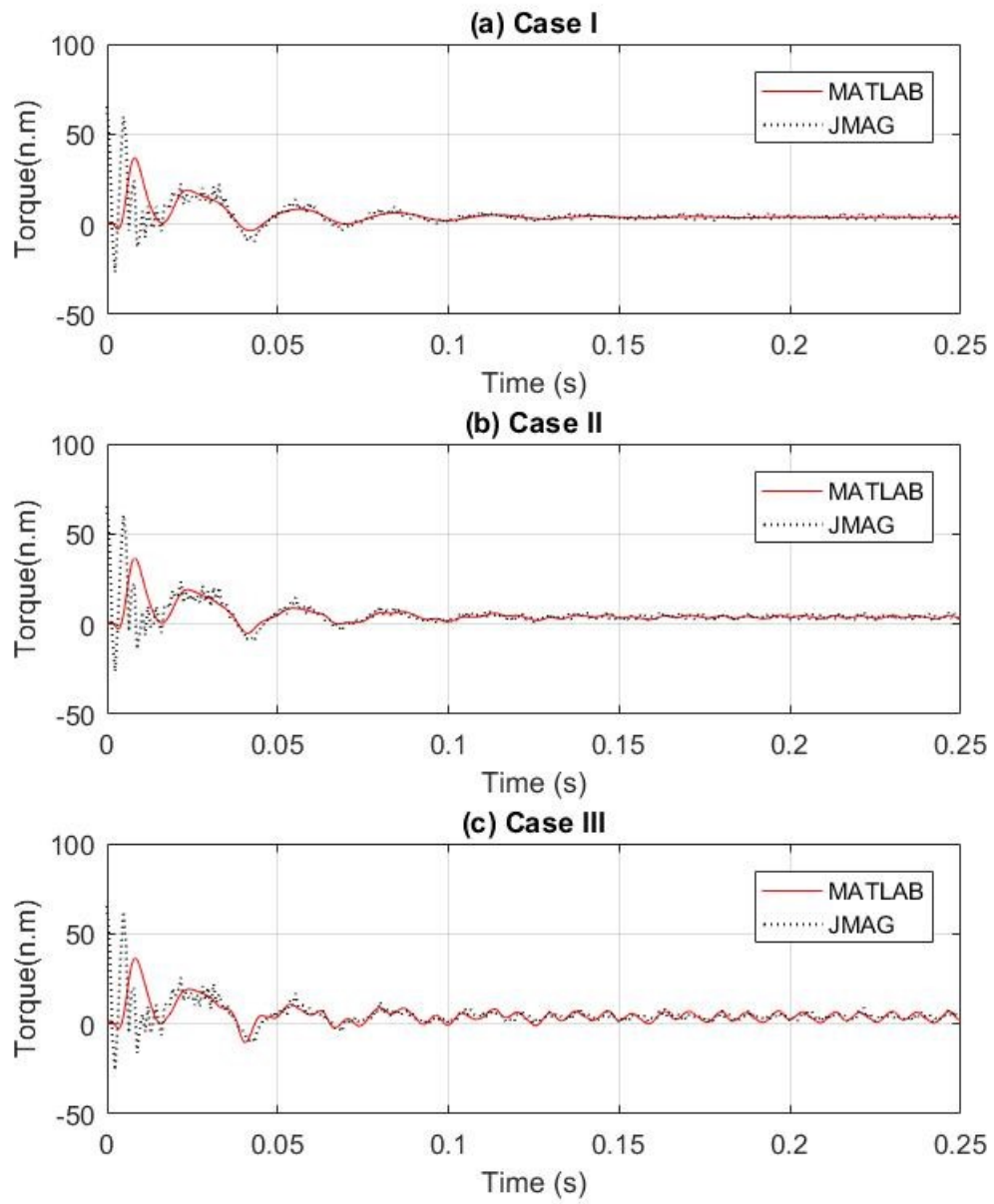


Figure 5.10 Motor torque at full load (a) Case I (b) Case II (c) Case III

## 5.4 Testing of LSPMSM under Stator Inter-Turn Fault

To verify effectiveness of the developed mathematical model under inter-turn short circuit fault, experimental, MATLAB and Finite element tests on the 1-hp motor were conducted. The parameters of the used motor are listed in table 5.1. The motor stator has 24 slots, with a single-layer winding and four coils per phase. Each coil consists of 86 turns, therefore, there are 344 turns per phase. To create the inter-turn fault via a low and high number of shorted turns, the motor was dismantled, and 6 access points were inserted into phase-a, as shown in Figure 5.11. It is clearly shown that the four access points ( $a_1$ ,  $a_2$ ,  $a_3$  and  $a_4$ ) are added to a coil, while the other two access points ( $a_5$  and  $a_6$ ) are added to another coil. Therefore, 8 inter-turn fault cases can be created. Table 5.3 indicates the access point combinations, with their respective number of turns and shorted turn percentages ( $\mu$ ). The access points inserted in the motor were at the level of 4, 9, 26, 40, 44, 66, 70, and 77 turns on phase-a.

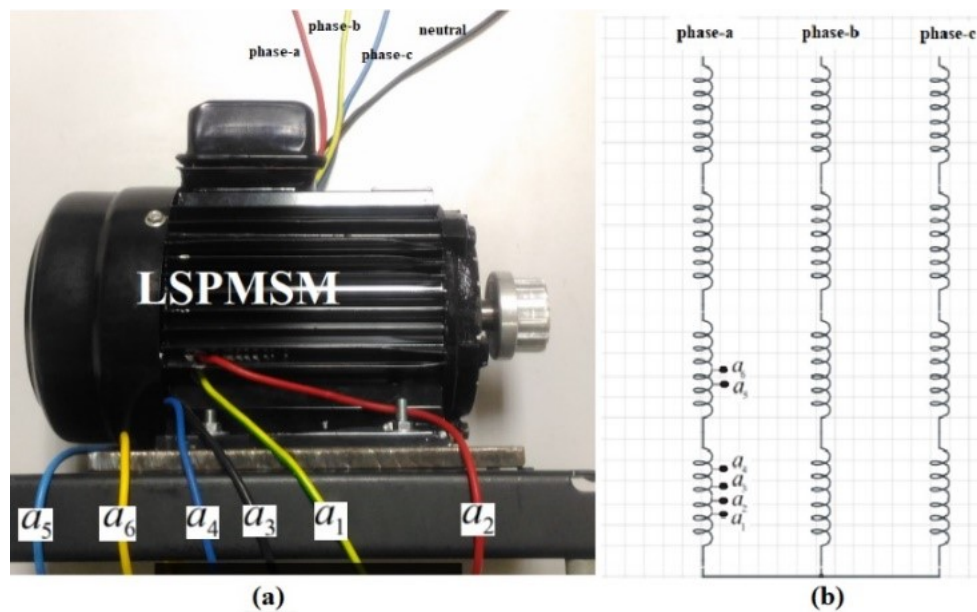
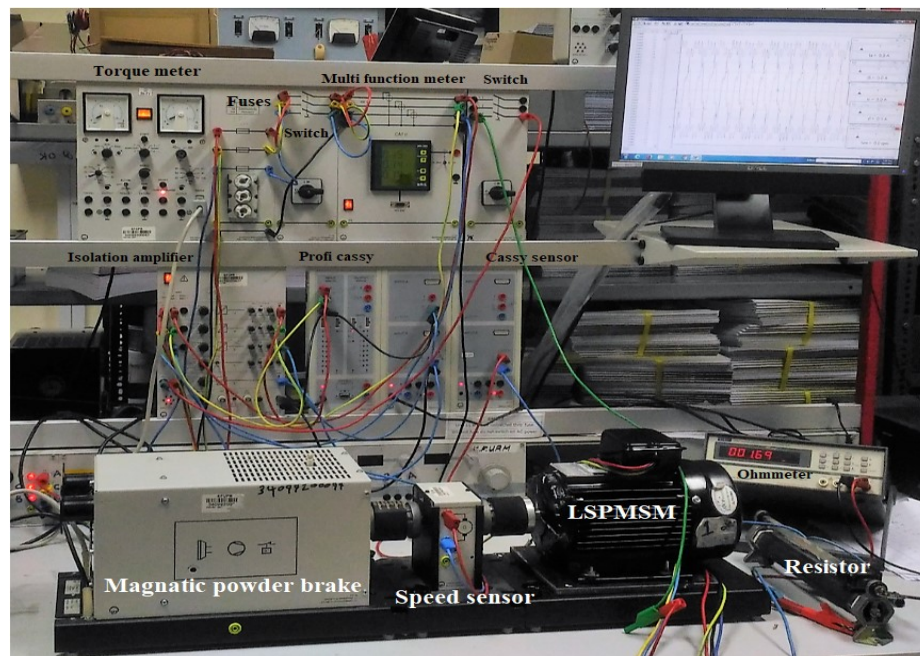


Figure 5.11 Configuration of the stator windings of the LSPMSM with center taps added in phase-a.

**Table 5.3 The shorted-turn cases for the faulty LSPMSM**

Tap cases	$N_{sh}$	$\mu$ (%)	Tap cases	$N_{sh}$	$\mu$ (%)
$a_1-a_2$	26	7.6	$a_2-a_4$	44	12.8
$a_1-a_3$	66	19.2	$a_3-a_4$	4	1.2
$a_1-a_4$	70	20.3	$a_4-a_5$	77	22.4
$a_2-a_3$	40	11.6	$a_5-a_6$	9	2.6

To perform the experimental tests, the experimental setup shown in Figure 5.12 was used. During the experimental tests, an external adjustable resistor was used to limit the fault current in the shorted turns of the motor stator windings to avoid damaging of the motor winding.



**Figure 5.12 Experimental setup**

The simulation and experimental results are presented in this section. The results were taken during acceleration after the system has been started to the synchronous speed

(1800 rpm) under a balanced three-phase voltage supply of 400 V<sub>rms</sub> line-to-line. The simulation and experimental tests were conducted for 0.8 sec to avoid overheating and damage of the motor windings. For a fair comparison, both the simulation and experimental step times were 0.1 msec. To study the effect of the inter-turn fault on the motor performance, both simulations and experiments with 8 different inter-turn fault cases under no load and full load were carried out. Figures 5.13 and 5.14 present the experimental and the simulation current and speed used to test the motor under no load for three different cases (healthy condition, 26 shorted turns and 40 shorted turns). The tests were carried out experimentally with a fault resistance of 0.8 Ω. On the other hand, for the simulation test, a 0.2 Ω extra resistance was added to the fault resistance to account for the wires used at the access points and their soldering connections.

Figures 5.13 and 5.14 show that both the experimental and simulation results are in good agreement. Figure 5.13 depicts that under all cases (healthy, 26 shorted turns and 40 shorted turns), the simulation stator phase-a current behaves like the experimental phase-a current in the transient and steady states, with small mismatches occurring especially during the transient period. The same is true for the speed in Figure 5.14.

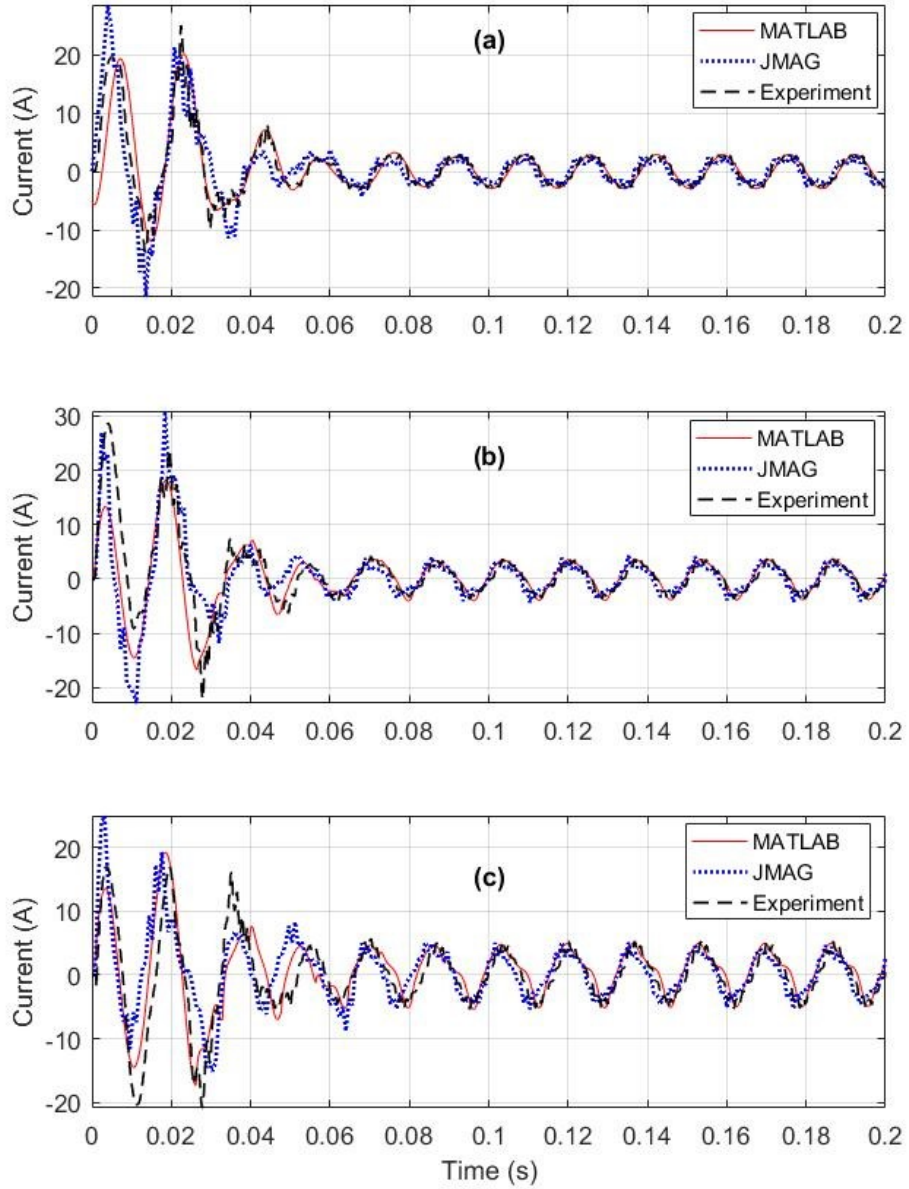
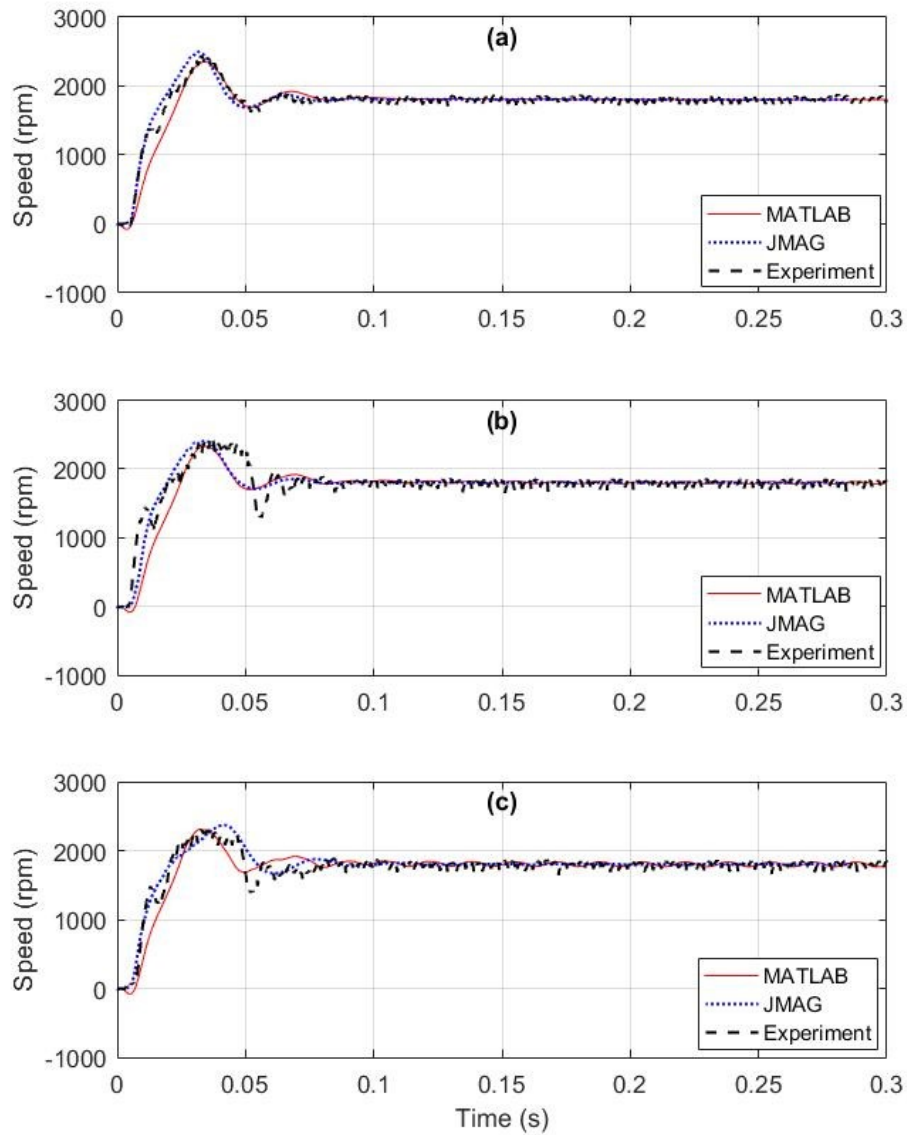


Figure 5.13 Stator phase-a current under no load: (a) healthy conditions, (b) 26 shorted turns, (c) 40 shorted turns



**Figure 5.14 Rotor speed under no load: (a) healthy conditions, (b) 26 shorted turns, (c) 40 shorted turns**

Figure 5.15 shows the stator current, speed and fault current results for the LSPMSM with 26 turns shorted under full load for both the simulation and experimental tests. The



tests were conducted with fault resistance of  $0.8 \Omega$ . The figure shows that the simulation and experimental results are in good agreement.

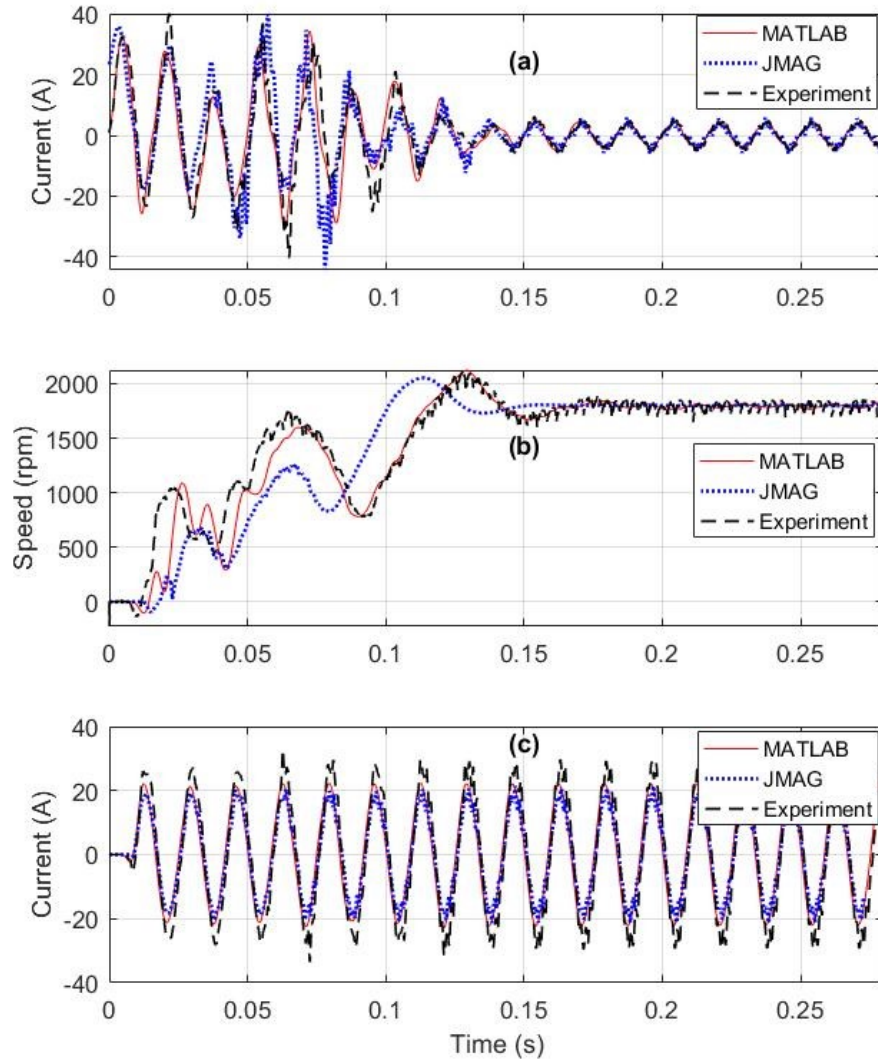


**Figure 5.15 Motor testing results under full load with 26 shorted turns: (a) stator phase-a, (b) rotor speed, (c) fault current**

To investigate the relationship between the fault current and the fault resistance/fault severity, both experimental and MATLAB simulation tests under no load were conducted for the possible inter-turn short circuit cases listed in Table 5.3. Figure 5.16 (a) shows the



relationship between the fault current and fault resistance for the three cases of shorted turns (9, 26 and 40 shorted turns). The figure clearly shows that the relationship is not linear and that the fault current increases as the fault resistance decreases. On the other hand, the relationship between the fault current and the fault severity at a constant fault resistance of  $0.9 \Omega$  is indicated in Figure 5.16 (b). It is observed that as the severity of the fault increases, the fault current increases. These findings prove that the developed model is in agreement with the experimental results.

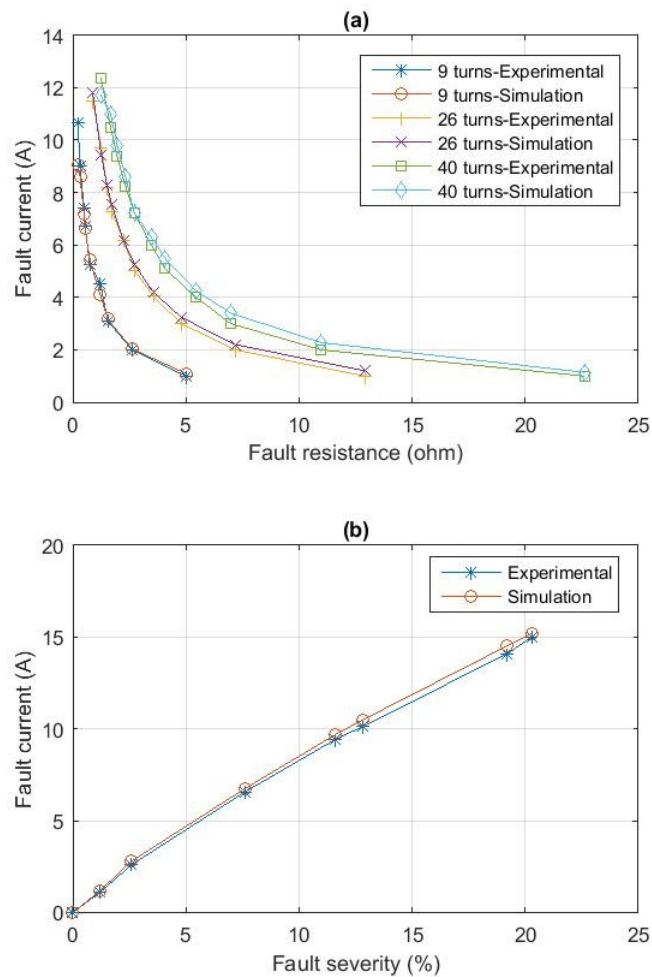
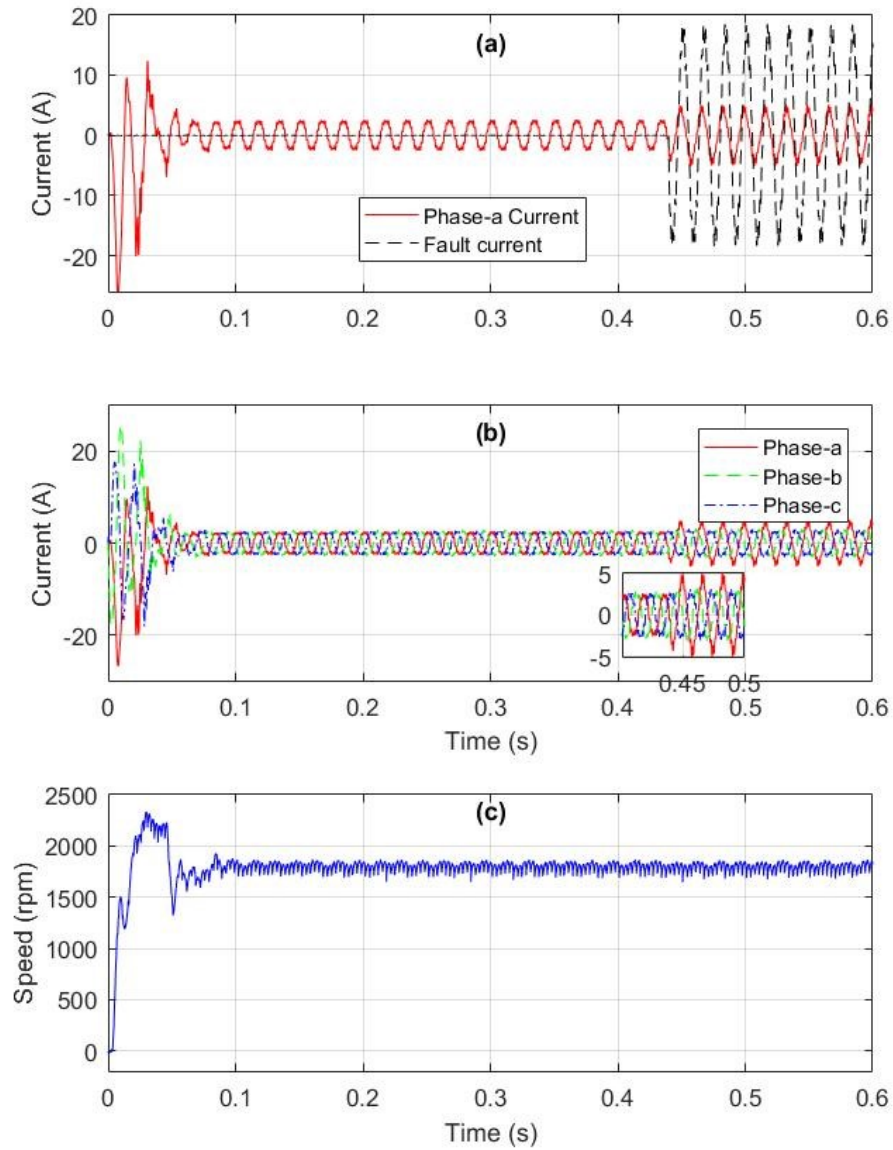


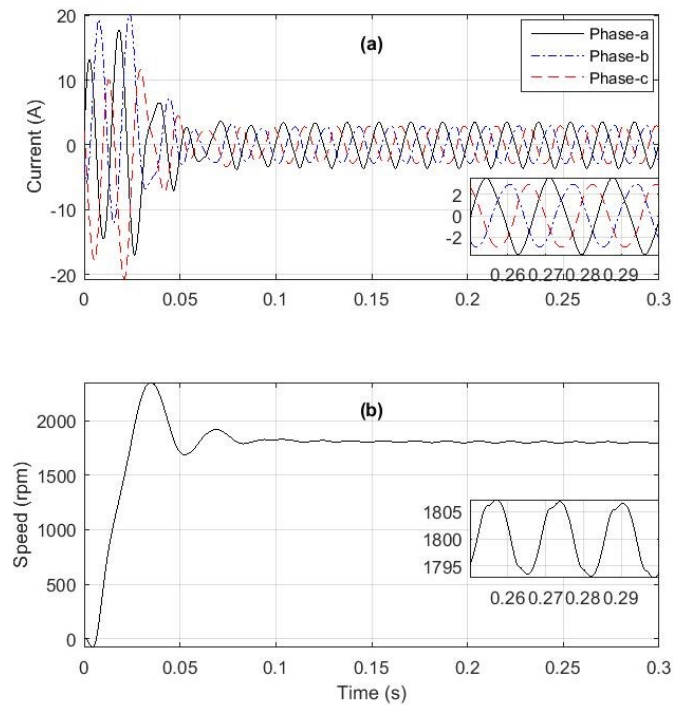
Figure 5.16 Experimental and MATLAB simulation results under no load: (a) fault current as a function of fault resistance, (b) fault current as a function of fault severity

Figures 5.17 and 5.18 show that the inter-turn fault will affect the current in the faulted phase more than that in the other phases.



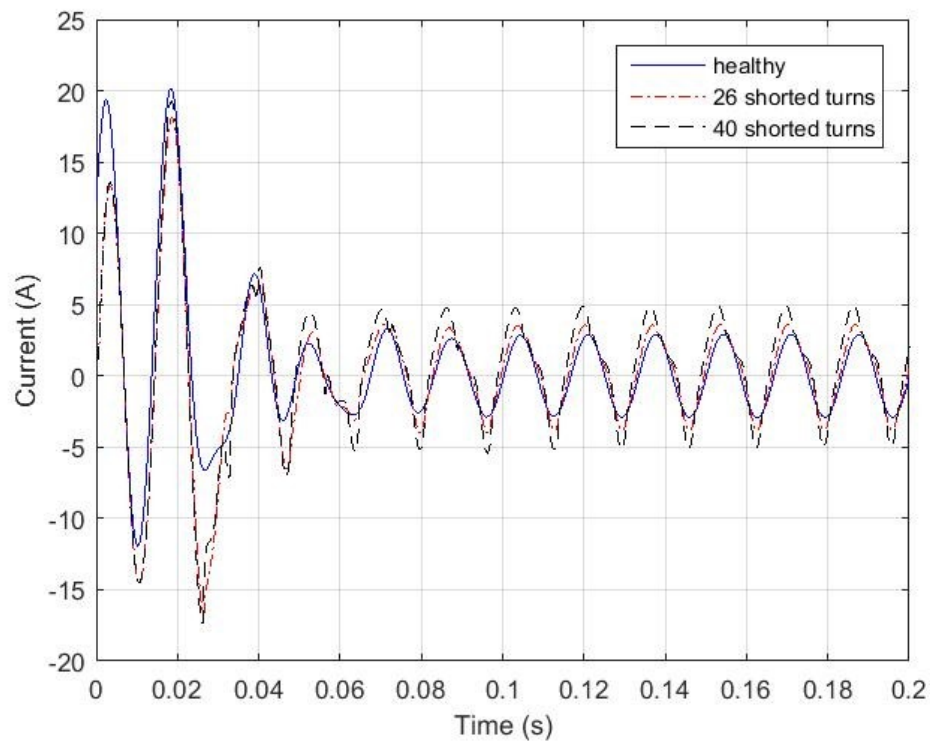
**Figure 5.17** Experimental results under 26 shorted turns occurring at 0.44 sec (a) stator phase-a current and fault (b) three phase current (c) speed

Figure 5.17-a shows the experimental transient response of the motor (three-phase current, speed and fault current) from system standstill to the synchronous speed for 0.6 sec, with the motor initially operated under healthy conditions and then subjected to a fault with 26 shorted turns and a  $0.4\text{-}\Omega$  fault resistance at 0.44 sec. Figure 17.b clearly shows that the current of phase-a is affected, while the other phase currents remain the same. On the other hand, figure 5.18 shows the three-phase current and speed when the motor is subjected to a fault of 9 shorted turns with a  $0.35\text{-}\Omega$  fault resistance. Figure 18.a clearly reveals that during the fault, the magnitude and time response of the phase-a (faulted-phase) current are affected much more than those of the other two phase currents. With this observation in mind, the developed model can be used to detect the possibility and location of the stator inter-turn fault in an LSPMSM.



**Figure 5.18 MATLAB simulation results under no load with 9 shorted turns (a) Three-phase stator current (b) speed**

To investigate the size of inter-turn faults on both current and the speed of the motor, MATLAB simulations for the motor under three different inter-turn cases (healthy, 26 shorted turns and 40 shorted turns) have been done. The results are depicted in both Figure 5.19, 5.20, 5.21 and 5.22. Figure 5.19 and 5.20 highlight that the magnitude of the current increases as the size of the fault increases. While Figure 5.21 and 5.22 shows that the oscillation in speed response at steady state increases with increase in the size of the fault.



**Figure 5.19 Phase-a current under no load for MATLAB simulation**

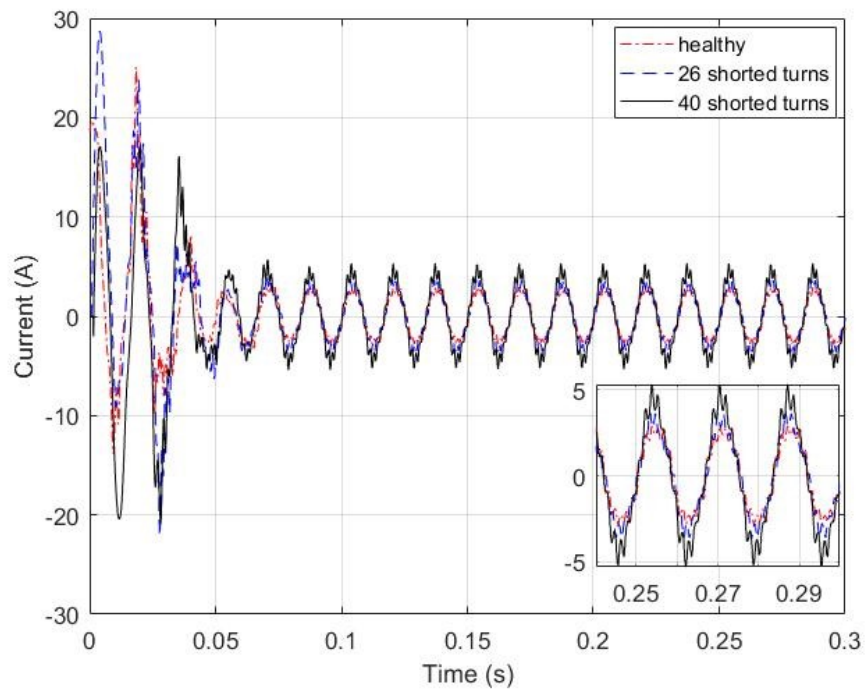


**Figure 5.20 Phase-a current under no load for experimental testing**

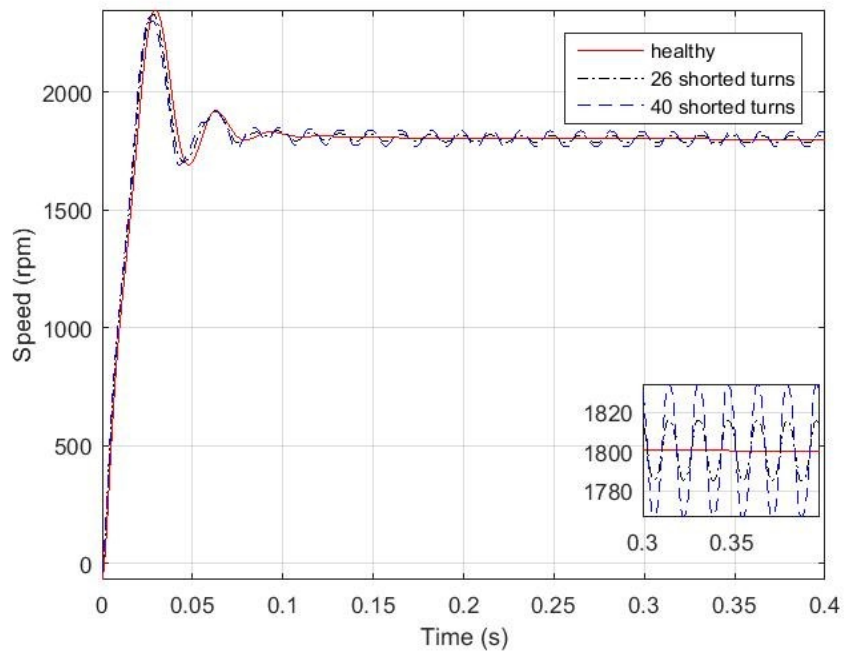


**Figure 5.21 Speed under no load for MATLAB simulation**

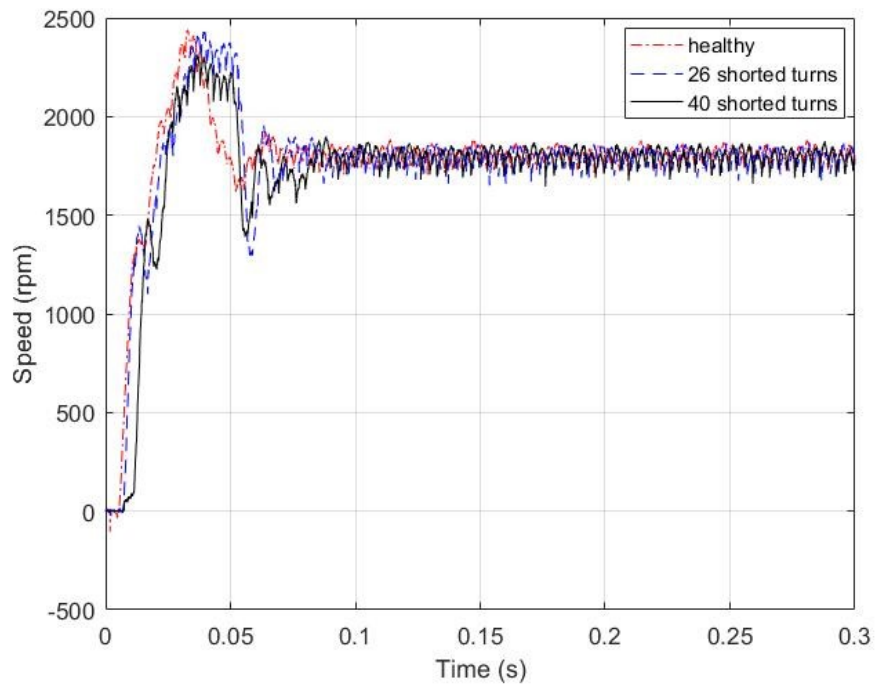


**Figure 5.22 Speed under no load for experimental testing**

In conclusion, the results presented in this chapter clearly show that the mathematical simulation results of the developed models are in very good agreement with the JMAG commercial software results and experimental findings.

## **CHAPTER 6**

# **DIAGNOSTIC TOOL DESIGN FOR DETECTING STATOR WINDING ABNORMALITIES**

### **6.1 Overview**

In this chapter, a neural network-based diagnosing tool that can predict stator winding abnormalities was developed. The developed mathematical models have been simulated using MATLAB under different loadings, abnormality types, and severity conditions. Since the stator currents and voltages are easily accessible without extra hardware, it has been decided to be used as the key signatures for developing the diagnostic tool. Several time and frequency based features have been extracted using motor current and voltage waveforms. The developed tool has been designed to correlate the extracted features with its corresponding type and severity of stator abnormalities. Finally, the designed tool has been tested using different unseen abnormality cases.

### **6.2 Features Extraction**

Extracting the fault representative features is a major step in the design of any fault diagnostic tool. In this section, time-based and frequency-based features were extracted from the stator steady state current response for stator winding abnormalities. The extracted

features were investigated to select the most distinct features of the faults. The following subsections show the feature extraction process.

### 6.2.1 Features Extraction for Inter-turn Fault

MATLAB comprehensive investigations of the motor performance under stator inter-turn fault has been done to select the most distinct and representative features. The shorted turn cases of 0, 9, 26 and 40 at phase-a are studied. In addition, experimental investigation for the same number of shorted turns has been done. Figure 6.1 shows the experimental and MATLAB phase-a (faulted phase) steady state stator current under no load condition.

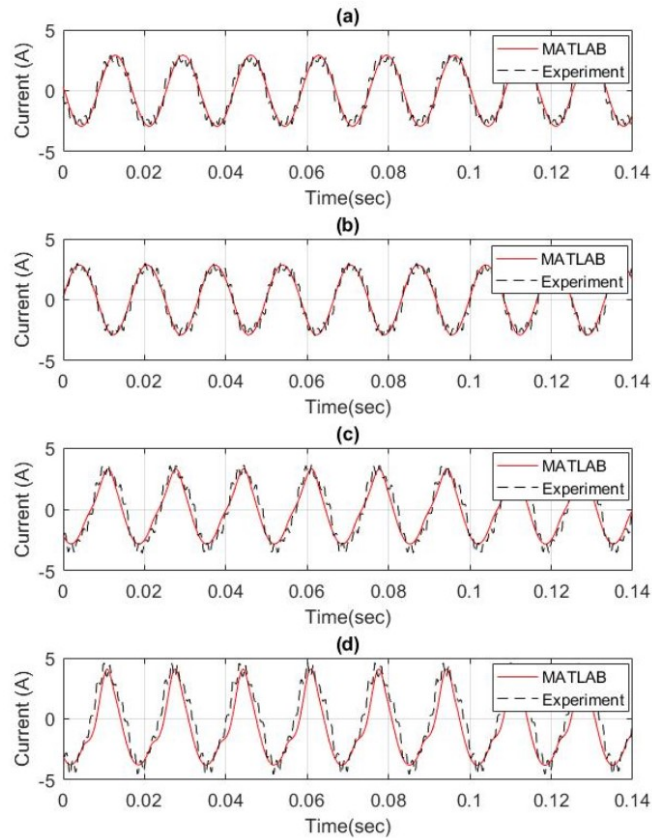
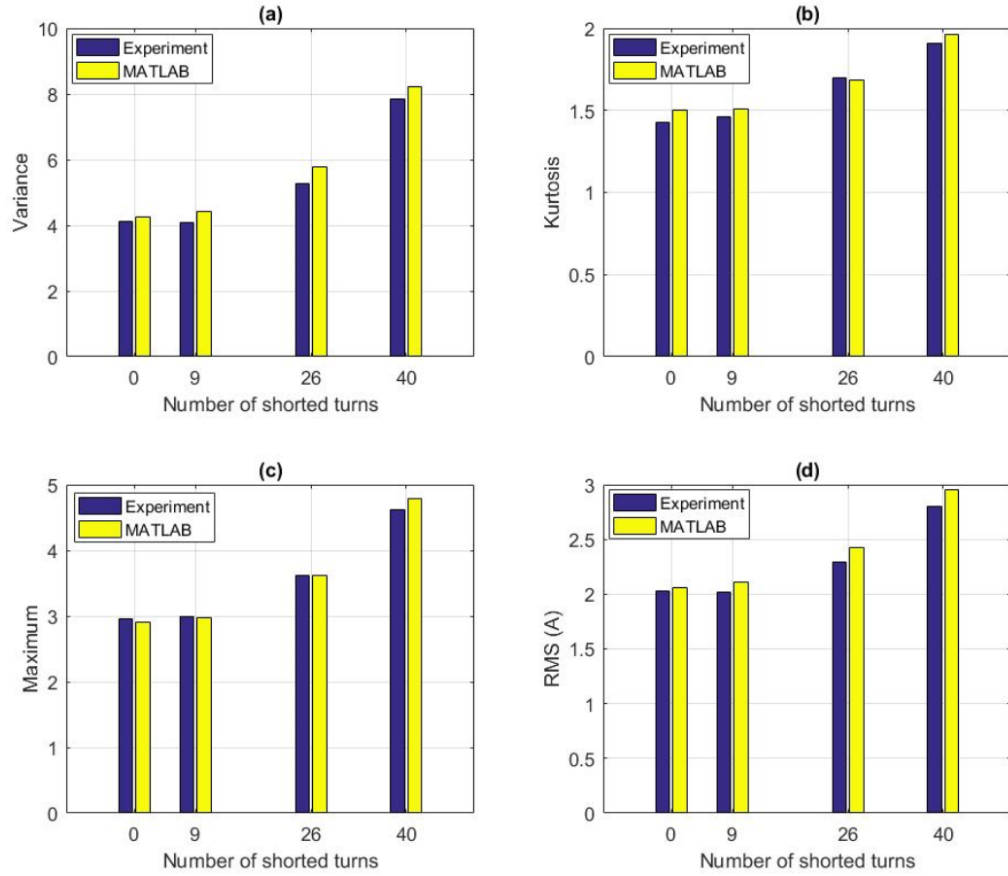


Figure 6.1 Phase-a steady state current under no load (a) 0 shorted turns (b) 9 shorted turns (c) 26 shorted turns (d) 40 shorted turns



It can be observed that both experimental and MATLAB results are in good agreements. Also, it can be noted that the current response of the faulted phase and its amplitude are affected with the size of inter-turn fault during steady state. As shown in chapter 5, the currents in the unfaulted phases have been slightly affected and hence are not shown.

Using the stator currents and supply voltages for the above studied cases, several features have been extracted and compared in order to determine their effectiveness in detecting the stator inter-turn fault. Among these feature; four time-based (Variance, Kurtosis, Maximum and RMS value) are extracted from the current of the faulted phase during steady state. In addition, two frequency-based features (the fundamental current magnitude and the fundamental power factor angle) are also extracted from the frequency response of the voltage and current of the faulted phase. Moreover, the power factor of the faulted phase and the stator current symmetrical components (positive, negative and zero) have also been extracted. Figures 6.2 to 6.3 show the extracted features under no load for the  $1\Omega$  fault resistor.



**Figure 6.2 Experimental and MATLAB extracted features at no load for 1Ω fault resistance: (a) variance (b) kurtosis (c) Maximum (d) RMS**

The results showed that the time based-extracted features (variance, kurtosis, maximum and RMS) increases as the number of shorted turns increases as shown in Figure 6.2. The fundamental current magnitude, the fundamental power factor angle as well as the power factor of the faulted phase are shown in figure 6.3, where it is proved that both the fundamental current component and the power factor increase as the number of shorted turns increases, while the fundamental power factor angle decreases as the shorted turns number increases. In addition, it is clear from Figure 6.2 and 6.3 that both experimental and MATLAB based extracted features are in good agreement.

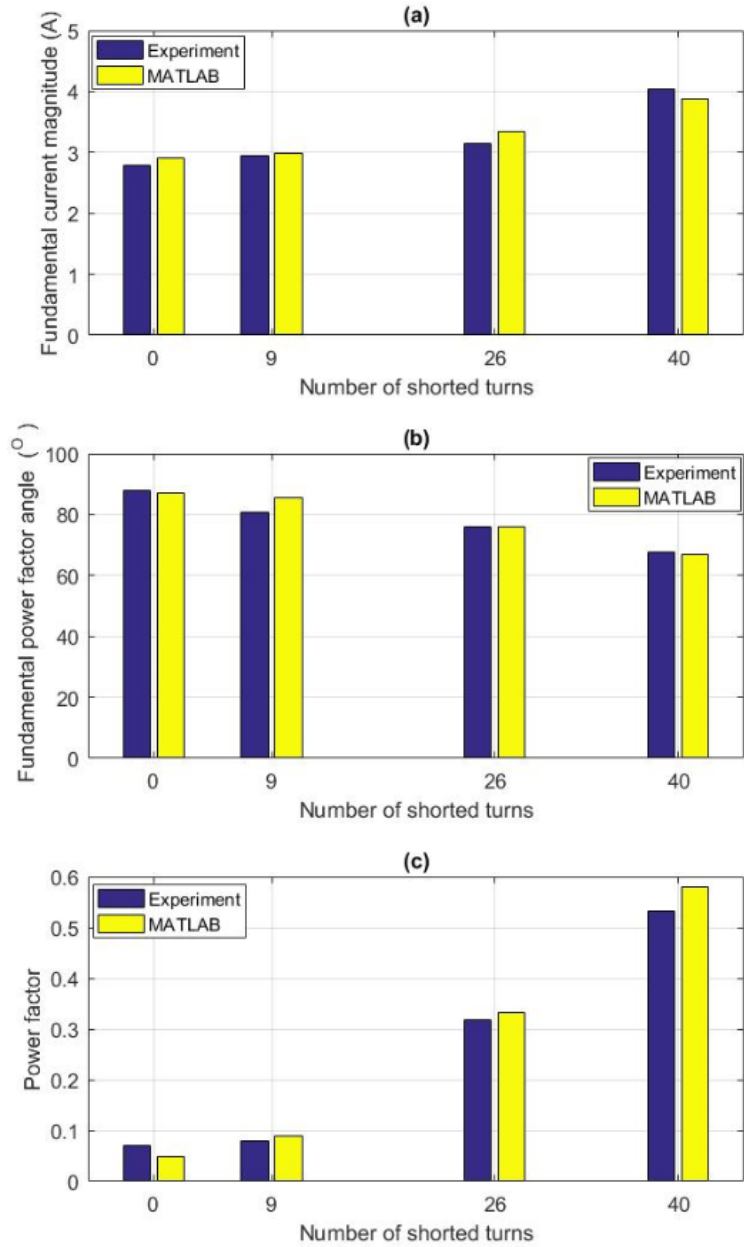


**Figure 6.3** Experimental and MATLAB extracted features at no load for  $1 \Omega$  fault resistance: (a) Fundamental current Magnitude (b) Fundamental power factor angle (c) Power factor

Figure 6.4 shows the symmetrical current components, where the positive sequence component for both MATLAB and experimental results are in good agreement for the four shorted turn cases.

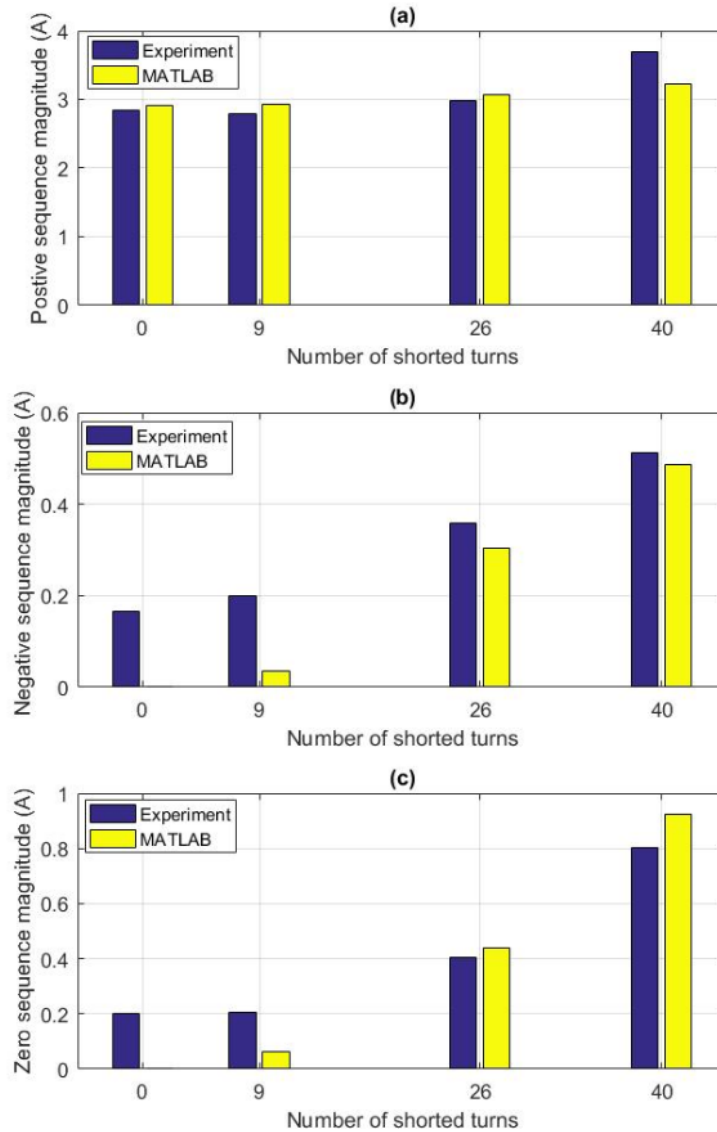


Figure 6.4 Experimental and MATLAB extracted features at no load for  $1\Omega$  fault resistance: (a) positive sequence component magnitude (b) negative sequence component magnitude (c) zero sequence component magnitude

### 6.2.1.1 Features under Fixed Fault Resistance and Variable Loading Levels

To study the effect of load variation on the extracted feature patterns at fixed fault resistor, the developed mathematical model was simulated for 14 cases of shorted turns conditions (0, 5, 10, 15, 20, 25, 30, 35, 40, 45, 50, 55, 60, and 65) and 9 loading

conditions (0 N.m, 0.5 N.m, 1 N.m, 1.5 N.m, 2 N.m, 2.5 N.m, 3 N.m, 3.5 N.m and 4 N.m ). Hence, the model was used to simulate 126 shorted turns/load combinations at the same fault resistor of 1  $\Omega$ . Figure 6.5 to 6.7 show the extracted features for the 126 simulated cases. Figure 6.5 reveals that the features such as variance, kurtosis, Maximum and RMS are load dependent and their values increase as the number of shorted turns increases. Also, it is clear that the variance, maximum and RMS features follow almost the same curve pattern for different loading conditions, but the feature curves are shifted up when the load is increased. However, for the Kurtosis, the curves are shifted down as the load is increased, Figure 6.5 (b).

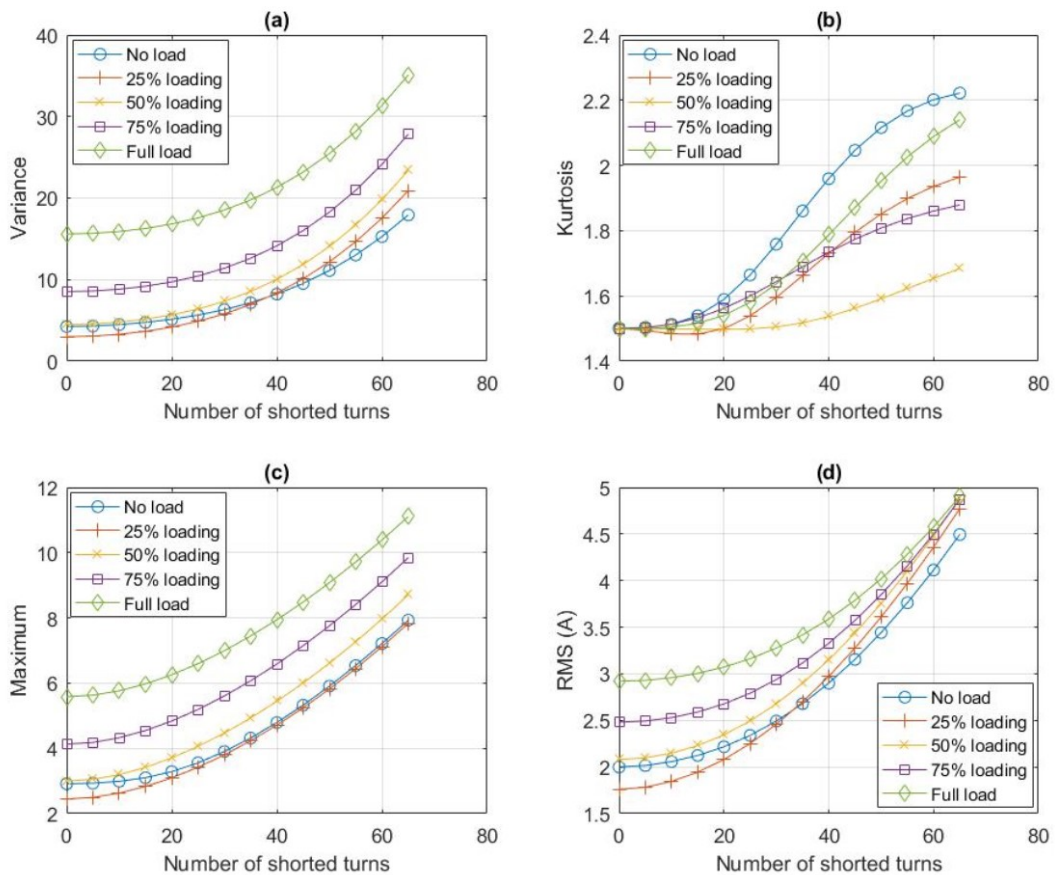


Figure 6.5 MATLAB extracted features at different loading condition for 1  $\Omega$  fault resistance (a) variance (b) kurtosis (c) Maximum (d) RMS

On the other hand, Figure 6.6 shows the fundamental current magnitude, the fundamental power factor angle and the power factor for the faulted phase at different loading conditions. It is evident from Figure 6.6(a) that the fundamental current magnitude increased with the increase in the number of shorted turns for a particular load size.

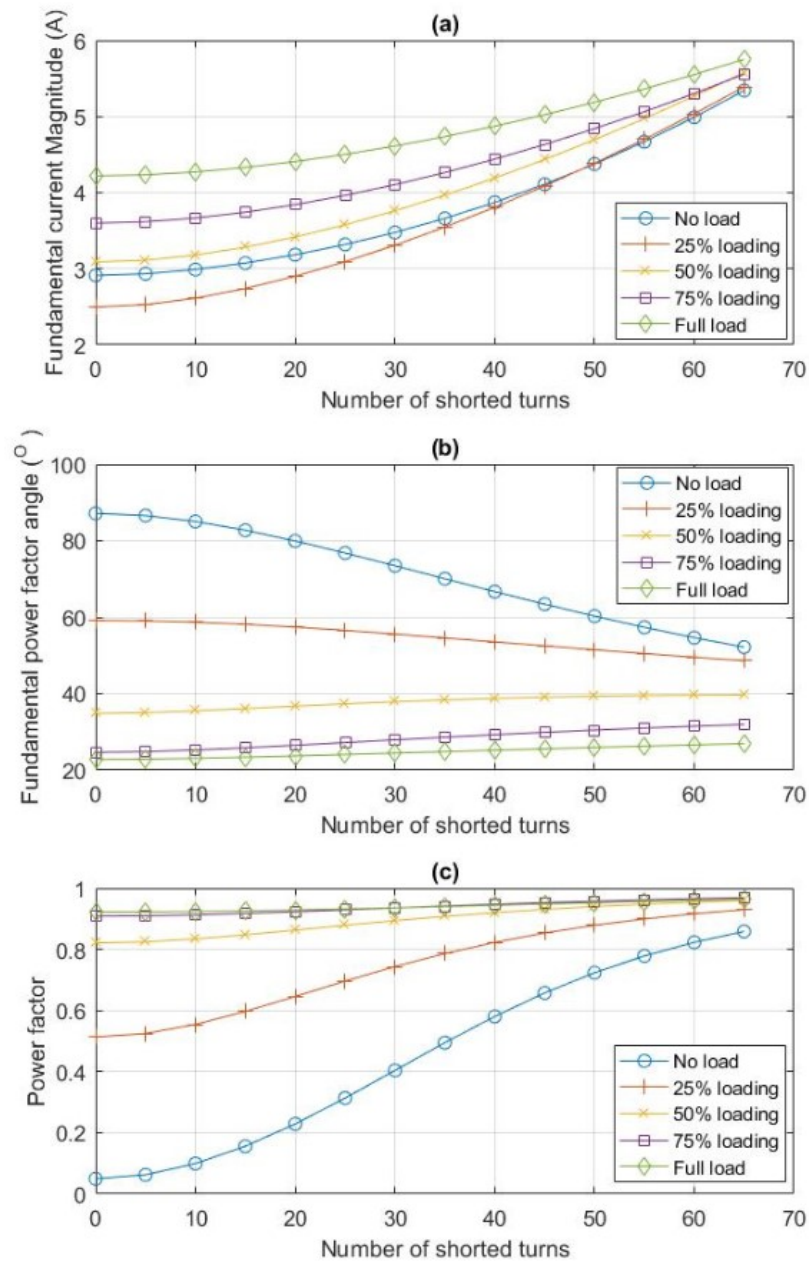
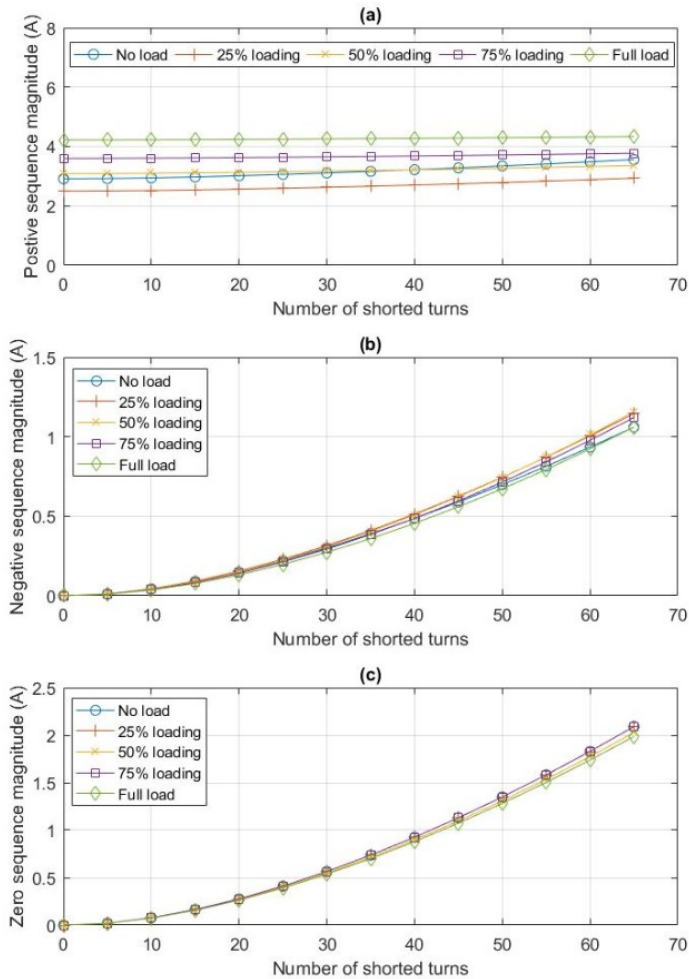


Figure 6.6 MATLAB extracted features at different loading condition for 1 Ω fault resistance (a) Fundamental current Magnitude (b) Fundamental power factor angle (c) power factor

Figure 6.6 (b) shows that the fundamental power factor angle decreases as the number of shorted turns increases at no load and 25% loading, while at a load of 50%, 75% and full load the feature value is slightly changed (increases slightly) as the number of shorted turns is increased. Figure 6.6(c) shows that the power factors are load dependent whereby the values are increased as the number of shorted turns increases for loads less than 50%, while the power factor is almost constant regardless of the number of shorted turns for the other load conditions (75% and 100% loading). The magnitudes of symmetrical components of the stator current are displayed in figure 6.7.



**Figure 6.7 MATLAB extracted features at different loading condition for 1  $\Omega$  fault resistance (a) positive sequence faulted current magnitude (b) negative sequence faulted current magnitude (c) zero sequence faulted current magnitude**

It is clear from figure 6.18 (a) that the positive sequence component feature is load dependent, while Figure 6.18 (b) and (c) confirms that the negative and zero sequence feature components are almost load independent. Therefore, the symmetrical current components could be good indicators for inter-turn fault under variable loading condition.

Therefore, one can conclude that the above analyzed features are distinct and follow a certain pattern that makes them very useful in designing a diagnostic tool. Moreover, the variation in each of the variance, maximum, RMS, fundamental current magnitude and positive sequence component values with respect to the number of shorted turns is approximately the same at different loading conditions.

### **6.2.1.2 Features under variable Fault Resistance and fixed Loading Condition**

To investigate the effect of inter-turn fault on the stator current signatures at different fault resistor values, the developed mathematical model was simulated at the case of 26-shorter turns in phase-a for four fault resistor values (0.4  $\Omega$ , 0.8  $\Omega$ , 1  $\Omega$ , and 1.2  $\Omega$ ). The MATLAB results are validated experimentally. MATLAB and experimental results for the current are shown in figure 6.8 where they are in good agreement. It is also clear that the magnitude of the faulted phase current increases as the fault resistance decreases as well as a notable effect on the time response of the current.



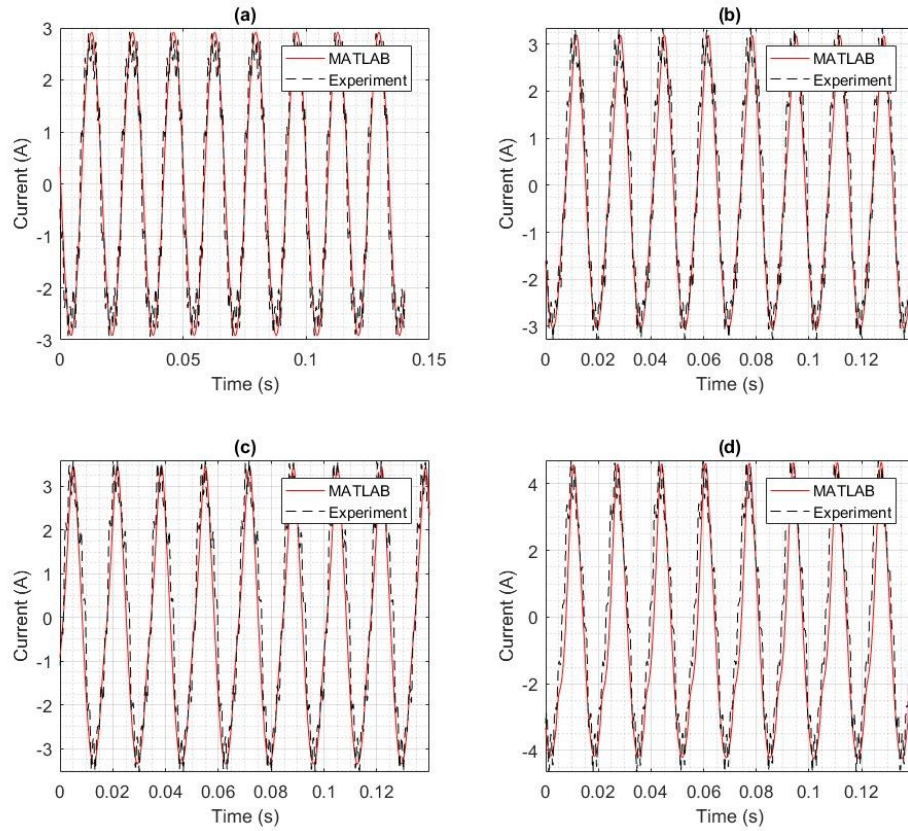


**Figure 6.8** Phase-a steady state current under no load for 26-shortened turns (a)  $R_f=1.2 \Omega$  (b)  $R_f=1 \Omega$  (c)  $R_f=0.8 \Omega$  (d)  $R_f=0.4 \Omega$

The effect of inter turn fault on the extracted features patterns at fixed load and variable fault resistor is studied for 14 cases of shorted turns (0, 5, 10, 15, 20, 25, 30, 35, 40, 45, 50, 55, 60, and 65) and five fault resistor values (0  $\Omega$ , 0.4  $\Omega$ , 0.8  $\Omega$ , 1  $\Omega$ , and 1.2  $\Omega$ ) at no load. In other words, the model was used to simulate 70 shorted turns/fault resistance values at no load condition. Figures 6.9 to 6.11 exhibit the extracted features for the 70 simulated cases. It is clear from the figures that the extracted features increase as the fault resistance decreases for a particular number of shorted turns, except the fundamental power factor angle in Figure 6.10 (b). Moreover, the features are distinct and follow certain patterns that make them very useful in designing a diagnostic tool. In addition, the effectiveness of the features increases as the fault resistance decreases. The same pattern

of distinct features has been observed under different loading condition while changing the fault resistance.

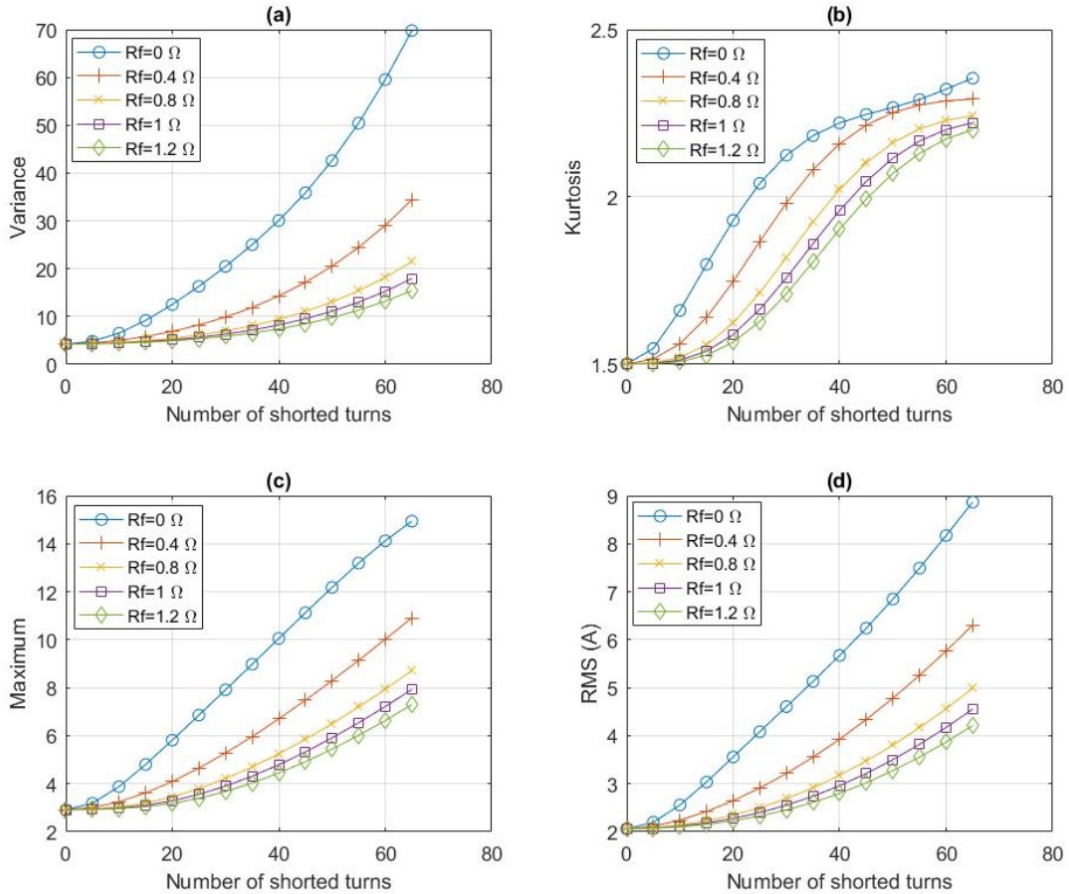


Figure 6.9 MATLAB extracted features for different fault resistor values at no load (a) variance (b) kurtosis (c) Maximum (d) RMS

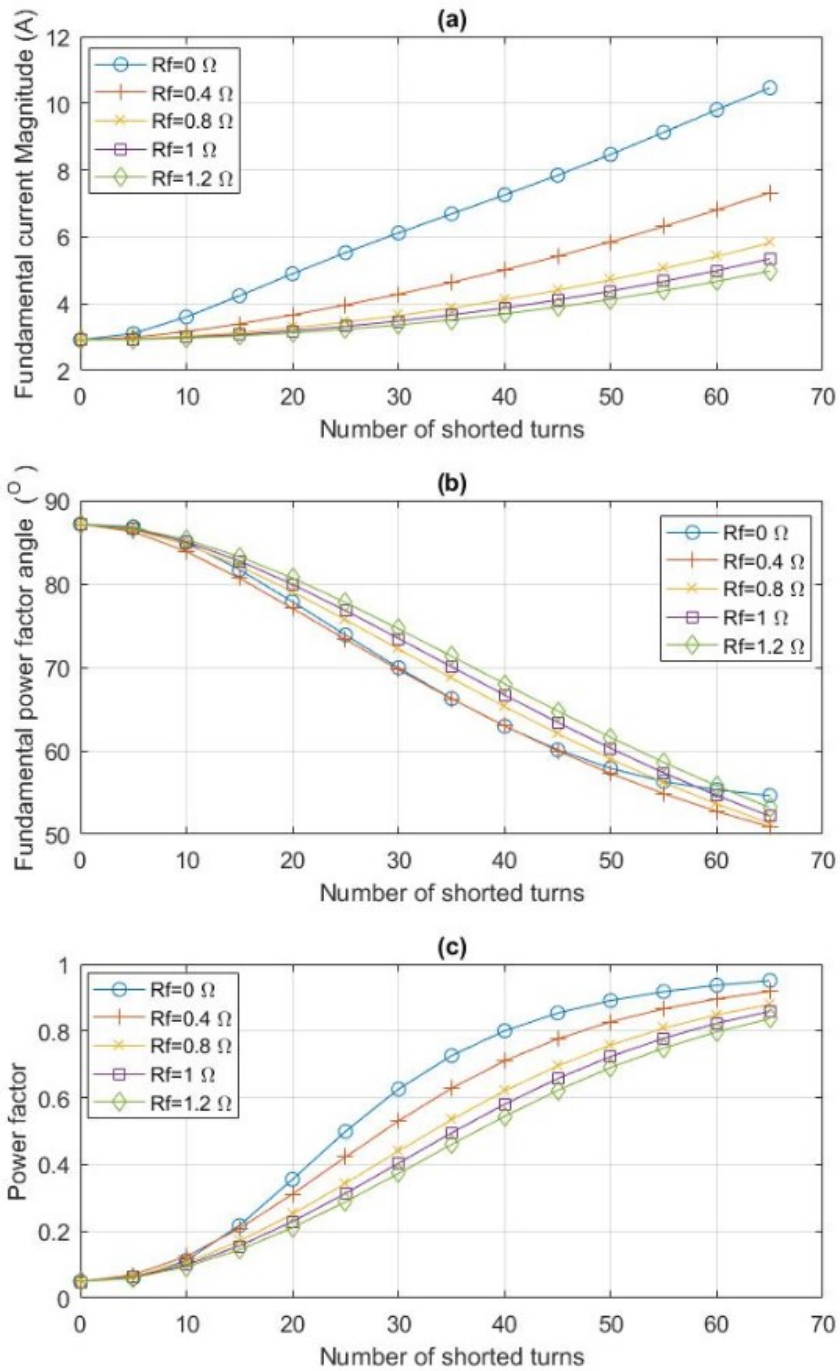


Figure 6.10 MATLAB extracted features for different fault resistor values at no load (a) Fundamental current Magnitude (b) Fundamental power factor angle (c) power factor

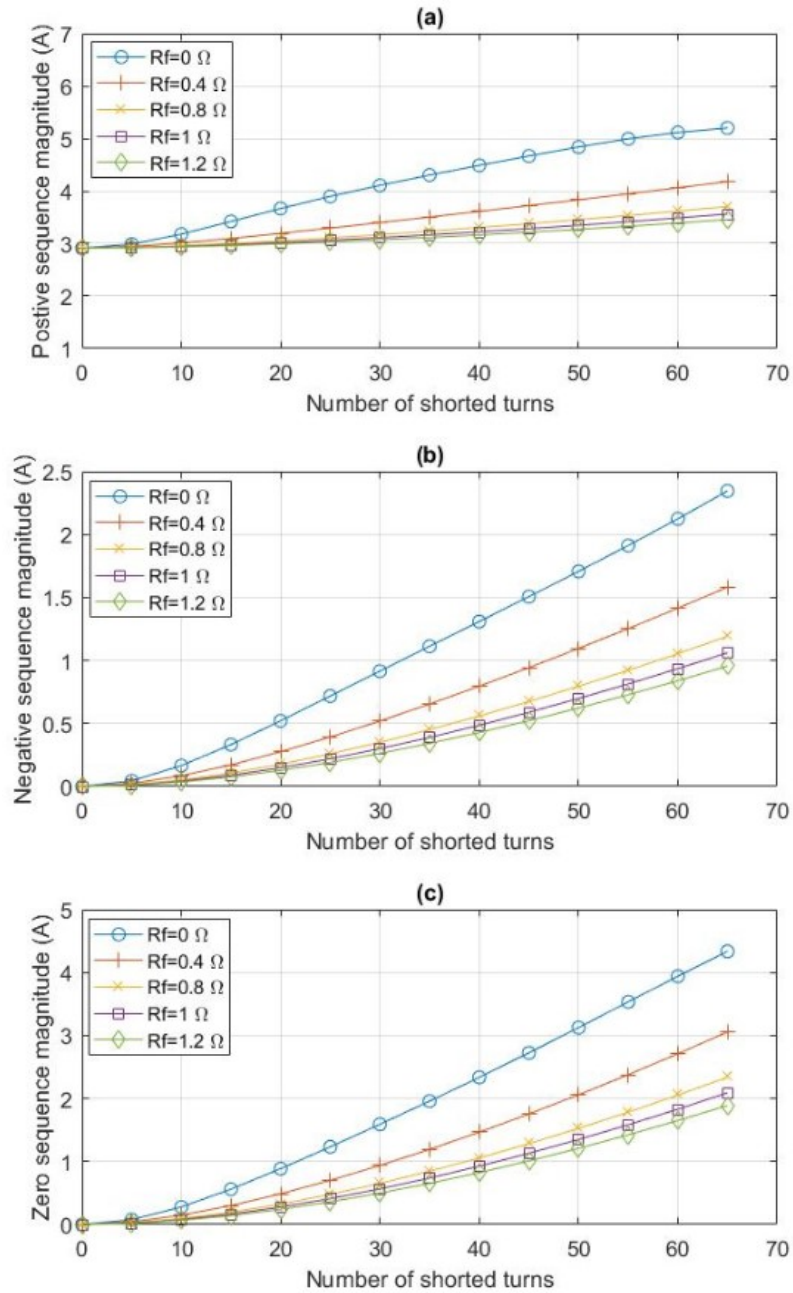


Figure 6.11 MATLAB extracted features for different fault resistor values at no load (a) positive sequence component magnitude (b) negative sequence component magnitude (c) zero sequence component magnitude

## 6.2.2 Features Extraction for the Asymmetry Condition

In this section, the same time and frequency-based features which are considered under inter-turn fault are investigated for the case of asymmetry condition under different load levels.

For the feature extraction, the developed mathematical model under asymmetry condition was simulated for 126 cases with different number of asymmetry turns in phase-a and different loading levels. For demonstration purposes, Figures 6.12-6.14 show the extracted features for the 126 simulated cases. Figures 6.12 to 6.14 show that the extracted features follow almost a certain pattern regardless of the load, also part of the features are less non-linear compare with the result under inter turn fault. In addition, for some of the features such as the zero sequence component, it values under inter-turn fault is less than for asymmetric condition at the same fault severity. Therefore, the extracted features will help in discriminating between the stator abnormalities and also in determining the size of the abnormalities.

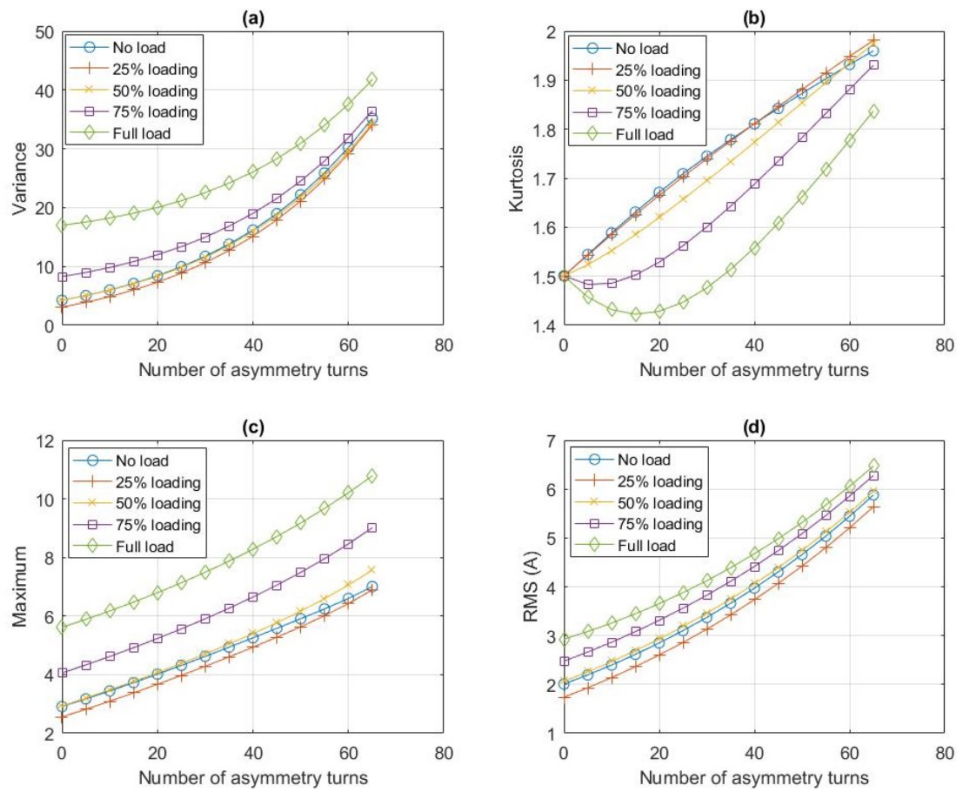


Figure 6.12 MATLAB extracted features under asymmetric condition in phase-a (a) variance (b) kurtosis (c) Maximum (d) RMS



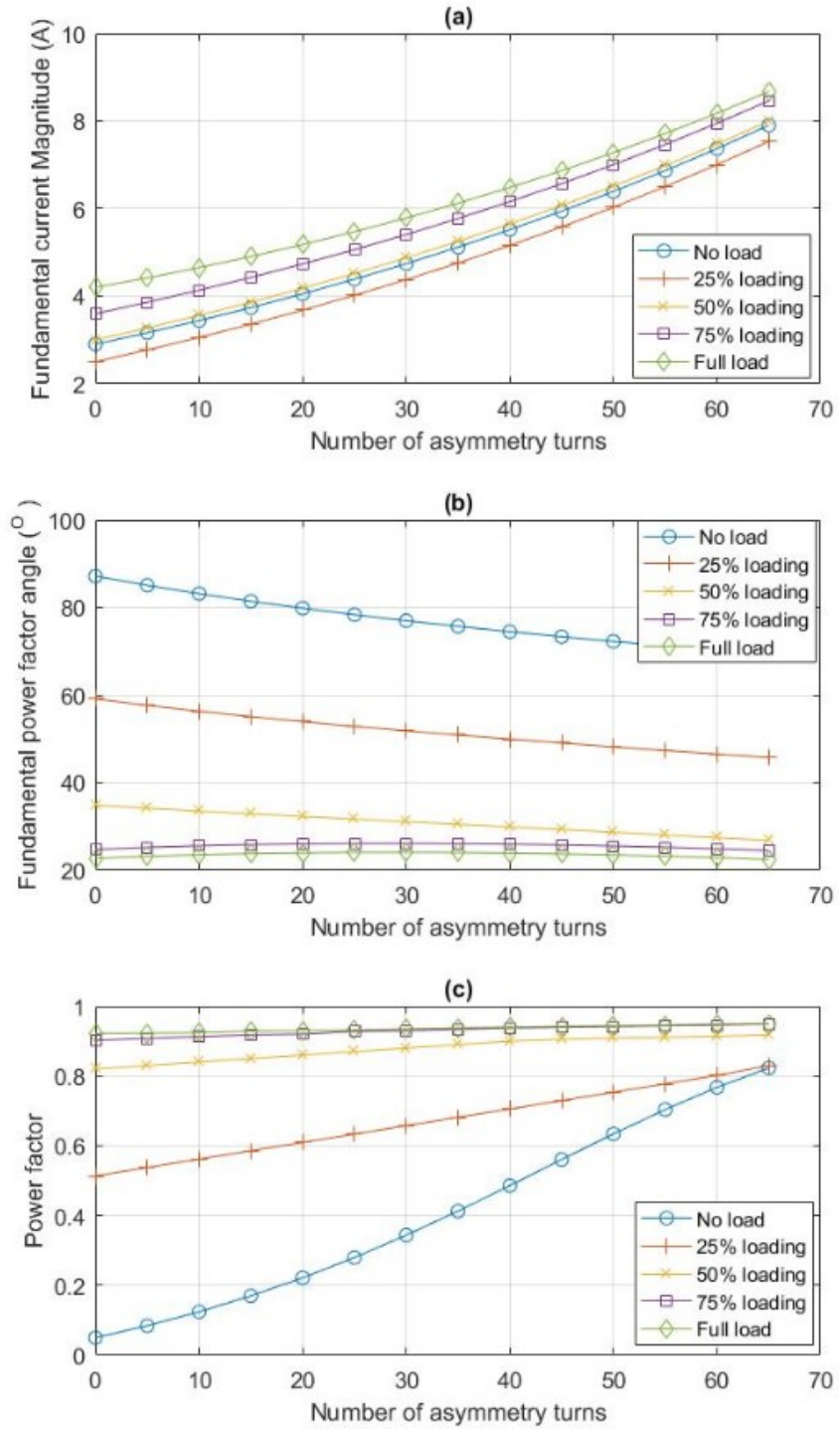


Figure 6.13 MATLAB extracted features under asymmetric condition in phase-a (a) Fundamental current Magnitude (b) Fundamental power factor angle (c) power factor

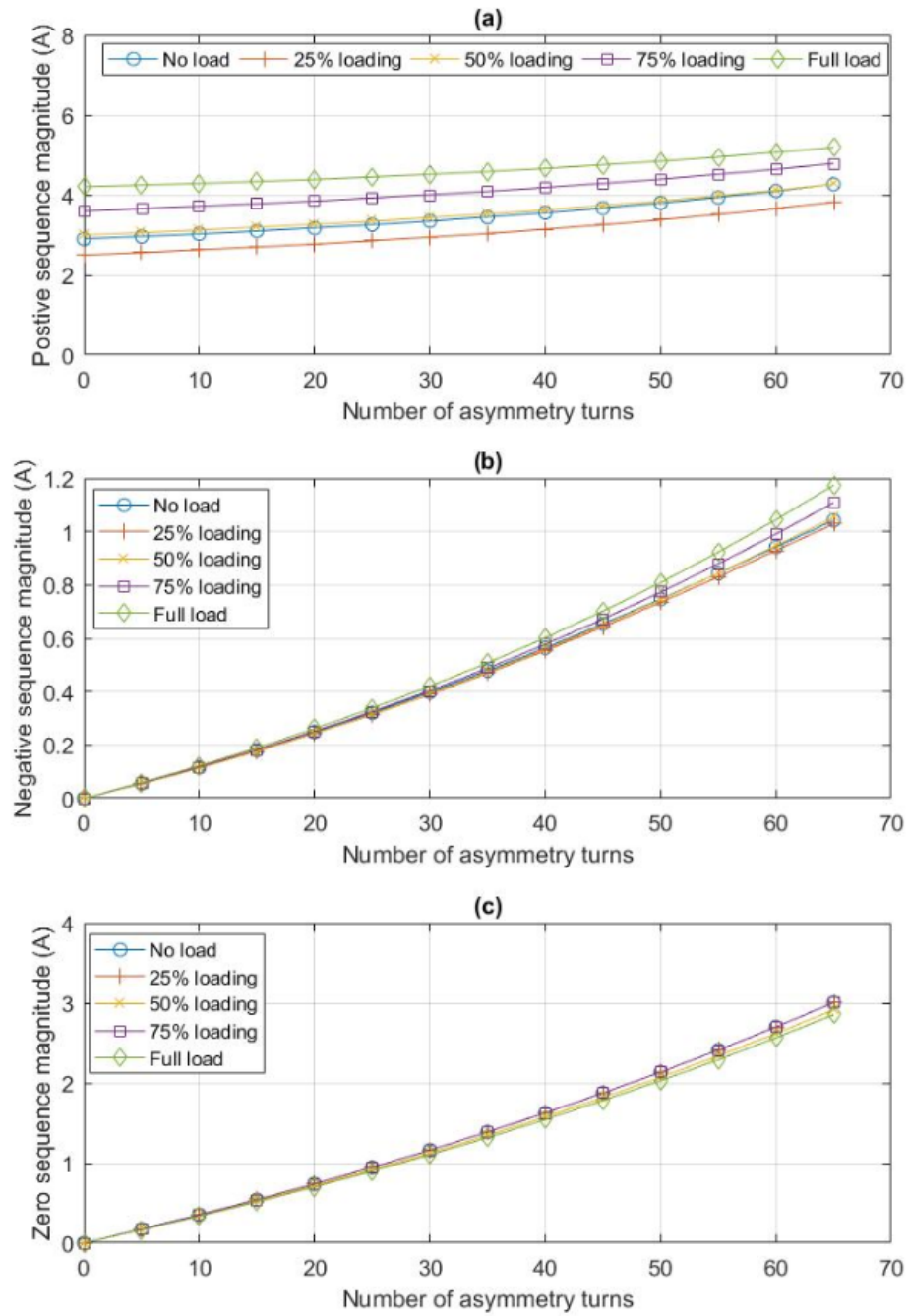


Figure 6.14 MATLAB extracted features under asymmetric condition in phase-a (a) positive sequence component magnitude (b) negative sequence component magnitude (c) zero sequence component magnitude

### 6.3 Neural Network Design

The most commonly used neural network for classification purposes is the multi-layer feed-forward neural network (MFNN). The feed-forward NN has the ability to learn various types of complex linear and nonlinear functions. Therefore, it can be utilized to learn different types of motor faults to accurately predict the type and severity of the fault. This type of detection is considered to be inexpensive and noninvasive. This section describes the design of ANN used as a tool for detecting the inter-turn fault and asymmetric condition in stator winding of LSPMSMs. The neural network has two outputs which represent the number of shorted turns and the number of asymmetry turns whereas 10 inputs were specified, including; Variance, Kurtosis, Maximum, RMS, fundamental current magnitude, fundamental power factor angle and power factor of the tested phase as well as the stator current symmetrical components (positive, negative and zero).

Different topologies of the feed-forward neural network with different number of hidden layers and hidden neurons have been tried to create suboptimal networks that correlate the extracted features with the corresponding abnormality type and severity. Figure 6.15 shows the topology of the designed neural network. The ANN consists of two hidden layers with 10 and 4 neurons, respectively. The activation function of all the neurons is 'tansig'. During the training of the ANN, 756 simulation cases have been used. These represent inter-turn faults and asymmetry conditions at different loading levels. For training, 14 sets of shorted turns (0, 5, 10, 15, 20, 25, 30, 35, 40, 45, 50, 55, 60 and 65) and 9 loading conditions (no load, 0.5N.m, 1N.m, 1.5N.m, 2N.m, 2.5N.m, 3N.m, 3.5N.m and 4N.m) as well as 5 fault resistance values (0  $\Omega$ , 0.4  $\Omega$ , 0.8  $\Omega$ , 1  $\Omega$ , and 1.2  $\Omega$ ) have



been considered. In addition, 14 sets of asymmetry condition and 9 loading levels have also been considered. It is worth mentioning that the number of shorted and asymmetry turns and loading values during testing are different from those for the training process.

Table 6.1 shows a sample of the 100 testing cases.

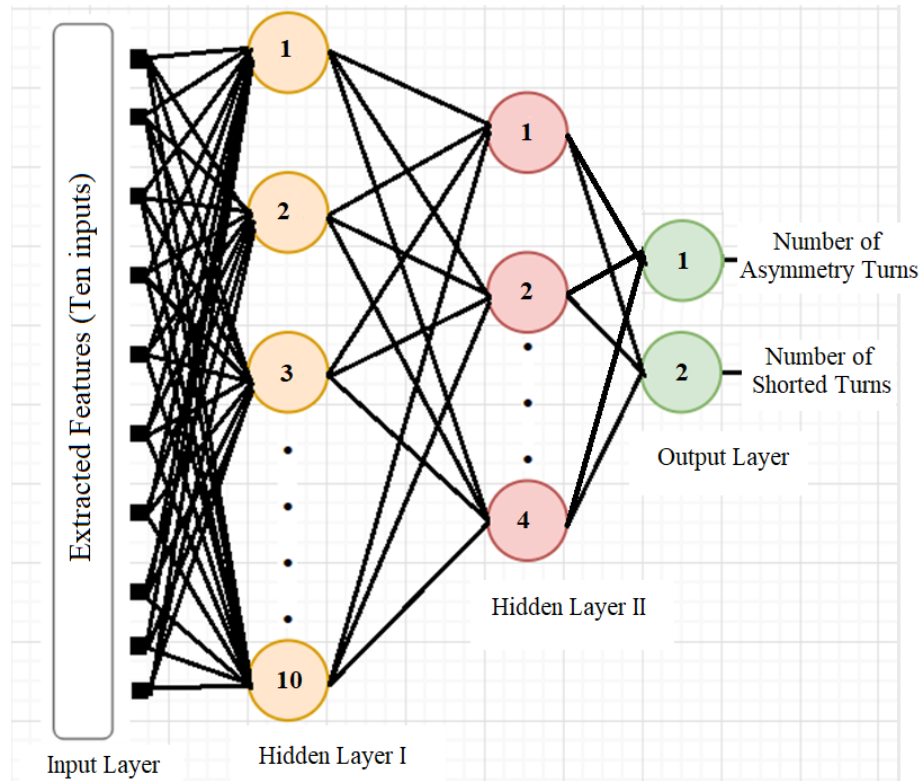


Figure 6.15 Neural network topology

The criterion of assuming a true (T) detection of abnormality is as follows: the detection is true if the difference between the predicted and the actual number of turns is less or equal to 2 turns. Otherwise, it is false (F). Based on this criterion, and for abnormalities that have never been seen by the trained neural network, the proposed diagnostic tool is found to have an accuracy of 96% in detecting the stator winding abnormalities, where only 4 cases out of 100 are identified to be wrongly detected. This reveals high accuracy of the developed diagnostic tool.

**Table 6.1 Sample of the testing results**

Case #	Load (N.m)	Rf (Ohm)	Actual shorted turns	Actual asymmetry turns	Detected shorted turns	Detected asymmetry turns	T/F detection
1	0	0	3	0	0	0	F
2	0.25	0.1	6	0	4	0	T
3	0.5	0.2	9	0	9	0	T
4	0.75	0.3	12	0	12	0	T
5	1	0.4	15	0	15	0	T
6	1.25	0.5	18	0	18	0	T
7	1.5	0.6	21	0	21	0	T
8	1.75	0.7	24	0	24	0	T
9	2	0.8	27	0	27	0	T
10	2.25	0.9	30	0	30	0	T
11	2.5	1	33	0	33	0	T
12	2.75	1.1	36	0	36	0	T
13	3	1.2	39	0	39	0	T
14	3.25	0	42	0	42	0	T
15	3.5	0.1	45	0	45	0	T
16	0	0	0	3	0	0	F
17	0.25	0	0	6	0	6	T
18	0.5	0	0	9	0	9	T
19	0.75	0	0	12	0	12	T
20	1	0	0	15	0	15	T
21	1.25	0	0	18	0	18	T
22	1.5	0	0	21	0	21	T
23	1.75	0	0	24	0	24	T
24	2	0	0	27	0	27	T
25	2.25	0	0	30	0	30	T
26	2.5	0	0	33	0	33	T
27	2.75	0	0	36	0	36	T
28	3	0	0	39	0	39	T
29	3.25	0	0	42	0	42	T
30	3.5	0	0	45	0	45	T

#### 6.4 Robustness of the developed Diagnostic Tool

The robustness of the proposed diagnostic tool against motor parameter variations (permanent magnet linkage flux, motor inertia, stator resistance and supply voltages) has been tested. In this section, the tool has been examined under five cases. In the first case the supply voltages were varied within  $\pm 3\%$ . In the second case the motor inertia was

varied within +3%. In the third case the stator resistance was varied within +3%. In the fourth case the flux linkage of the permanent magnet was varied within -3%. In the last case both supply voltages and motor inertia were varied by  $\pm 3\%$  and +3%, respectively. Tables 6.2 – 6.6 show samples of the testing result (30 pattern of the 100 testing pattern) for each of the five cases. It has been found that the abnormality detection accuracy decreased by no more than 3%.

**Table 6.2 Sample of the testing results under variation in the supply voltages**

Case #	Voltage (v)	Actual shorted turns	Actual asymmetry turns	Detected shorted turns	Detected asymmetry turns	T/F detection
1	388.0	3	0	0	0	F
2	389.0	6	0	2	0	F
3	390.0	9	0	6	0	F
4	391.0	12	0	10	0	T
5	392.0	15	0	15	0	T
6	393.0	18	0	19	0	T
7	394.0	21	0	21	0	T
8	395.0	24	0	24	0	T
9	396.0	27	0	27	0	T
10	397.0	30	0	30	0	T
11	398.0	33	0	33	0	T
12	399.0	36	0	36	0	T
13	400.0	39	0	39	0	T
14	401.0	42	0	42	0	T
15	402.0	45	0	45	0	T
16	388.0	0	3	0	6	F
17	389.0	0	6	0	7	T
18	390.0	0	9	0	10	T
19	391.0	0	12	0	12	T
20	392.0	0	15	0	15	T
21	393.0	0	18	0	18	T
22	394.0	0	21	0	21	T
23	395.0	0	24	0	24	T
24	396.0	0	27	0	27	T
25	397.0	0	30	0	30	T
26	398.0	0	33	0	33	T
27	399.0	0	36	0	36	T
28	400.0	0	39	0	39	T
29	401.0	0	42	0	42	T
30	402.0	0	45	0	45	T

**Table 6.3 Sample of the testing results under variation in the motor inertia**

Case #	Inertia (J)	Actual shorted turns	Actual asymmetry turns	Detected shorted turns	Detected asymmetry turns	T/F detection
1	0.0007019	3	0	0	0	F
2	0.0007027	6	0	4	0	T
3	0.0007034	9	0	9	0	T
4	0.0007042	12	0	12	0	T
5	0.0007049	15	0	15	0	T
6	0.0007057	18	0	18	0	T
7	0.0007065	21	0	21	0	T
8	0.0007072	24	0	24	0	T
9	0.0007080	27	0	27	0	T
10	0.0007087	30	0	30	0	T
11	0.0007095	33	0	33	0	T
12	0.0007102	36	0	36	0	T
13	0.0007110	39	0	39	0	T
14	0.0007117	42	0	42	0	T
15	0.0007125	45	0	45	0	T
16	0.0007019	0	3	0	0	F
17	0.0007029	0	6	0	6	T
18	0.0007039	0	9	0	9	T
19	0.0007049	0	12	0	12	T
20	0.0007060	0	15	0	15	T
21	0.0007070	0	18	0	18	T
22	0.0007080	0	21	0	21	T
23	0.0007090	0	24	0	24	T
24	0.0007100	0	27	0	27	T
25	0.0007110	0	30	0	30	T
26	0.0007120	0	33	0	33	T
27	0.0007130	0	36	0	36	T
28	0.0007140	0	39	0	39	T
29	0.0007150	0	42	0	42	T
30	0.0007160	0	45	0	45	T

**Table 6.4 Sample of the testing results under variation in stator resistance**

Case #	Rs (Ohm)	Actual shorted turns	Actual asymmetry turns	Detected shorted turns	Detected asymmetry turns	T/F detection
1	5.5527	3	0	0	0	F
2	5.5587	6	0	3	0	F
3	5.5646	9	0	8	0	T
4	5.5706	12	0	11	0	T
5	5.5765	15	0	15	0	T
6	5.5825	18	0	18	0	T
7	5.5884	21	0	21	0	T
8	5.5944	24	0	24	0	T
9	5.6003	27	0	27	0	T
10	5.6063	30	0	30	0	T
11	5.6122	33	0	33	0	T
12	5.6182	36	0	36	0	T
13	5.6241	39	0	39	0	T
14	5.6301	42	0	42	0	T
15	5.6360	45	0	45	0	T
16	5.5527	0	3	0	1	T
17	5.5607	0	6	0	5	T
18	5.5686	0	9	0	9	T
19	5.5765	0	12	0	12	T
20	5.5845	0	15	0	15	T
21	5.5924	0	18	0	18	T
22	5.6003	0	21	0	21	T
23	5.6083	0	24	0	24	T
24	5.6162	0	27	0	27	T
25	5.6241	0	30	0	30	T
26	5.6320	0	33	0	33	T
27	5.6400	0	36	0	36	T
28	5.6479	0	39	0	39	T
29	5.6558	0	42	0	42	T
30	5.6638	0	45	0	45	T

**Table 6.5 Sample of the testing results under variation in PM flux linkage**

Case #	Flux linkage	Actual shorted turns	Actual asymmetry turns	Detected shorted turns	Detected asymmetry turns	T/F detection
1	0.5797	3	0	0	0	F
2	0.5799	6	0	2	0	F
3	0.5801	9	0	7	0	T
4	0.5803	12	0	11	0	T
5	0.5806	15	0	14	0	T
6	0.5808	18	0	17	0	T
7	0.5810	21	0	20	0	T
8	0.5812	24	0	23	0	T
9	0.5814	27	0	26	0	T
10	0.5816	30	0	29	0	T
11	0.5818	33	0	33	0	T
12	0.5820	36	0	36	0	T
13	0.5822	39	0	39	0	T
14	0.5825	42	0	42	0	T
15	0.5827	45	0	45	0	T
16	0.5797	0	3	0	0	F
17	0.5800	0	6	0	4	T
18	0.5803	0	9	0	7	T
19	0.5806	0	12	0	11	T
20	0.5808	0	15	0	14	T
21	0.5811	0	18	0	17	T
22	0.5814	0	21	0	20	T
23	0.5817	0	24	0	24	T
24	0.5820	0	27	0	27	T
25	0.5822	0	30	0	30	T
26	0.5825	0	33	0	33	T
27	0.5828	0	36	0	36	T
28	0.5831	0	39	0	39	T
29	0.5834	0	42	0	42	T
30	0.5837	0	45	0	45	T

**Table 6.6 Sample of the testing results under variation in both supply voltages and motor inertia**

case #	Voltage (v)	Inertia (J)	Actual shorted turns	Actual asymmetry turns	Detected shorted turns	Detected asymmetry turns	T/F detection
1	388.0	0.0007019	3	0	0	0	F
2	389.0	0.0007027	6	0	2	0	F
3	390.0	0.0007034	9	0	6	0	F
4	391.0	0.0007042	12	0	10	0	T
5	392.0	0.0007049	15	0	14	0	T
6	393.0	0.0007057	18	0	19	0	T
7	394.0	0.0007065	21	0	21	0	T
8	395.0	0.0007072	24	0	24	0	T
9	396.0	0.0007080	27	0	27	0	T
10	397.0	0.0007087	30	0	30	0	T
11	398.0	0.0007095	33	0	33	0	T
12	399.0	0.0007102	36	0	36	0	T
13	400.0	0.0007110	39	0	39	0	T
14	401.0	0.0007117	42	0	42	0	T
15	402.0	0.0007125	45	0	45	0	T
16	388.0	0.0007019	0	3	0	6	F
17	389.0	0.0007029	0	6	0	9	F
18	390.0	0.0007039	0	9	0	11	T
19	391.0	0.0007049	0	12	0	12	T
20	392.0	0.0007060	0	15	0	15	T
21	393.0	0.0007070	0	18	0	18	T
22	394.0	0.0007080	0	21	0	21	T
23	395.0	0.0007090	0	24	0	24	T
24	396.0	0.0007100	0	27	0	27	T
25	397.0	0.0007110	0	30	0	30	T
26	398.0	0.0007120	0	33	0	33	T
27	399.0	0.0007130	0	36	0	36	T
28	400.0	0.0007140	0	39	0	39	T
29	401.0	0.0007150	0	42	0	42	T
30	402.0	0.0007160	0	45	0	45	T

## 6.5 Diagnostic Tool Deployment

The deployment of the diagnostic tool in reality could be realized as shown in Figure 6.16. The proposed fault detection tool starts by measuring the three phase currents and voltages signals using current and voltages sensors, respectively, which are connected to a computer through a data acquisition system. In the computer, the captured currents and voltages signals undergoes time and frequency domain analysis to extract the desired time- and frequency-based features. The extracted features are applied to the trained neural network, which gives the type and severity of the abnormality.

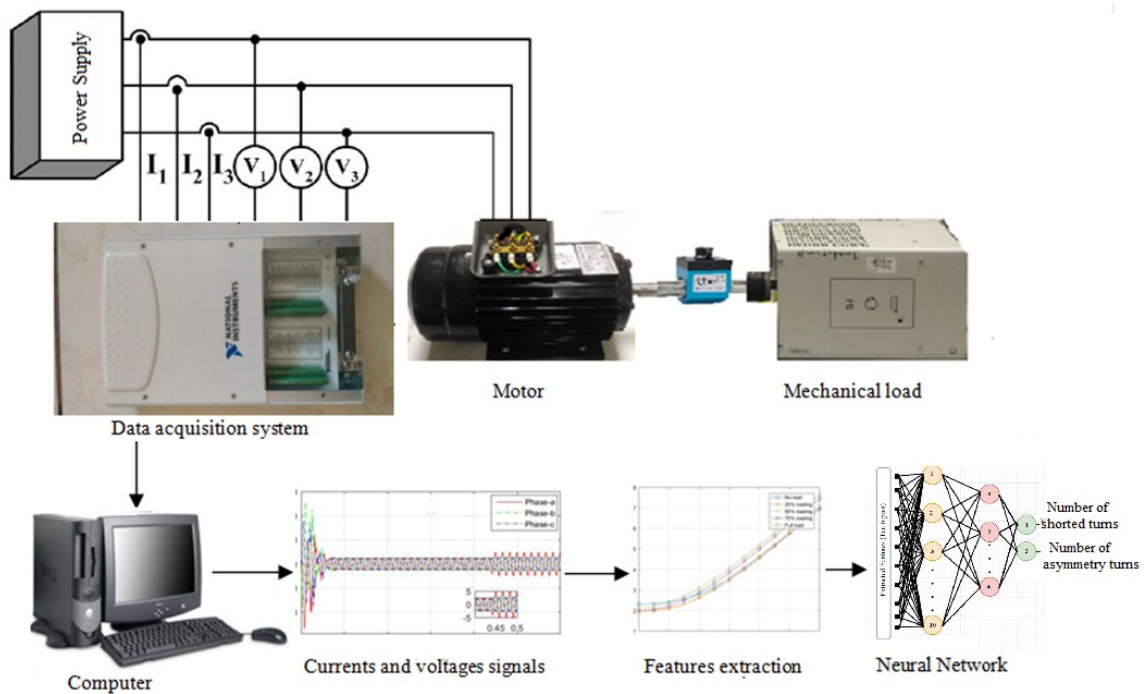


Figure 6.16 Diagnostic tool deployment.



## CHAPTER 7

### CONCLUSION AND FUTURE WORK

#### 7.1 Conclusion

This research work presents novel mathematical models for LSPMSM under stator under asymmetrical stator winding and inter-turn fault. In addition, a diagnostic tool for detecting the type and severity of these abnormalities was developed. The developed tool is based on a combination of signal processing technique and artificial neural network.

The main achievements of this dissertation can be summarized as follows:

- A QD0-mathematical and JMAG<sup>TM</sup> finite-element based models for interior-mount LSPMSM under asymmetrical stator phases winding have been developed. The developed QD0-mathematical model has been implemented and simulated using MATLAB software. Under asymmetrical stator phases winding conditions, MATLAB and JMAG<sup>TM</sup> simulation results show good agreement. In addition, the results revealed that under different asymmetric percentage between stator phases, different levels of oscillations are present in the motor speed and torque responses where oscillations increase as the asymmetry between stator phase winding increases.
- A QD0-mathematical and JMAG<sup>TM</sup> finite-element based models for interior-mount LSPMSM under stator inter-turn faults have been developed. The

developed mathematical model has been implemented using MATLAB, simulated and experimentally tested using a 1-hp interior-mount LSPMSM. The accuracy of the mathematical model was verified by comparing the results obtained from the MATLAB simulation and experimental tests as well as JMAG model under different numbers of shorted turns and fault resistance at different loading levels. Additionally, the simulation and experimental results show that the inter-turn fault affects the current (magnitude and time response profile) in the phase that contains the shorted turns. The effect increases as the number of shorted turns increases under the same fault resistance. In addition, the results show that the inter-turn fault introduces oscillations in the speed response at steady state.

- A set of experimental tests were conducted in the electric machine laboratory at KFUPM on a 1hp Interior-mount LSPMSM to measure the electric circuit parameters. The tests include; DC test to measure the stator DC resistance, AC single phase (rotor not included) test to measure stator AC resistance and leakage inductance, block rotor test to measure rotor resistance and leakage inductance in both d and q-axis, DC step test to measure the magnetizing inductance in d and q-axis, and the open circuit test to measure the flux linkage from the permanent magnets. The measured parameters are used in the developed QD0 mathematical models. The simulation and experimental testing confirm the accuracy of the measured parameters.
- A neural network based tool for detecting the severity of stator winding abnormalities under different loading condition has been developed. The stator

currents and voltages are used as fault indicators. Several time-based and frequency-based features (Variance, Kurtosis, Maximum, RMS value, the magnitude of the fundamental current component, fundamental power factor angle, power factor of the faulted phase and the three phase current symmetrical components) were extracted from the fault indicators for the two types of abnormalities. These features were found to be distinct and hence are used in developing the neural network that is capable of accurately predicting the type and severity of stator winding abnormalities. The input to the developed tool are the 10 extracted features while the output are two (the size of inter-turn fault and the size of asymmetry condition). The accuracy of the developed tool was confirmed by testing 100 unseen cases. The overall accuracy of detecting the stator winding abnormalities is 96% .

- Finally, the robustness of the proposed diagnostic tool against motor parameter variations (permanent magnet linkage flux, motor inertia, stator resistance and supply voltages) has been investigated. It has been found that the abnormality detection accuracy decreased by no more than 3%.

## 7.2 Future Work

In order to develop a general-purpose tool for detecting the possible type and size of faults associated with LSPMSMs, a number of problems must be solved. These problems suggest a variety of research directions that need to be pursued to make such a system available. The following presents some suggestion of these research topics.

- The developed diagnostic tool can be generalized to detect multiple types of faults, such as a combination of inter-turn and broken bar and/or inter-turn and eccentricity.
- Developing a mathematical model that investigates the effect of inter-turn fault on PM performance (Demagnetization). In addition, the effect of core saturation can be considered.
- Considering the spatial harmonics components in the development of the mathematical model.
- Investigating the use of conventional neural network or neuro-fuzzy system for the development of the diagnostic tool.
- Investigating the use of the developed LSPMSM mathematical model in variable frequency drives.

## References

- [1] L. Maraaba, Z. Al-Hamouz, A. Milhem, and M. Abido, "Modeling of Interior-Mount LSPMSM under Asymmetrical Stator Winding," *IET Electric Power Applications*, 2018.
- [2] B. Yan, X. Wang, and Y. Yang, "Starting Performance Improvement of Line-Start Permanent-Magnet Synchronous Motor Using Composite Solid Rotor," *IEEE Transactions on Magnetics*, vol. 54, pp. 1-4, 2018.
- [3] J. C. Quiroz, N. Mariun, M. R. Mehrjou, M. Izadi, N. Misron, and M. A. M. Radzi, "Fault detection of broken rotor bar in LS-PMSM using random forests," *Measurement*, vol. 116, pp. 273-280, 2018.
- [4] B. Wang, J. Wang, A. Griffo, and B. Sen, "Stator Turn Fault Detection by 2nd Harmonic in Instantaneous Power for a Triple Redundant Fault-tolerant PM Drive," *IEEE Transactions on Industrial Electronics*, 2018.
- [5] Y. Qi, E. Bostanci, V. Gurusamy, and B. Akin, "A Comprehensive Analysis of Short Circuit Current Behavior in PMSM Inter Turn Short Circuit Faults," *IEEE Transactions on Power Electronics*, 2018.
- [6] A. Zhang, Y. Bai, B. Yang, and H. Li, "Analysis of Nonlinear Vibration in Permanent Magnet Synchronous Motors under Unbalanced Magnetic Pull," *Applied Sciences*, vol. 8, p. 113, 2018.
- [7] M. Zhu, W. Hu, and N. C. Kar, "Acoustic Noise-Based Uniform Permanent-Magnet Demagnetization Detection in SPMSM for High-Performance PMSM Drive," *IEEE Transactions on Transportation Electrification*, vol. 4, pp. 303-313, 2018.
- [8] H. Talhaoui, A. Menacer, A. Kessal, and A. Tarek, "Experimental diagnosis of broken rotor bars fault in induction machine based on Hilbert and discrete wavelet transforms," *The International Journal of Advanced Manufacturing Technology*, vol. 95, pp. 1399-1408, 2018.
- [9] W. T. Thomson and M. Fenger, "Current signature analysis to detect induction motor faults," *IEEE Industry Applications Magazine*, vol. 7, pp. 26-34, 2001.

- [10] W. Fei, P. C.-K. Luk, J. Ma, J.-X. Shen, and G. Yang, "A high-performance line-start permanent magnet synchronous motor amended from a small industrial three-phase induction motor," *IEEE Transactions on Magnetics*, vol. 45, pp. 4724-4727, 2009.
- [11] R. Ugale and B. Chaudhari, "Rotor Configurations for Improved Starting and Synchronous Performance of Line Start Permanent-Magnet Synchronous Motor," *IEEE Transactions on Industrial Electronics*, vol. 64, pp. 138-148, 2017.
- [12] H. Zhu and J. Huang, "Compensation control of suspension force for LS-BLPMSM," *IET Electric Power Applications*, vol. 11, pp. 622-630, 2017.
- [13] K. Kim, S. J. Kim, W. H. Kim, J. B. Im, S. Cho, and J. Lee, "The optimal design of the rotor bar for LSPMSM considering the starting torque and magnetic saturation," in *Electromagnetic Field Computation (CEFC), 2010 14th Biennial IEEE Conference on*, 2010, pp. 1-1.
- [14] W. Fei, P. C.-K. Luk, J. Ma, J.-X. Shen, and G. Yang, "A high-performance line-start permanent magnet synchronous motor amended from a small industrial three-phase induction motor," *IEEE Transactions on Magnetics*, vol. 45, pp. 4724-4727, 2009.
- [15] X. Feng, L. Liu, J. Kang, and Y. Zhang, "Super premium efficient line start-up permanent magnet synchronous motor," in *Electrical Machines (ICEM), 2010 XIX International Conference on*, 2010, pp. 1-6.
- [16] A. H. Isfahani, S. Vaez-Zadeh, and S. Hasanzadeh, "An educational toolbox for performance analysis of line-start permanent magnet synchronous motors," *Computer Applications in Engineering Education*, vol. 22, pp. 452-462, 2014.
- [17] X. Lu, K. L. V. Iyer, K. Mukherjee, and N. C. Kar, "Development of a novel magnetic circuit model for design of premium efficiency three-phase line start permanent magnet machines with improved starting performance," *IEEE Transactions on Magnetics*, vol. 49, pp. 3965-3968, 2013.
- [18] X. Z. Xu, Y. H. Cui, X. D. Wang, and Z. Zhang, "Starting Performance Analysis of Line-Start Permanent Magnet Synchronous Motor with Novel Rotor Structure," in *Applied Mechanics and Materials*, 2013, pp. 291-295.

- [19] A. H. Isfahani and S. Vaez-Zadeh, "Line start permanent magnet synchronous motors: Challenges and opportunities," *Energy*, vol. 34, pp. 1755-1763, 2009.
- [20] D. Stoia, O. CHIRILĂ, M. Cernat, and B. Drago, "THE BEHAVIOUR OF THE LSPSM IN ASYNCHRONOUS OPERATION," in *14 th International Power Electronics and Motion Control Conference*, 2010.
- [21] J. Soulard and H.-P. Nee, "Study of the synchronization of line-start permanent magnet synchronous motors," in *Industry Applications Conference, 2000. Conference Record of the 2000 IEEE*, 2000, pp. 424-431.
- [22] C. Jedryczka, R. M. Wojciechowski, and A. Demenko, "Finite element analysis of the asynchronous torque in LSPMSM with non-symmetrical squirrel cage winding," *International Journal of Applied Electromagnetics and Mechanics*, vol. 46, pp. 367-373, 2014.
- [23] X. Lu, K. L. V. Iyer, K. Mukherjee, and N. C. Kar, "A Novel Two-Axis Theory-Based Experimental Approach Towards Determination of Magnetization Characteristics of Line-Start Permanent Magnet Synchronous Machines," *IEEE Transactions on Magnetics*, vol. 49, pp. 4733-4737, 2013.
- [24] E. Muljadi and J. Green, "Cogging torque reduction in a permanent magnet wind turbine generator," in *ASME 2002 Wind Energy Symposium*, 2002, pp. 340-342.
- [25] C. Breton, J. Bartolome, J. Benito, G. Tassinario, I. Flotats, C. Lu, *et al.*, "Influence of machine symmetry on reduction of cogging torque in permanent-magnet brushless motors," *IEEE Transactions on Magnetics*, vol. 36, pp. 3819-3823, 2000.
- [26] E. Peralta-Sánchez and A. Smith, "Line-start permanent-magnet machines using a canned rotor," *IEEE Transactions on industry applications*, vol. 45, pp. 903-910, 2009.
- [27] E. Peralta-Sanchez and A. Smith, "Line-start permanent-magnet machines using a canned rotor," in *Electric Machines & Drives Conference, 2007. IEMDC'07. IEEE International*, 2007, pp. 1084-1089.
- [28] H. Behbahanifard and A. Sadoughi, "Cogging Torque Reduction in Line Start Permanent Magnet Synchronous Motor," *Journal of Electrical Engineering & Technology*, vol. 11, pp. 878-888, 2016.

- [29] V. Elistratova, "Optimal design of line-start permanent magnet synchronous motors of high efficiency," Ecole Centrale de Lille, 2015.
- [30] C.-M. Ong, *Dynamic simulation of electric machinery: using MATLAB/SIMULINK* vol. 5: Prentice Hall PTR Upper Saddle River, NJ, 1998.
- [31] X. Lu, K. Iyer, K. Mukherjee, and N. C. Kar, "A Novel Two-Axis Theory-Based Experimental Approach Towards Determination of Magnetization Characteristics of Line-Start Permanent Magnet Synchronous Machines," *Magnetics, IEEE Transactions on*, vol. 49, pp. 4733-4737, 2013.
- [32] M. H. Soreshjani, A. Ghafari, and M. Haghparast, "Direct Torque and Flux Controlled Space Vector Modulated (DTFC-SVM) Based on Fuzzy Logic Controller for Line-Start Permanent Magnet Synchronous and Permanent Magnet Synchronous Machines," *Journal of Control Engineering and Applied Informatics*, vol. 16, pp. 75-83, 2014.
- [33] P. M. S. MOTORS, "Educational Bench of Line-Start Permanent Magnet Synchronous Motors Part I: Operating Point Of Permanent Magnet," 2009.
- [34] D. STOIA, M. Cernat, H. HAMEYER, and D. Ban, "Line-start permanent magnet synchronous motors. analysis and design," in *15 th International Conference on Electrical Drives and Power Electronics, EDPE 2009*, 2009.
- [35] J. Kinnunen, "Direct-on-line axial flux permanent magnet synchronous generator static and dynamic performance," *Acta Universitatis Lappeenrantaensis*, 2007.
- [36] Y.-Y. Choe, S.-Y. Oh, S.-H. Ham, I.-S. Jang, S.-Y. Cho, J. Lee, *et al.*, "Comparison of concentrated and distributed winding in an IPMSM for vehicle traction," *Energy Procedia*, vol. 14, pp. 1368-1373, 2012.
- [37] U. A. Bakshi and V. U. Bakshi, *Electrical Circuits and Machines: Technical Publications*, 2009.
- [38] J. K. Tangudu, "On modeling and design of fractional-slot concentrated-winding interior permanent magnet machines," University of Wisconsin--Madison, 2011.
- [39] G. Pellegrino, A. Vagati, P. Guglielmi, and B. Boazzo, "Performance comparison between surface-mounted and interior PM motor drives for electric vehicle application," *IEEE Transactions on Industrial Electronics*, vol. 59, pp. 803-811, 2012.



- [40] V. Giurgiutiu and S. E. Lyshevski, *Micromechatronics: Modeling, analysis, and design with MATLAB*: CRC Press, 2016.
- [41] C. U. Ogbuka, C. M. Nwosu, and M. U. Agu, "Performance comparison of line-start permanent magnet synchronous motors with interior and surface rotor magnets," *Indian Journal of Science and Technology*, vol. 9, 2016.
- [42] P. Huang, S. Mao, M. Tsai, and C. Liu, "Investigation of line start permanent magnet synchronous motors with interior-magnet rotors and surface-magnet rotors," in *Electrical Machines and Systems, 2008. ICEMS 2008. International Conference on*, 2008, pp. 2888-2893.
- [43] S. Nandi, H. A. Toliyat, and X. Li, "Condition monitoring and fault diagnosis of electrical motors—A review," *IEEE transactions on energy conversion*, vol. 20, pp. 719-729, 2005.
- [44] H. Abdallah and K. Benatman, "Stator winding inter-turn short-circuit detection in induction motors by parameter identification," *IET Electric Power Applications*, vol. 11, pp. 272-288, 2017.
- [45] D. G. Jerkan, D. D. Reljic, and D. Marcetic, "Broken Rotor Bar Fault Detection of IM Based on the Counter-Current Braking Method," *IEEE Transactions on Energy Conversion*, 2017.
- [46] J.-X. Shen, P. Li, M.-J. Jin, and G. Yang, "Investigation and countermeasures for demagnetization in line start permanent magnet synchronous motors," *IEEE Transactions on Magnetics*, vol. 49, pp. 4068-4071, 2013.
- [47] H. Henao, G.-A. Capolino, M. Fernandez-Cabanas, F. Filippetti, C. Bruzzese, E. Strangas, *et al.*, "Trends in fault diagnosis for electrical machines: A review of diagnostic techniques," *IEEE industrial electronics magazine*, vol. 8, pp. 31-42, 2014.
- [48] L. Maraaba, Z. Al-Hamouz, and M. Abido, "Modeling and simulation of line start permanent magnet synchronous motors with asymmetrical stator windings," in *Industrial Electronics Society, IECON 2016-42nd Annual Conference of the IEEE*, 2016, pp. 1698-1703.
- [49] R. Yan, R. X. Gao, and X. Chen, "Wavelets for fault diagnosis of rotary machines: a review with applications," *Signal Processing*, vol. 96, pp. 1-15, 2014.

- [50] S. Nandi, H. A. Toliyat, and X. Li, "Condition monitoring and fault diagnosis of electrical motors-a review," *IEEE Transactions on Energy Conversion*, vol. 20, pp. 719-729, 2005.
- [51] J. Pons-Llinares, J. A. Antonino-Daviu, M. Riera-Guasp, S. B. Lee, T. j. Kang, and C. Yang, "Advanced Induction Motor Rotor Fault Diagnosis Via Continuous Time and Discrete Frequency Tools," *IEEE Transactions on Industrial Electronics*, vol. 62, pp. 1791-1802, 2015.
- [52] M. Karami, N. Mariun, M. Rezazadeh Mehrjou, M. Z. A. Ab Kadir, N. Misron, and M. A. Mohd Radzi, "Static eccentricity fault recognition in three-phase line start permanent magnet synchronous motor using finite element method," *Mathematical Problems in Engineering*, vol. 2014, 2014.
- [53] M. Mehrjou, N. Mariun, M. Karami, N. Misron, and M. Mohd Radzi, "Broken Rotor Bar Detection in LS-PMSMs Based on Statistical Features Analysis of Start-up Current Envelope," in *Smart Instrumentation, Measurement and Application (ICSIMA), 2015 IEEE The International Conference on*, 2015.
- [54] A. M. C. MA Cruz, S, "Rotor cage fault diagnosis in three-phase induction motors by extended Park's vector approach," *Electric Machines & Power Systems*, vol. 28, pp. 289-299, 2000.
- [55] S. B. Lee, K. Younsi, and G. B. Kliman, "An online technique for monitoring the insulation condition of AC machine stator windings," *Energy Conversion, IEEE Transactions on*, vol. 20, pp. 737-745, 2005.
- [56] A. Singh, B. Grant, R. DeFour, C. Sharma, and S. Bahadoorsingh, "A review of induction motor fault modeling," *Electric Power Systems Research*, vol. 133, pp. 191-197, 2016.
- [57] M. Arkan, D. Kostic-Perovic, and P. Unsworth, "Modelling and simulation of induction motors with inter-turn faults for diagnostics," *Electric Power Systems Research*, vol. 75, pp. 57-66, 2005.
- [58] W. Liu, L. Liu, I.-Y. Chung, D. A. Cartes, and W. Zhang, "Modeling and detecting the stator winding fault of permanent magnet synchronous motors," *Simulation Modelling Practice and Theory*, vol. 27, pp. 1-16, 2012.

- [59] S. Wiak, A. Krawczyk, I. Dolezel, J. Ahmed Farooq, T. Raminosoa, A. Djerdir, *et al.*, "Modelling and simulation of stator winding inter-turn faults in permanent magnet synchronous motors," *COMPEL-The international journal for computation and mathematics in electrical and electronic engineering*, vol. 27, pp. 887-896, 2008.
- [60] T. Kawady, A. Afify, A. Osheiba, and A. Taalab, "Modeling and experimental investigation of stator winding faults in induction motors," *Electric Power Components and Systems*, vol. 37, pp. 599-611, 2009.
- [61] R. M. Tallam, T. G. Habetler, and R. G. Harley, "Transient model for induction machines with stator winding turn faults," in *Industry Applications Conference, 2000. Conference Record of the 2000 IEEE*, 2000, pp. 304-309.
- [62] L. Liu and E. Collins, "ROBUST FAULT DETECTION AND DIAGNOSIS FOR PERMANENT MAGNET SYNCHRONOUS MOTORS ," 2006.
- [63] P. Tavner and A. Anderson, "Core faults in large generators," *IEE Proceedings-Electric Power Applications*, vol. 152, pp. 1427-1439, 2005.
- [64] R. Romary, C. Demian, P. Schlupp, and J.-Y. Roger, "Offline and online methods for stator core fault detection in large generators," *IEEE Transactions on Industrial Electronics*, vol. 60, pp. 4084-4092, 2013.
- [65] E. Ajily, M. Ardebili, and K. Abbaszadeh, "Magnet defect and rotor eccentricity modeling in axial-flux permanent-magnet machines via 3-D field reconstruction method," *IEEE Transactions on Energy Conversion*, vol. 31, pp. 486-495, 2016.
- [66] Y. Li, Q. Lu, and Z.-Q. Zhu, "Unbalanced magnetic force prediction in permanent magnet machines with rotor eccentricity by improved superposition method," *IET Electric Power Applications*, 2017.
- [67] A. Hofmann, F. Qi, C. Weiss, T. Kojima, and R. De Doncker, "The acoustic impact of rotor eccentricity in switched reluctance machines," *EPE Journal*, vol. 26, pp. 47-57, 2016.
- [68] M. Y. Kaikaa, M. Hadjami, and A. Khezzar, "Effects of the simultaneous presence of static eccentricity and broken rotor bars on the stator current of induction machine," *IEEE Transactions on Industrial Electronics*, vol. 61, pp. 2452-2463, 2014.

- [69] J.-K. Park and J. Hur, "Detection of inter-turn and dynamic eccentricity faults using stator current frequency pattern in IPM-type BLDC motors," *IEEE Transactions on Industrial Electronics*, vol. 63, pp. 1771-1780, 2016.
- [70] S. Bindu and V. V. Thomas, "Detection of Static Air-Gap Eccentricity in Three-Phase Squirrel Cage Induction Motor Through Stator Current and Vibration Analysis," in *Advances in Power Systems and Energy Management*, ed: Springer, 2018, pp. 511-518.
- [71] J. Faiz and S. M. M. Moosavi, "Detection of mixed eccentricity fault in doubly-fed induction generator based on reactive power spectrum," *IET Electric Power Applications*, 2017.
- [72] G. Georgoulas, V. Climente-Alarcon, J. A. Antonino-Daviu, I. P. Tsoumas, C. D. Stylios, A. Arkkio, *et al.*, "The Use of a Multilabel Classification Framework for the Detection of Broken Bars and Mixed Eccentricity Faults Based on the Start-Up Transient," *IEEE Transactions on Industrial Informatics*, vol. 13, pp. 625-634, 2017.
- [73] Y. Li, Q. Lu, Z. Zhu, D. Wu, and G. Li, "Superposition method for cogging torque prediction in permanent magnet machines with rotor eccentricity," *IEEE Transactions on Magnetics*, vol. 52, pp. 1-10, 2016.
- [74] W. T. Thomson and R. J. Gilmore, "Motor current signature analysis to detect faults in induction motor drives-fundamentals, Data interpretation, and industrial case histories," in *Proceedings of 32nd Turbo machinery Symposium, A&M University, Texas, USA*, 2003.
- [75] J. Faiz and M. Ojaghi, "Different indexes for eccentricity faults diagnosis in three-phase squirrel-cage induction motors: A review," *Mechatronics*, vol. 19, pp. 2-13, 2009.
- [76] B. M. Ebrahimi, M. Javan Roshtkhari, J. Faiz, and S. V. Khatami, "Advanced eccentricity fault recognition in permanent magnet synchronous motors using stator current signature analysis," *Industrial Electronics, IEEE Transactions on*, vol. 61, pp. 2041-2052, 2014.
- [77] K. Yahia, A. Cardoso, A. Ghoggal, and S. Zouzou, "Induction motors airgap-eccentricity detection through the discrete wavelet transform of the apparent

- power signal under non-stationary operating conditions," *ISA transactions*, vol. 53, pp. 603-611, 2014.
- [78] J. Pons-Llinares, J. Antonino-Daviu, J. Roger-Folch, D. Moríñigo-Sotelo, and O. Duque-Pérez, "Mixed eccentricity diagnosis in Inverter-Fed Induction Motors via the Adaptive Slope Transform of transient stator currents," *Mechanical Systems and Signal Processing*, vol. 48, pp. 423-435, 2014.
- [79] Y.-T. Yu, C. Bi, P. N. Hla, Q. Jiang, S. Lin, N. L. H. Aung, *et al.*, "Incline unbalanced magnetic pull induced by misalignment rotor in PMSM," *Magnetics, IEEE Transactions on*, vol. 49, pp. 2709-2714, 2013.
- [80] S. Bindu and V. V. Thomas, "Diagnoses of internal faults of three phase squirrel cage induction motor—A review," in *Advances in Energy Conversion Technologies (ICAECT), 2014 International Conference on*, 2014, pp. 48-54.
- [81] Y.-H. Kim, Y.-W. Youn, D.-H. Hwang, J.-H. Sun, and D.-S. Kang, "High-resolution parameter estimation method to identify broken rotor bar faults in induction motors," *IEEE Transactions on Industrial Electronics*, vol. 60, pp. 4103-4117, 2013.
- [82] K. N. Gyftakis, J. A. Antonino-Daviu, R. Garcia-Hernandez, M. D. McCulloch, D. A. Howey, and A. J. M. Cardoso, "Comparative experimental investigation of broken bar fault detectability in induction motors," *IEEE Transactions on Industry Applications*, vol. 52, pp. 1452-1459, 2016.
- [83] J. Pons-Llinares, J. A. Antonino-Daviu, M. Riera-Guasp, S. B. Lee, T.-J. Kang, and C. Yang, "Advanced induction motor rotor fault diagnosis via continuous and discrete time–frequency tools," *IEEE Transactions on Industrial Electronics*, vol. 62, pp. 1791-1802, 2015.
- [84] S. Nandi and H. Toliyat, "Fault diagnosis of electrical machines-a review," in *Electric Machines and Drives, 1999. International Conference IEMD'99*, 1999, pp. 219-221.
- [85] J. Ilonen, J.-K. Kamarainen, T. Lindh, J. Ahola, H. Kälviäinen, and J. Partanen, "Diagnosis tool for motor condition monitoring," *Industry Applications, IEEE Transactions on*, vol. 41, pp. 963-971, 2005.

- [86] A. Ordaz-Moreno, R. de Jesus Romero-Troncoso, J. A. Vite-Frias, J. R. Rivera-Gillen, and A. Garcia-Perez, "Automatic online diagnosis algorithm for broken-bar detection on induction motors based on discrete wavelet transform for FPGA implementation," *Industrial Electronics, IEEE Transactions on*, vol. 55, pp. 2193-2202, 2008.
- [87] M. Haji and H. A. Toliyat, "Pattern recognition-a technique for induction machines rotor broken bar detection," *Energy Conversion, IEEE Transactions on*, vol. 16, pp. 312-317, 2001.
- [88] A. M. Da Silva, R. J. Povinelli, and N. A. Demerdash, "Induction machine broken bar and stator short-circuit fault diagnostics based on three-phase stator current envelopes," *Industrial Electronics, IEEE Transactions on*, vol. 55, pp. 1310-1318, 2008.
- [89] K. M. Siddiqui, K. Sahay, and V. Giri, "Health monitoring and fault diagnosis in induction motor-a review," *International Journal of Advanced Research in Electrical, Electronics and Instrumentation Engineering*, vol. 3, pp. 6549-6565, 2014.
- [90] M. R. Mehrjou, N. Mariun, M. Karami, N. Misron, and M. A. M. Radzi, "Broken Rotor Bar Detection in LS-PMSMs Based on Statistical Features Analysis of Start-up Current Envelope."
- [91] M. R. Mehrjou, N. Mariun, M. Karami, N. Misron, and M. A. M. Radzi, "Statistical Features Analysis of Transient Current Signal for Broken Bars Fault Detection in LS-PMSMs."
- [92] M. Akar and M. Eker, "Demagnetization fault diagnosis in permanent magnet synchronous motors," *Przegląd Elektrotechniczny*, vol. 89, pp. 229-233, 2013.
- [93] X. Tang, X. Wang, G. Li, and M. Tian, "Demagnetization study of line-start permanent magnet synchronous motor under out-of-step and supersynchronous faults," in *Industrial Electronics and Applications (ICIEA), 2016 IEEE 11th Conference on*, 2016, pp. 1496-1501.
- [94] W. Lu, M. Liu, Y. Luo, and Y. Liu, "Influencing factors on the demagnetization of line-start permanent magnet synchronous motor during its starting process," in

- Electrical Machines and Systems (ICEMS), 2011 International Conference on*, 2011, pp. 1-4.
- [95] X. Xiao and C. Chen, "Reduction of torque ripple due to demagnetization in PMSM using current compensation," *Applied Superconductivity, IEEE Transactions on*, vol. 20, pp. 1068-1071, 2010.
- [96] K.-C. Kim, S.-B. Lim, D.-H. Koo, and J. Lee, "The shape design of permanent magnet for permanent magnet synchronous motor considering partial demagnetization," *Magnetics, IEEE Transactions on*, vol. 42, pp. 3485-3487, 2006.
- [97] J. Rosero, J. Cusido, A. Garcia, J. Ortega, and L. Romeral, "Study on the permanent magnet demagnetization fault in permanent magnet synchronous machines," in *The 32nd Annual Conference of the IEEE Industrial Electronics Society, IECON06, Paris-FRANCE*, 2006, pp. 879-884.
- [98] A. Abbas, H. Yousef, and O. Sebakhly, "FE parameters sensitivity analysis of an industrial LS interior PM synchronous motor," in *Power and Energy Society General Meeting-Conversion and Delivery of Electrical Energy in the 21st Century, 2008 IEEE*, 2008, pp. 1-6.
- [99] M. D. Prieto, A. G. Espinosa, J.-R. Ruiz, J. C. Urresty, and J. A. Ortega, "Feature extraction of demagnetization faults in permanent-magnet synchronous motors based on box-counting fractal dimension," *Industrial Electronics, IEEE Transactions on*, vol. 58, pp. 1594-1605, 2011.
- [100] C. A. Lopez, A. S. Babel, and E. G. Strangas, "Detecting uniform and partial demagnetization for an interior permanent magnet machine," in *Electrical Machines (ICEM), 2016 XXII International Conference on*, 2016, pp. 2874-2880.
- [101] J. Wang, D. Lieu, W. Lorimer, and A. Hartman, "Comparison of lumped parameter and finite element magnetic modeling in a brushless DC motor," *IEEE transactions on Magnetics*, vol. 33, pp. 4092-4094, 1997.
- [102] A. Cassat, C. Espanet, and N. Wavre, "BLDC motor stator and rotor iron losses and thermal behavior based on lumped schemes and 3-D FEM analysis," *IEEE Transactions on Industry Applications*, vol. 39, pp. 1314-1322, 2003.

- [103] K. Boughrara, N. Takorabet, R. Ibtouen, O. Touhami, and F. Dubas, "Analytical analysis of cage rotor induction motors in healthy, defective, and broken bars conditions," *IEEE Transactions on Magnetics*, vol. 51, pp. 1-17, 2015.
- [104] N. Féki, G. Clerc, and P. Vex, "Gear and motor fault modeling and detection based on motor current analysis," *Electric power systems research*, vol. 95, pp. 28-37, 2013.
- [105] J. Faiz, A. Exiri, and H. Nejadi-Koti, "Current-based inter-turn short circuit fault modeling in permanent magnet synchronous machine using magnetic equivalent circuit model," in *Compatibility, Power Electronics and Power Engineering (CPE-POWERENG), 2016 10th International Conference on*, 2016, pp. 265-270.
- [106] N. H. Obeid, T. Boileau, and B. Nahid-Mobarakeh, "Modeling and diagnostic of incipient interturn faults for a three-phase permanent magnet synchronous motor," *IEEE Transactions on Industry Applications*, vol. 52, pp. 4426-4434, 2016.
- [107] J. Faiz, M. Ghasemi-Bijan, and B. Mahdi Ebrahimi, "Modeling and diagnosing eccentricity fault using three-dimensional magnetic equivalent circuit model of three-phase squirrel-cage induction motor," *Electric Power Components and Systems*, vol. 43, pp. 1246-1256, 2015.
- [108] D. C. Patel and M. C. Chandorkar, "Modeling and analysis of stator interturn fault location effects on induction machines," *IEEE Transactions on Industrial Electronics*, vol. 61, pp. 4552-4564, 2014.
- [109] H. Qian, H. Guo, and X. Ding, "Modeling and analysis of interturn short fault in permanent magnet synchronous motors with multistrands windings," *IEEE Transactions on Power Electronics*, vol. 31, pp. 2496-2509, 2016.
- [110] A. Gaeta, G. Scelba, and A. Consoli, "Modeling and control of three-phase PMSMs under open-phase fault," *IEEE transactions on industry applications*, vol. 49, pp. 74-83, 2013.
- [111] P. Shi, Z. Chen, Y. Vagapov, and Z. Zouaoui, "A new diagnosis of broken rotor bar fault extent in three phase squirrel cage induction motor," *Mechanical Systems and Signal Processing*, vol. 42, pp. 388-403, 2014.



- [112] S. Asgari, M. Jannati, and N. Idris, "Modeling of three-phase induction motor with two stator phases open-circuit," in *Energy Conversion (CENCON), 2014 IEEE Conference on*, 2014, pp. 231-236.
- [113] I. Jeong, B. J. Hyon, and K. Nam, "Dynamic modeling and control for SPMSMs with internal turn short fault," *IEEE Transactions on Power Electronics*, vol. 28, pp. 3495-3508, 2013.
- [114] P. Dewangan, D. K. Singh, and M. D. Sharma, "Modeling And Simulation Of Rotor Side Fault Diagnosis Of Induction Motor By Using Fuzzy Based Controlled Identifier," *International Journal of Engineering Research and General Science*, vol. 3, 2015.
- [115] M. Zafarani, T. Goktas, B. Akin, and S. E. Fedigan, "Modeling and dynamic behavior analysis of magnet defect signatures in permanent magnet synchronous motors," *IEEE Transactions on Industry Applications*, vol. 52, pp. 3753-3762, 2016.
- [116] M. h. Drif and A. J. M. Cardoso, "Stator fault diagnostics in squirrel cage three-phase induction motor drives using the instantaneous active and reactive power signature analyses," *IEEE Transactions on Industrial Informatics*, vol. 10, pp. 1348-1360, 2014.
- [117] B. Vaseghi, N. Takorabet, B. Nahid-Mobarakeh, and F. Meibody-Tabar, "Modelling and study of PM machines with inter-turn fault dynamic model–FEM model," *Electric Power Systems Research*, vol. 81, pp. 1715-1722, 2011.
- [118] A. Gandhi, T. Corrigan, and L. Parsa, "Recent advances in modeling and online detection of stator interturn faults in electrical motors," *IEEE Transactions on Industrial Electronics*, vol. 58, pp. 1564-1575, 2011.
- [119] Y.-S. Lee, K.-T. Kim, and J. Hur, "Finite-element analysis of the demagnetization of IPM-type BLDC motor with stator turn fault," *IEEE Transactions on Magnetics*, vol. 50, pp. 889-892, 2014.
- [120] B. Vaseghi, N. Takorabet, and F. Meibody-Tabar, "Analytical circuit-based model of PMSM under stator inter-turn short-circuit fault validated by time-stepping finite element analysis," in *Electrical Machines (ICEM), 2010 XIX International Conference on*, 2010, pp. 1-6.

- [121] M. Fitouri, Y. Bensalem, and M. N. Abdelkrim, "Modeling and detection of the short-circuit fault in PMSM using Finite Element Analysis," *IFAC-PapersOnLine*, vol. 49, pp. 1418-1423, 2016.
- [122] A. Berzoy, A. A. Mohamed, and O. Mohammed, "Complex-Vector Model of Interturn Failure in Induction Machines for Fault Detection and Identification," *IEEE Transactions on Industry Applications*, vol. 53, pp. 2667-2678, 2017.
- [123] L. Romeral, J. C. Urresty, J.-R. R. Ruiz, and A. G. Espinosa, "Modeling of surface-mounted permanent magnet synchronous motors with stator winding interturn faults," *IEEE Transactions on Industrial Electronics*, vol. 58, pp. 1576-1585, 2011.
- [124] J.-H. Choi, B.-G. Gu, and C.-Y. Won, "Modeling and analysis of PMSMs under inter turn short faults," *Journal of Electrical Engineering and Technology*, vol. 8, pp. 1243-1250, 2013.
- [125] V. C. Leite, J. G. B. da Silva, G. F. C. Veloso, L. E. B. da Silva, G. Lambert-Torres, E. L. Bonaldi, *et al.*, "Detection of localized bearing faults in induction machines by spectral kurtosis and envelope analysis of stator current," *IEEE Transactions on Industrial Electronics*, vol. 62, pp. 1855-1865, 2015.
- [126] K. N. Gyftakis, M. h. Drif, and A. J. Cardoso, "Thorough investigation of the third current harmonic in delta-connected induction motors suffering from a stator inter-turn fault," in *Diagnostics for Electrical Machines, Power Electronics and Drives (SDEMPED), 2015 IEEE 10th International Symposium on*, 2015, pp. 7-13.
- [127] M. Eftekhari, M. Moallem, S. Sadri, and M.-F. Hsieh, "A novel indicator of stator winding inter-turn fault in induction motor using infrared thermal imaging," *Infrared Physics & Technology*, vol. 61, pp. 330-336, 2013.
- [128] N. Lashkari, J. Poshtan, and H. F. Azgomi, "Simulative and experimental investigation on stator winding turn and unbalanced supply voltage fault diagnosis in induction motors using artificial neural networks," *ISA transactions*, vol. 59, pp. 334-342, 2015.

- [129] A. M. da Silva, R. J. Povinelli, and N. A. Demerdash, "Rotor bar fault monitoring method based on analysis of air-gap torques of induction motors," *IEEE Transactions on Industrial Informatics*, vol. 9, pp. 2274-2283, 2013.
- [130] T. Kato, K. Inoue, and K. Yoshida, "Diagnosis of Stator-Winding-Turn Faults of Induction Motor by Direct Detection of Negative Sequence Currents," *Electrical Engineering in Japan*, vol. 186, pp. 75-84, 2014.
- [131] J.-C. Urresty, J.-R. Riba, M. Delgado, and L. Romeral, "Detection of demagnetization faults in surface-mounted permanent magnet synchronous motors by means of the zero-sequence voltage component," *IEEE transactions on Energy conversion*, vol. 27, pp. 42-51, 2012.
- [132] K. N. Gyftakis, D. V. Spyropoulos, J. C. Kappatou, and E. D. Mitronikas, "A novel approach for broken bar fault diagnosis in induction motors through torque monitoring," *IEEE Transactions on Energy Conversion*, vol. 28, pp. 267-277, 2013.
- [133] P. Lamim Filho, R. Pederiva, and J. Brito, "Detection of stator winding faults in induction machines using flux and vibration analysis," *Mechanical Systems and Signal Processing*, vol. 42, pp. 377-387, 2014.
- [134] S. Jelassi, R. Romary, and J.-F. Brudny, "Vibro-acoustic behaviour of an induction machine with stator inter-turn short-circuit," *The European Physical Journal Applied Physics*, vol. 73, p. 10904, 2016.
- [135] J. S. Hsu, "Monitoring of defects in induction motors through air-gap torque observation," *IEEE Transactions on Industry Applications*, vol. 31, pp. 1016-1021, 1995.
- [136] H. A. Toliyat and T. A. Lipo, "Transient analysis of cage induction machines under stator, rotor bar and end ring faults," *IEEE Transactions on Energy Conversion*, vol. 10, pp. 241-247, 1995.
- [137] S. Choi, M. S. Haque, A. Arafat, and H. Toliyat, "Detection and Estimation of Extremely Small Fault Signature by Utilizing Multiple Current Sensor Signals in Multiphase Electric Machines," *IEEE Transactions on Industry Applications*, 2017.

- [138] Q. Wu and S. Nandi, "Fast single-turn sensitive stator interturn fault detection of induction machines based on positive-and negative-sequence third harmonic components of line currents," *IEEE Transactions on Industry Applications*, vol. 46, pp. 974-983, 2010.
- [139] K.-H. Kim, "Simple online fault detecting scheme for short-circuited turn in a PMSM through current harmonic monitoring," *IEEE Transactions on Industrial Electronics*, vol. 58, pp. 2565-2568, 2011.
- [140] A. M. Da Silva, R. J. Povinelli, and N. A. Demerdash, "Induction machine broken bar and stator short-circuit fault diagnostics based on three-phase stator current envelopes," *IEEE Transactions on Industrial Electronics*, vol. 55, pp. 1310-1318, 2008.
- [141] S. M. Cruz and A. M. Cardoso, "Multiple reference frames theory: A new method for the diagnosis of stator faults in three-phase induction motors," *IEEE Transactions on Energy Conversion*, vol. 20, pp. 611-619, 2005.
- [142] P. Barendse, B. Herndler, M. Khan, and P. Pillay, "The application of wavelets for the detection of inter-turn faults in induction machines," in *Electric Machines and Drives Conference, 2009. IEMDC'09. IEEE International, 2009*, pp. 1401-1407.
- [143] J. Rosero, L. Romeral, J. Cusido, A. Garcia, and J. Ortega, "On the short-circuiting fault detection in a PMSM by means of stator current transformations," in *Power Electronics Specialists Conference, 2007. PESC 2007. IEEE, 2007*, pp. 1936-1941.
- [144] J. A. Rosero, L. Romeral, J. A. Ortega, and E. Rosero, "Short-circuit detection by means of empirical mode decomposition and Wigner–Ville distribution for PMSM running under dynamic condition," *IEEE Transactions on Industrial Electronics*, vol. 56, pp. 4534-4547, 2009.
- [145] K. Zhang, F. Yuan, J. Guo, and G. Wang, "A novel neural network approach to transformer fault diagnosis based on momentum-embedded BP neural network optimized by genetic algorithm and fuzzy c-means," *Arabian Journal for Science and Engineering*, vol. 41, pp. 3451-3461, 2016.

- [146] A. Prasad and J. B. Edward, "Importance of artificial neural networks for location of faults in transmission systems: A survey," in *Intelligent Systems and Control (ISCO), 2017 11th International Conference on*, 2017, pp. 357-362.
- [147] A. Nag and A. Yadav, "Fault classification using Artificial Neural Network in combined underground cable and overhead line," in *Power Electronics, Intelligent Control and Energy Systems (ICPEICES), IEEE International Conference on*, 2016, pp. 1-4.
- [148] W. Chine, A. Mellit, V. Lughi, A. Malek, G. Sulligoi, and A. M. Pavan, "A novel fault diagnosis technique for photovoltaic systems based on artificial neural networks," *Renewable Energy*, vol. 90, pp. 501-512, 2016.
- [149] G. M. Joksimovic and J. Penman, "The detection of inter-turn short circuits in the stator windings of operating motors," *IEEE Transactions on Industrial Electronics*, vol. 47, pp. 1078-1084, 2000.
- [150] P. V. J. Rodríguez and A. Arkkio, "Detection of stator winding fault in induction motor using fuzzy logic," *Applied Soft Computing*, vol. 8, pp. 1112-1120, 2008.
- [151] M. B. K. Bouzid, G. Champenois, N. M. Bellaaj, L. Signac, and K. Jelassi, "An effective neural approach for the automatic location of stator interturn faults in induction motor," *IEEE transactions on industrial electronics*, vol. 55, pp. 4277-4289, 2008.
- [152] N. Lashkari and J. Poshtan, "Detection and discrimination of stator interturn fault and unbalanced supply voltage fault in induction motor using neural network," in *Power Electronics, Drives Systems & Technologies Conference (PEDSTC), 2015 6th*, 2015, pp. 275-280.
- [153] G. H. Bazan, P. R. Scalassara, W. Endo, A. Goedtel, W. F. Godoy, and R. H. C. Palácios, "Stator fault analysis of three-phase induction motors using information measures and artificial neural networks," *Electric Power Systems Research*, vol. 143, pp. 347-356, 2017.
- [154] V. N. Ghate and S. V. Dudul, "Optimal MLP neural network classifier for fault detection of three phase induction motor," *Expert Systems with Applications*, vol. 37, pp. 3468-3481, 2010.

- [155] V. N. Ghate and S. V. Dudul, "Cascade neural-network-based fault classifier for three-phase induction motor," *IEEE Transactions on Industrial Electronics*, vol. 58, pp. 1555-1563, 2011.
- [156] J. F. Martins, V. F. Pires, and A. Pires, "Unsupervised neural-network-based algorithm for an on-line diagnosis of three-phase induction motor stator fault," *IEEE Transactions on Industrial Electronics*, vol. 54, pp. 259-264, 2007.
- [157] S. Moosavi, A. Djerdir, Y. Ait-Amirat, and D. Khaburi, "ANN based fault diagnosis of permanent magnet synchronous motor under stator winding shorted turn," *Electric Power Systems Research*, vol. 125, pp. 67-82, 2015.
- [158] B. Bessam, A. Menacer, M. Boumehraz, and H. Cherif, "Wavelet transform and neural network techniques for inter-turn short circuit diagnosis and location in induction motor," *International Journal of System Assurance Engineering and Management*, vol. 8, pp. 478-488, 2017.
- [159] F. Cira, M. Arkan, and B. Gumus, "Detection of Stator Winding Inter-Turn Short Circuit Faults in Permanent Magnet Synchronous Motors and Automatic Classification of Fault Severity via a Pattern Recognition System," *J. Electr. Eng. Technol*, vol. 11, pp. 416-424, 2016.
- [160] G. Rajamany and S. Srinivasan, "An Artificial Neural Networks Application for the Automatic Detection of Severity of Stator Inter Coil Fault in Three Phase Induction Motor," *Journal of Electrical Engineering & Technology*, vol. 12, pp. 2219-2226, 2017.
- [161] V. Giurgiutiu and S. E. Lyshevski, *Micromechatronics: Modeling, analysis, and design with MATLAB*: CRC Press, 2009.
- [162] P. C. Krause, O. Wasynczuk, S. D. Sudhoff, and S. Pekarek, *Analysis of electric machinery and drive systems* vol. 75: John Wiley & Sons, 2013.
- [163] Lu, Xiaomin, "Dual Benefits of Adding Damper Bars in PMSMs for Electrified Vehicles: Improved Machine Dynamics and Simplified Integrated Charging" (2014). *Electronic Theses and Dissertations*. 5194.
- [164] C.-M.-M. O. Ong, *Dynamic simulation of electric machinery using Matlab/Simulink*: Prentice-Hall PTR, 1998.

- [165] R. Krishnan, *Permanent magnet synchronous and brushless DC motor drives*: CRC press, 2009.
- [166] M. S. Sarma and M. K. Pathak, *Electric machines*: Cengage Learning, 2010.
- [167] R. M. Tallam, T. G. Habetler, and R. G. Harley, "Transient model for induction machines with stator winding turn faults," *IEEE Transactions on Industry Applications*, vol. 38, pp. 632-637, 2002.
- [168] A. Berzoy, A. Mohamed, and O. Mohammed, "Dynamic space-vector model of induction machines with stator inter-turn short-circuit fault," in *Industrial Electronics Society, IECON 2015-41st Annual Conference of the IEEE*, 2015, pp. 003620-003625.
- [169] R. A. Patel and M. A. Alam, "Stator Inter-turn Fault Detection using MCSA."
- [170] S. M. Cruz and A. M. Cardoso, "Diagnosis of stator inter-turn short circuits in DTC induction motor drives," *IEEE Transactions on Industry Applications*, vol. 40, pp. 1349-1360, 2004.
- [171] S. Cruz and A. Cardoso, "The method of multiple reference frames applied to the diagnosis of stator faults in three-phase induction motors," in *Power Electronics and Motion Control Conference, 2004. IPEMC 2004. The 4th International*, 2004, pp. 603-609.
- [172] M. Sahraoui, A. Ghoggal, S. E. Zouzou, A. Aboubou, and H. Razik, "Modelling and detection of inter-turn short circuits in stator windings of induction motor," in *IEEE Industrial Electronics, IECON 2006-32nd Annual Conference on*, 2006, pp. 4981-4986.
- [173] L. M. R. Baccarini, B. R. de Menezes, and W. M. Caminhas, "Fault induction dynamic model, suitable for computer simulation: Simulation results and experimental validation," *Mechanical Systems and Signal Processing*, vol. 24, pp. 300-311, 2010.
- [174] S. E. Lyshevski, *Electromechanical systems, electric machines, and applied mechatronics* vol. 3: CRC press, 1999.
- [175] R. Krishnan, *Switched reluctance motor drives: modeling, simulation, analysis, design, and applications*: CRC press, 2001.

- [176] F. Khorrami, P. Krishnamurthy, and H. Melkote, *Modeling and adaptive nonlinear control of electric motors*: Springer Science & Business Media, 2003.
- [177] B. Vaseghi, N. Takorabet, and F. Meibody-Tabar, "Fault analysis and parameter identification of permanent-magnet motors by the finite-element method," *IEEE Transactions on Magnetics*, vol. 45, pp. 3290-3295, 2009.
- [178] K. L. V. Iyer, X. Lu, K. Mukherjee, and N. C. Kar, "A novel two-axis theory-based approach towards parameter determination of line-start permanent magnet synchronous machines," *IEEE Transactions on Magnetics*, vol. 48, pp. 4208-4211, 2012.
- [179] T. Marcic, B. Stumberger, and G. Stumberger, "Differential-evolution-based parameter identification of a line-start IPM synchronous motor," *IEEE Transactions on Industrial Electronics*, vol. 61, pp. 5921-5929, 2014.
- [180] X. Ji and T. Noguchi, "Off-line parameter identification of interior permanent magnet motor by searching minimum point of current norm characteristics," in *Power Electronics, Electrical Drives, Automation and Motion (SPEEDAM), 2014 International Symposium on*, 2014, pp. 279-284.
- [181] D. Jing, "Computational analysis of a permanent magnet synchronous machine using numerical techniques," 2005.
- [182] C. Debruyne, M. Polikarpova, S. Derammelaere, P. Sergeant, J. Pyrhonen, J. J. Desmet, *et al.*, "Evaluation of the efficiency of line-start permanent-magnet machines as a function of the operating temperature," *IEEE Transactions on Industrial Electronics*, vol. 61, pp. 4443-4454, 2014.
- [183] F. Lazăr, A. Simion, L. Livadaru, and I. Daniel, "FEM analysis of a 3 kW line-start permanent magnet synchronous machine," in *Electrical and Power Engineering (EPE), 2014 International Conference and Exposition on*, 2014, pp. 402-405.
- [184] M. R. Mehrjou, N. Mariun, M. Karami, N. Misron, and M. A. M. Radzi, "Performance analysis of line-start permanent magnet synchronous motor in presence of rotor fault," in *Research and Development (SCORED), 2014 IEEE Student Conference on*, 2014, pp. 1-4.



- [185] F. Ghoroghchian, A. D. Aliabad, E. Amiri, and B. Poudel, "Line start permanent magnet synchronous motor with dual magnetic polarity," in *Electric Machines and Drives Conference (IEMDC), 2017 IEEE International*, 2017, pp. 1-6.
- [186] E. Sarani and S. Vaez-Zadeh, "Design Procedure and Optimal Guidelines for Overall Enhancement of Steady State and Transient Performances of Line Start Permanent Magnet Motors," *IEEE Transactions on Energy Conversion*, 2017.
- [187] A. Takahashi, S. Kikuchi, H. Mikami, K. Ide, and A. Binder, "dq Space vector analysis for line-starting permanent magnet synchronous motors," in *Electrical Machines (ICEM), 2012 XXth International Conference on*, 2012, pp. 136-142.
- [188] V. Elistratova, M. Hecquet, P. Brochet, D. Vizireanu, and M. Dessoude, "Analytical approach for optimal design of a line-start internal permanent magnet synchronous motor," in *Power Electronics and Applications (EPE), 2013 15th European Conference on*, 2013, pp. 1-7.
- [189] S. Ahmed, D. Tremelling, H. Kim, Z. Zhang, N. Frank, and R. McElveen, "Modeling, simulation and performance evaluation of cage rotor permanent magnet motor fed by variable speed drive," in *Energy Conversion Congress and Exposition (ECCE), 2016 IEEE*, 2016, pp. 1-6.
- [190] W. Kemmetmuller, D. Faustner, and A. Kugi, "Modeling of a permanent magnet synchronous machine with internal magnets using magnetic equivalent circuits," *IEEE Transactions on Magnetics*, vol. 50, pp. 1-14, 2014.
- [191] K. M. Rahman and S. Hiti, "Identification of machine parameters of a synchronous motor," *IEEE Transactions on Industry Applications*, vol. 41, pp. 557-565, 2005.
- [192] M. Haque and M. Rahman, "Dynamic model and parameter measurement of interior permanent magnet synchronous motor," in *Proceedings of the 2006 Australasian Universities Power Engineering Conference (AUPEC'06)*, 2006, pp. 10-13.
- [193] A. Cavagnino, M. Lazzari, F. Profumo, and A. Tenconi, "Axial flux interior PM synchronous motor: parameters identification and steady-state performance measurements," *IEEE Transactions on Industry Applications*, vol. 36, pp. 1581-1588, 2000.

- [194] T. Marcic, G. Stumberger, B. Stumberger, M. Hadziselimovic, and P. Vrtic, "Determining parameters of a line-start interior permanent magnet synchronous motor model by the differential evolution," *IEEE Transactions on Magnetics*, vol. 44, pp. 4385-4388, 2008.
- [195] M. O. Sonnaillon, G. Bisheimer, C. D. Angelo, and G. O. García. (2007, Automatic induction machine parameters measurement using standstill frequency-domain tests. *IET Electric Power Applications 1(5)*, 833-838. Available: [http://digital-library.theiet.org/content/journals/10.1049/iet-epa\\_20060512](http://digital-library.theiet.org/content/journals/10.1049/iet-epa_20060512)
- [196] S. Chapman, *Electric machinery fundamentals*: Tata McGraw-Hill Education, 2005.
- [197] "IEEE Standard Test Procedure for Polyphase Induction Motors and Generators," *IEEE Std 112-1996*, p. i, 1997.
- [198] R. Zeni, "Investigation of the sensorless capability of an Induction Motor with intentionally created saliency. Simulations and measurements," 2013.
- [199] S. Ayasun and C. O. Nwankpa, "Induction motor tests using MATLAB/Simulink and their integration into undergraduate electric machinery courses," *IEEE Transactions on education*, vol. 48, pp. 37-46, 2005.
- [200] O. I. Okoro, *Dynamic and thermal modelling of induction machine with non-linear effects*: Kassel University Press Kassel, 2002.
- [201] V. Bobek, "Pmsm electrical parameters measurement," *Freescale Semiconductor*, 2013.
- [202] M. Cisneros-Gonzalez, C. Hernandez, R. Escarela-Perez, and M. Arjona, "Determination of equivalent-circuit parameters of a synchronous generator based on the standstill DC decay test and a hybrid optimization method," *Electric Power Components and Systems*, vol. 39, pp. 645-659, 2011.
- [203] D. Y. Ohm, "Dynamic model of PM synchronous motors," *Drivetech, Inc., Blacksburg, Virginia, www.drivetechinc.com*, vol. 16, 2000.

## Publications

### Published Journal Papers

- J1. L. Maraaba, Z. Al-Hamouz, and M. Abido, "An Efficient Stator Inter-Turn Fault Diagnosis Tool for Induction Motors," *Energies*, vol. 11, p. 653, 2018.**
- J2. Maraaba, L., Al-Hamouz, Z., Milhem, A., & Abido, M. "Modeling of Interior-Mount LSPMSM under Asymmetrical Stator Winding". IET Electric Power Applications. 2018.**

### Submitted Publications

- J1. Luqman Maraaba, Zakariya Al-Hamouz, Abdulaziz Milhem, Mohammad Abido, "Neural Network-based Diagnostic Tool for Detecting Stator Inter-Turn Faults in LSPMSMs" IEEE Access.**
- J2. L. S. Maraaba, Z. M. Al-Hamouz and M. A. Abido, Mathematical Modeling, Simulation, and Experimental Testing of Interior-Mount LSPMSM Under Stator Inter-Turn Fault, IEEE Transaction on Energy Conversion**

### Published/Accepted Conference Papers

- C3. L. S. Maraaba, Z. M. Al-Hamouz and M. A. Abido, "Modeling and simulation of line start permanent magnet synchronous motors with asymmetrical stator windings," IECON 2016 - 42nd Annual Conference of the IEEE Industrial Electronics Society, Florence, 2016, pp. 1698-1703.doi: 10.1109/IECON.2016.7793412(ISI)**

## Vitae

Name	:Luqman Sulyman Faez Maraaba
Nationality	:Palestinian
Date of Birth	:7/12/1987
Email	:Luqman.sylyman@gmail.com, lmaraaba@kfupm.edu.sa
Address	:Dhahran, Khobar, Saudi Arabia
Academic Background	: Electrical Engineering M.Sc. with 4.00/4.00 GPA – KFUPM, King Fahd University of Petroleum and Minerals, graduation date, December 2013.  Electrical Engineering B.Sc. First Class Honored Graduate with 90.1% GPA– Al-Najah National University, graduation date, May 2010. Research interest includes machine failures modelling and detection, high voltage insulators.